2016

Cascading Failure Risk Estimation and Mitigation in Power Systems

Pooya Rezaei
University of Vermont

CASCADING FAILURE RISK ESTIMATION AND MITIGATION IN POWER SYSTEMS

A Dissertation Presented

by

Pooya Rezaei

to

The Faculty of the Graduate College

of

The University of Vermont

In Partial Fullfillment of the Requirements
for the Degree of Doctor of Philosophy
Specializing in Electrical Engineering

January, 2016

Defense date: September 25, 2015
Dissertation Examination Committee:

Paul D. H. Hines, Ph.D., Advisor
Byung S. Lee, Ph.D., Chairperson
Margaret J. Eppstein, Ph.D.
Eric M. Hernandez, Ph.D.
Mads Almassalkhi, Ph.D.
Cynthia J. Forehand, Ph.D., Dean of the Graduate College

Abstract

Electricity is a critical component in our daily life. Because it is almost always available, we take it for granted. However, given the proper conditions, blackouts do happen every once in a while and can cause discomfort at a minimum, and a catastrophe in rare circumstances. The largest blackouts typically include cascading failures, which are sequences of interdependent outages. Although timely and effective operator intervention can often prevent a cascade from spreading, such interventions require ample situational awareness.

The goals of this dissertation are twofold: to provide power system operators with insight into the risk of blackouts given the space of potential initiating outages, and to evaluate control systems that might mitigate cascading failure risk. Accordingly, this dissertation proposes a novel method to estimate cascading failure risk. It is shown that this method is at least two orders of magnitude faster in estimating risk, compared with a traditional Monte-Carlo simulation in two test systems including a large-scale real power grid model. This method allows one to find critical components in a system and suggests ideas for how to reduce blackout risk by preventive measures, such as adjusting initial dispatch of a system.

In addition to preventive measures, it is also possible to use corrective control strategies to reduce blackout sizes. These methods could be used once the system is under stress (for example if some of the elements are overloaded) to stop a potential cascade before it unfolds. This dissertation focuses on a distributed receding horizon model predictive control strategy to mitigate overloads in a system, in which each node can only control other nodes in its local neighborhood. A distributed approach not only needs less communication and computation, but is also a more natural fit with modern power system operations, in which many control centers manage disjoint regional networks. In addition, a distributed controller may be more robust to random failures and attacks. A central controller benefits from perfect information, and thus provides the optimal solution. This dissertation shows that as long as the local neighborhood of the distributed method is large enough, distributed control can provide high quality solutions that are similar to what an omniscient centralized controller could achieve, but with less communication requirements (per node), relative to the centralized approach.

Citations

Material from this dissertation has been published in the following forms:

Rezaei, P., Hines, P.D.H., Eppstein, M.J.. (2015). Estimating Cascading Failure Risk with Random Chemistry. IEEE Transactions on Power Systems, Vol. 30, No. 5, 2726-2735.

AND

Rezaei, P., Eppstein, M.J., Hines, P.D.H.. (2015). Rapid Assessment, Visualization and Mitigation of Cascading Failure Risk in Power Systems. 2015 48$^{\text{th}}$ Hawaii International Conference on System Sciences (HICSS).

AND

Rezaei, P., Hines, P.D.H., Eppstein, M.J.. (2014). Estimating Cascading Failure Risk: Comparing Monte Carlo Sampling and Random Chemistry. 2014 IEEE PES General Meeting.

AND

Rezaei, P., Hines, P.D.H.. (2014). Changes in Cascading Failure Risk with Generator Dispatch Method and System Load Level. 2014 IEEE PES Transmission and Distribution Conference and Exposition (T&D).

AND

Material from this dissertation has been submitted for publication to 2016 IEEE PES General Meeting on November, 9, 2015 in the following form:

Rezaei, P., Hines, P.D.H.. Simulating Cascading Failures using AC Power Flow. 2016 IEEE PES General Meeting.

To my wife Saghar,

for her love and support

Acknowledgements

During my doctoral studies, I have been very fortunate to get support form many people, some of whom are acknowledged below.

First of all, I would like to thank my advisor Professor Paul Hines for providing really interesting ideas in my research, and giving invaluable feedback to my work. During my time at UVM, he supported me to attend many fascinating conferences and summer/winter schools that helped considerably in my research and also in shaping my future career. He is an excellent advisor and an amazing friend, always willing to do his best whenever his help is needed. I also like to thank his wife Vanessa for her kindness and support to me and my wife.

Thanks are also due the other members of my dissertation committee: Professors Byung Lee, Maggie Eppstein, Eric Hernandez and Mads Almassalkhi. Thank you to Professor Lee for agreeing to be the committee chair not very long before my defense. I was lucky to collaborate with Professor Eppstein on a chapter of this dissertation and publish a few articles with her, which made me learn a lot. Thank you to Professor Hernandez for answering my reliability questions, and to Professor Almassalkhi for fruitful discussions about his experience on some of the work in this dissertation. Thanks to other Professors at UVM who have been inspiring in teaching and my research. In particular, I want to thank Professor Frolik for co-advising me in a previous project on electric vehicle charging management, for his help in our publication, and supporting my job search. Thanks to Professors Taras Lakoba and Chris Danforth for their very inspirational teaching and continued support during my career applications.

This work was supported in part by the U.S. Department of Energy and the U.S. National Science Foundation. Many thanks to my fellow students at UVM and my friends who have directly or indirectly supported my work. In particular, I want to thank Dr. Goodarz Ghanavati and Professor Eduardo Cotilla-Sanchez, who assisted me in many ways when I

first joined the Energy Systems research group. Thanks also to the UVM IGERT Smart Grid research fellows for being vibrant colleagues and making our office a brighter and happier place. I like to especially thank Curtis Saunders, Mark Wagy, Emily Cody, Cathleen Balantic, Kelsey Linnell, Tom McAndrew, Katie Aho, Dan Fredman, and Christopher Clement (among others), not only for their friendship but also for engaging in intellectual conversations.

Finally, I want to thank my family for supporting me along this work. My parents, Soheila and Mohsen, have always provided their unconditional support in my life, encouraging me to continue higher education although it caused me to be more distant from them. My sister Pegah has been an amazing source of happiness for me. Most importantly, I want to thank my wonderful wife Saghar, without whom I would not be where I am now. She has been an open ear for all my worries, encouraged me substantially during my work, helped me whenever needed, and accompanied me in my career decisions. I love you.

Table of Contents

List of Figures

List of Tables

Chapter 1

Introduction

In August 2003, a transmission line outage in Ohio, combined with a software glitch and some operator errors, triggered a sequence of events that left over 50 million people without electricity in eight US states and one province of Canada [1]. In addition to days of discomfort and chaos, this blackout led to many more emergencies than usual. For example, respiratory emergency medical service calls increased by 189% [2]. Many important lessons were learned from that blackout. For example, reliability measures including vegetation management should have been enforced more strictly for utilities. Despite these lessons, another blackout happened eight years later (September 2011) in Southwest US causing nearly seven million people to lose power. The report for the 2011 blackout identified inadequate situational awareness and planning as causes [3], much like the 2003 blackout. The problem of large blackouts is not unique to North America. Recent blackouts in India (July 2012) and Turkey (March 2015) affected over 600 million and about 70 million people, respectively.

Large blackouts are often caused by cascading failures, which are sequences of interdependent outages initiated by one or more disturbances [4]. The events above are all examples of such large cascading blackouts, illustrating that past efforts have not yet eliminated large blackout problem. In fact, previous data show that large blackouts are much

more common in the US than what would result from an exponentially tailed distribution, such as the Gaussian or the Weibull distributions, and that they have a heavy-tailed distribution similar to the power-law [5, 6]. This behavior could be explained, at least in part, by the fact that power networks are naturally nonlinear dynamical systems with many components that are constantly interacting. Rapid growth of smart grid technology, where more sophisticated control and communication schemes are being used in power systems, adds to the network complexity. This level of complexity enables a new level of flexibility in power system operation, promising to increase reliability, decrease costs, and reduce harmful environmental impacts, but might also contribute to new ways that the system could fail.

The fact that large blackouts continue to happen, often as a result of cascading failures, is also evidence of shortcomings in how power grids are currently operated under stressed conditions. To address these shortcomings, more work is needed to understand and mitigate cascading failure risk. Risk generally combines two factors: the probability of a disturbance to a system and its consequences. When it comes to estimating cascading failure risk, both of these factors give rise to two critical challenges. Firstly, large blackouts are rare. The number of combinations of failures (also known as contingencies in power system analysis) that could lead to a large blackout grows exponentially with the number of elements in the system. Most of these combinations do not lead to a large blackout, but given the right conditions, some of them do. Therefore, traditional methods of reliability analysis, such as Monte-Carlo simulation, will do a poor job in estimating risk for any realistically-sized system, because of slow convergence. Chapter 2 of this dissertation presents a method that can efficiently estimate blackout risk significantly faster than classical Monte-Carlo.

The other challenge for computing blackout risk is estimating the consequences of blackouts. This challenge appears both in estimating the consequences after an initial set of failures in a power system, i.e., the size of the blackout in MW, and also in calculating the

social costs of a blackout given its size. The latter problem is outside the scope of this dissertation. The reader can refer to [7] as an example of such study. The challenge in estimating blackout size arises because many different failure mechanisms are involved in any given cascading blackout. These include, but are not limited to: overloads, contact between vegetation and conductors, voltage instability, transient instability, frequency instability, relay failures and operator errors. Some of these mechanisms can be modeled with some degree of accuracy in small systems, but designing models that accurately capture all of these mechanisms for all possible initiating disturbances is infeasible for realistically sized systems.

Because there are limited data about historical cascading blackouts, and because it is not possible to experiment with cascading failures in real power systems, simulation models are a necessary element of most cascading failure analysis methods. Because many failure processes are likely to contribute to any particular cascade, a trade-off exists between the level of detail in a cascading failure simulator and its practicality. Chapter 3 describes a cascading failure simulator based on ac power flow model (a nonlinear system of algebraic equations to solve power flow). The ac power flow equations, which are generally a good approximation of power system operation, do not have a solution for many configurations of high load and are thus less good at representing extreme cases. The challenge in simulating cascading failures with ac power flow is that extreme cascading failure cases frequently find these solution-less cases, which leads to a phenomenon known as voltage collapse. Chapter 3 explains an effective method to find an amount of load shedding that restores a system to solvability. This method provides a numerically reliable way to simulate voltage collapse during a cascade.

Given that we can assess blackout risk efficiently, the next natural question is how to mitigate it, when it is high. The approaches that could mitigate blackout risk fall roughly into four categories:

1. investing in new transmission capacity,
2. changing the normal operating point using available controls, e.g., generator dispatch,
3. mitigating overloads after contingencies before they trigger cascades, and
4. improving restoration methods.

Generally the first two items are pre-contingency and the last two are post-contingency strategies. Pre-contingency methods involve some change in normal operation of the system to mitigate blackouts. For example, the initial dispatch of a system could be modified in a way to reduce the amount of stress (e.g., overload) to the system after some critical contingencies occurred. Chapter 2 shows how risk estimation can be used to identify critical components in a system and suggests strategies to reduce risk by reducing the outage probabilities of critical transmission lines (item 1), e.g., by more vegetation management, or by changing the initial dispatch of the system (item 2) .

Post-contingency methods take effect after some stress is detected in the system (item 3), or after the blackout (item 4). Restoration methods are outside the scope of this dissertation, but are nevertheless critical to reducing social costs after a blackout has occurred. Chapter 4 focuses on mitigating overloads to reduce the size of blackouts (item 4), in terms of the MW of unserved load. The chapter describes a distributed predictive emergency control method to identify the best local loads to shed and generators to reduce to mitigate stress in a system before a large cascade results. The method can reduce blackout sizes after an initial set of contingencies that would otherwise lead to a large blackout.

The rest of this chapter is organized as follows. Section 1.1 reviews cascading failure simulators described in the literature, and Section 1.2 explains in detail, DCSimSep, a simulator based on the dc power flow model. This model, which was previously developed in our group, is used in this dissertation (Chapter 2) for quickly estimating blackout risk.

1.1 Simulating cascading failures in power systems

As previously mentioned, real cascading failures propagate by many different mechanisms. Simulating every failure and control mechanism in a power system can be impractical for several reasons. Firstly, more detailed simulators need more computing resources and take longer to run. In addition, to produce useful statistical results, a simulator needs to have a similar level of detail in modeling different control and failure processes. For example, a detailed tool that is specialized to model transient stability may give misleading statistical results in studying cascading failures because of its focus on transient stability and insufficient detail about other failure mechanisms.

Finally, more complex models need more input parameters, each of which could potentially be inaccurate. And even after a model is tuned to reproduce the behavior of one particular event, we do not know if it will accurately describe all possible events. In fact, there are many cases where tuning a model to fit one particular sequence will cause it to less accurately capture other types of events. Consider, for example, the August 10, 1996 cascading failure in the Western US. An engineering research team led by Kosterev [8] endeavored to recreate the sequence of events using a detailed dynamic model. Numerous changes to the model's parameters, including automatic generation control (AGC) systems, droop control, and voltage control systems dispersed throughout the interconnection, were needed before the model could even roughly approximate the observed cascading behavior. The behavior of power systems depends on the parameters of millions of devices, each with numerous settings. While not all of these are critical to cascading behavior, many of them are. Knowing which parameters are important to the ultimate outcomes of interest is a critical area of ongoing research [9].

A particularly notable uncertainty is the behavior of loads during extreme events. Since loads depend on the aggregate behavior of many different devices, virtually none of which

can be directly observed by power grid operators, understanding how loads behave during periods of fast dynamics and abnormal voltage swings is an important and difficult aspect of cascading failure modeling. Another source of uncertainty for cascading failure models is the many exogenous, non-power-system influences on cascading behavior. For example, wind speeds and the distances between vegetation and transmission equipment are important factors affecting the amount of time that a transmission line can operate in a heavily loaded state before a fault occurs. Similarly the behavior of grid operators and the energy management software systems that enable situational awareness have been critical factors in many historical cascades, but are notably difficult to capture in simulation models [10]. Finally, one of the key aspects of cascading failure modeling is understanding the set of possible exogenous initiating events. Weather can initiate faults in transmission lines. Generators may fail due to operator errors. Maintenance errors, such as the one that initiated the 2011 blackout in the southwestern US, can cause transmission system outages. Modeling these exogenous disturbances is key to accurately describing cascading failure risk in a power system.

As a result of this complexity, it is impossible for models of cascading to accurately capture all of the possible failure mechanisms (both exogenous and endogenous) that might factor into all potential cascades. However, models that capture a subset of these mechanisms can produce valuable insight, and as these models improve over time this insight will become increasingly valuable.

Existing cascading failure models can, roughly, be divided into three categories. The first are purely topological models that neglect the physics of power flow. There is substantial evidence that such models can be misleading [11], since they typically assume that cascades propagate locally. For example, if component a fails, the next component to fail, after the failure of a, is one that is topologically connected to a. Real cascading failures propagate non-locally (see Fig. 1.1) such that the next component to fail after a fails, may be hundreds

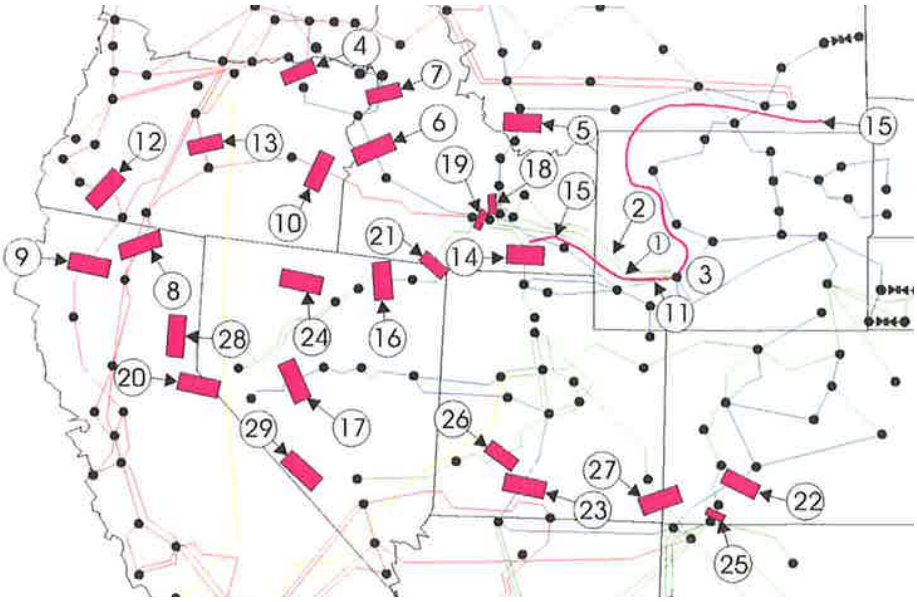

Figure 1.1: An illustration of the event sequence for the Western US blackout on July 2, 1996 (from [12]). The sequence jumps across hundreds of kilometers at several points, such as from ③ - ④ and from ⑦ - ⑧ .

of miles away from a.

The second, and most common, type of model is a quasi-steady-state (QSS) model based on either the dc or ac power flow models. In QSS models, the impacts of component outages are computed using standard steady-state power flow equations. When outages cause overloads elsewhere in the network, those components subsequently outage based on some criteria, which may be deterministic or based on some type of random threshold. There are a number of QSS models developed based on the dc approximations, such as OPA [13], DCSimSep [14], [15], [16], and [17].

QSS models based on the ac power flow equations are described in [18–21]. Models based on dc power flow equations are often useful for testing new approaches to cascading failure risk analysis, since they do not require one to make assumptions about how voltages react during low voltage conditions and do not experience voltage collapse. On the other hand, ac power flow equations are clearly a better approximation of the steady state operation of

actual power grids and are likely to be important for industry-grade analysis tools. One of the key challenges in the design of ac models of cascading is dealing with the non-convergent power flows that result from voltage collapse. Chapter 3 discusses one approach to dealing with this problem and several other challenges associated with the design of an ac model of cascading.

One of the challenges with QSS modeling of cascades is dealing with imbalances between supply and demand that result when a network separates into non-connected islands, when generators shut down, or when load shedding occurs. The conventional power-flow assumption that all of the imbalance is taken up by a "slack" bus clearly is not a particularly good model of a real system's response to large power imbalances. In real systems these imbalances are re-balanced through a hierarchy of system dynamics and feedback control systems including machine inertial responses, droop control (primary frequency response), automatic generation control (secondary response), spinning reserves (tertiary response), and (in extreme cases) under-frequency load shedding schemes or generator over-speed relays. However, accurately capturing these dynamic responses in a steady-state model is not possible, making it necessary to employ heuristics that approximate this behavior. One common approach, described in [22], is to assume that supply and demand imbalances are resolved through equal fractions of generator ramping and load shedding. Another approach, used in both DCSimSep (Section 1.2) and ACSimSep (Chapter 3), is to allow generators to do some up/down ramping in response to imbalances and then trip generators or shed loads if the initial response is insufficient.

In order to avoid these types of heuristics, and to capture a broader range of dynamic phenomena that have frequently contributed to large cascading failures, dynamic models are necessary. There is substantial existing literature on mid-term and long-term dynamic stability modeling [23, 24], but few existing models are explicitly focused on the modeling of the complex dynamics during cascading failure. Reference [9] presents one approach to

the dynamic cascading failure simulation problem and highlights a number of important challenges. For example, [9] shows that the type of load model used can have a dramatic impact on the resulting distribution of blackout sizes.

1.2 DCSimSep: A dc power flow model of cascading

Using a dc power flow model is a useful starting point for cascading failure research, allowing one to gain physical insight that goes beyond what one would get from an abstract model of cascading, while avoiding some of the numerical difficulties associated with non-convergent power flows. The dc power flow equations are a linearized and simplified estimate of the more accurate ac power flow equations. They are mostly used in analyzing market applications [25]. They provide many advantages (such as fast and always existing solution) if they give an acceptable estimate of power flows, for which there is no guarantee. However, some conditions such as higher ratio of X (reactance) to R (resistance) in transmission lines, result in a better estimate.

This section explains one model based on dc power flow, named DCSimSep. It was first used in [11], and then in [14] to find many $n-k$ outages (for $2 \leq k \leq 5$) that cause large blackouts in a large-scale power system (a model of the Polish grid). Fig. 1.2 and the following paragraphs describe how this model works. Note that some of the components from this model are also used in developing ACSimsSep (Chapter 3).

Step 1: ($t = 0$) Compute power flows within an initially balanced (with respect to generation and load) in a power system.

Step 2: Implement an initiating contingency (typically one or more branch outages) at $t = 1$ sec.

Step 3: Find the number of islands (sub-grids), and the set of buses/branches in each

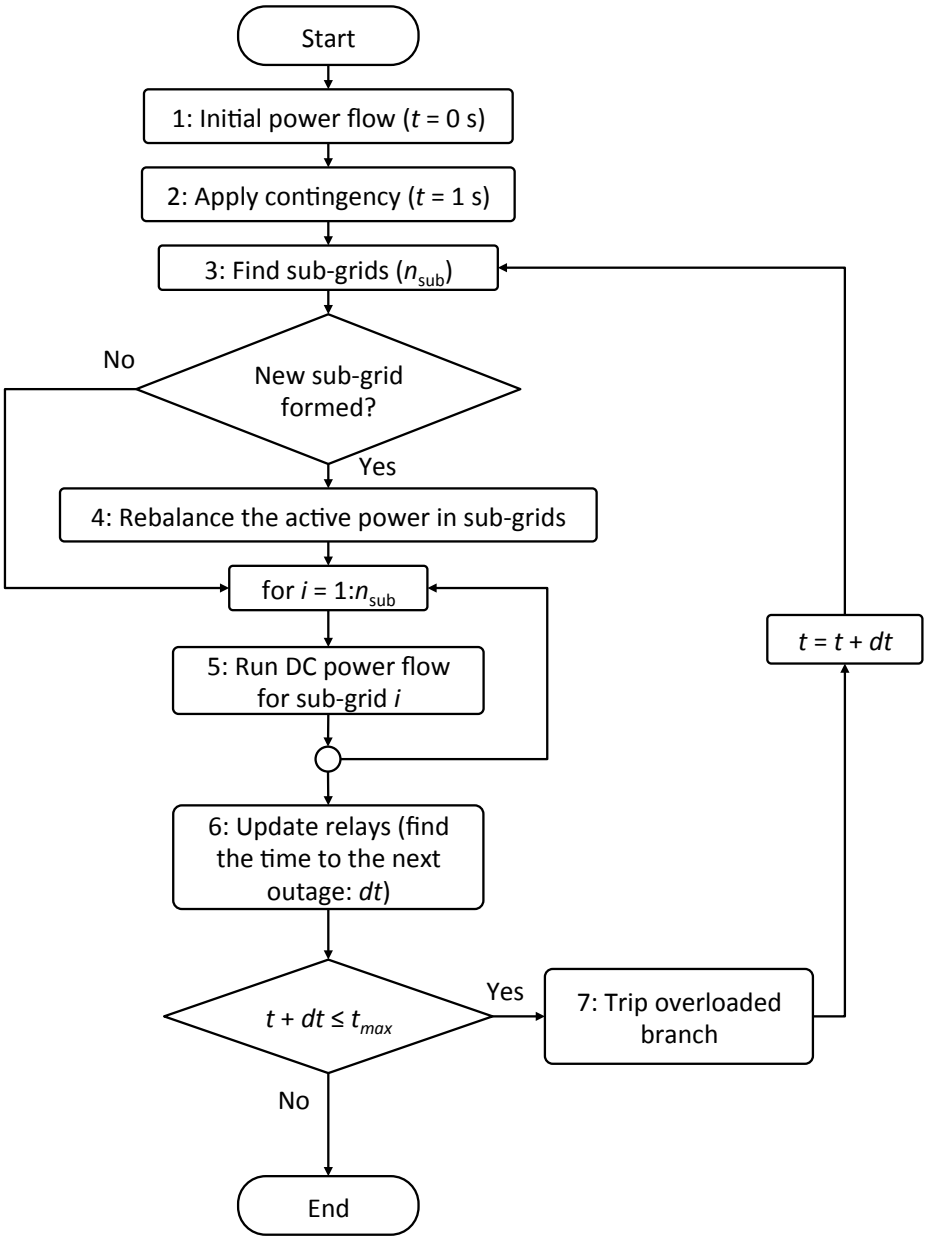

*Figure 1.2: Algorithm flowchart for DCSimSep: A **DC** power flow **Sim**ulator of power system **Sep**aration*

island, since the contingency may have caused the system to separate into non-connected islands.

Step 4: If the number of islands has changed since the previous iteration, re-balance

generation and load in each island. A standard power flow calculation can eliminate imbalance using the "slack" bus, but this is an inaccurate representation of how real power systems respond to large imbalances. Therefore, in this step, generators within the unbalanced islands are first allowed to ramp up/down for one minute, given their ramp rate limits. The assumption here is that the imbalance can be tolerated for up to one minute, during which various generation controls, such as droop control and AGC, within the island compensate for the imbalance. If this amount of re-balancing is insufficient, load shedding and generator tripping, which would be implemented by under frequency or over-speed relays, are implemented to eliminate the remaining imbalance. A surplus of generation is compensated by tripping generators starting from the smallest until the surplus is eliminated. A deficit in generation is balanced by shedding all loads in the island by the same fraction $\sum P_{G,i}/\sum P_{D,i}$, where $P_{G,i}$ and $P_{D,i}$ denote, respectively, generations and loads in that island. Note that step 4 is skipped if the number of islands does not increase with the previous line outage.

Step 5: Compute power flows within each island using the dc approximations. Because the islands are balanced, power flow results are independent of the reference bus chosen.

Step 6: If overloads remain in the network, find the amount of time (dt) until the next transmission line outage will occur. DCSimSep emulates a time-delayed overcurrent relay to trip transmission lines. Each line has an overload state variable o_j that increases over time if the line is overloaded. The change in o_j over a particular time period Δt at time t is computed as follows:

$$\Delta o_j(t, \Delta t) = \begin{cases} \int_t^{t+\Delta t} (f_j(t) - \overline{f_j}) dt & \text{if } f_j(t) > \overline{f_j} \\ 0 & \text{otherwise} \end{cases} \tag{1.1}$$

where $\Delta o_j(t, \Delta t)$ is the change in o_j from t to $t + \Delta t$, $f_j(t)$ represents flow of line j at time t, and $\overline{f_j}$ is line j's flow limit. Fig. 1.3 shows the inverse time overcurrent characteristic

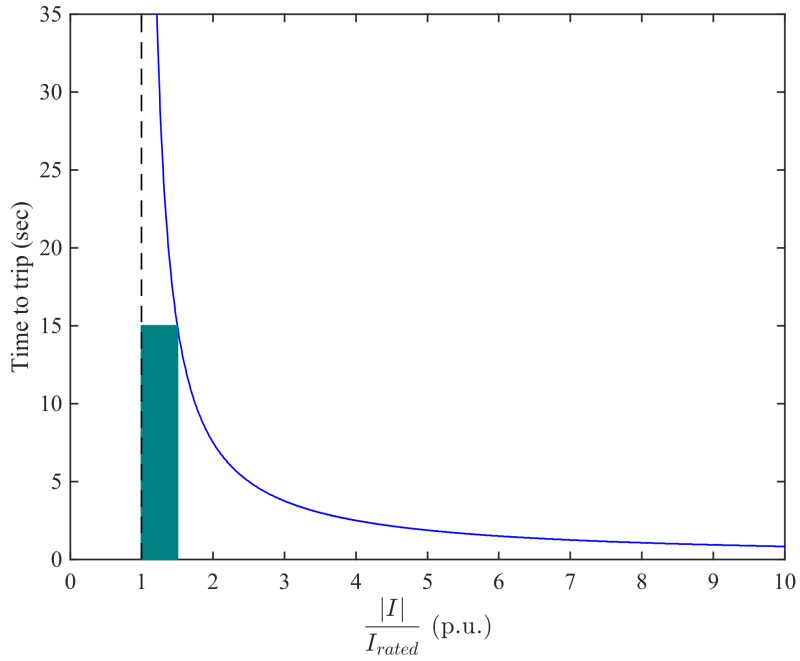

Figure 1.3: Inverse time overcurrent relay characteristic. The area of cyan rectangle is equal to the limit on o_j for all lines.

that is implemented here. When a line current changes over time, as soon as the integral in (1.1) is equal to to the area of cyan rectangle in Fig. 1.3, the line trips.

In our simulations, we use the long-term emergency (LTE) for the limit $\overline{f_j}$, which is higher than the normal rating but lower than the short-term emergency (STE) rating. This approach intends to roughly capture a variety of mechanisms by which overloaded lines might trip, including the overheating of conductors and sagging into vegetation and the reaction of Zone 2 or Zone 3 distance relays. The limit on o_j is set such that a branch with a 50% overload (a flow of 1.5 times the LTE rating) will trip in 15 seconds. Based on (1.1) a larger overload will cause a line to trip more quickly, and more moderate overload will lead to a longer time before tripping.

Step 7: If dt is short enough, such that $t + dt$ is smaller than the maximum allowed simulation time (t_{max}), trip the overloaded branch, move time to $t + dt$ and go to step 3.

t_{max} represents the time duration that, for some reason, operators are not intervening in the power system operation, e.g., because they are not aware of the situation due to a malfunction in the alarm system. This value is typically set to 15 to 30 minutes in our simulations.

DCSimSep provides us with an estimate of the blackout size caused by any set of initiating contingencies in a power system. Next, we need an efficient method to estimate cascading failure risk in reasonable time. Chapter 2 explains such a method.

Chapter 2

Estimating Cascading Failure Risk with Random Chemistry [1]

Abstract

The potential for cascading failure in power systems adds substantially to overall reliability risk. Monte Carlo sampling can be used with a power system model to estimate this impact, but doing so is computationally expensive. This chapter presents a new approach to estimating the risk of large cascading blackouts triggered by multiple contingencies. The method uses a search algorithm (Random Chemistry) to identify blackout-causing contingencies, and then combines the results with outage probabilities to estimate overall risk. Comparing this approach with Monte Carlo sampling for two test cases (the IEEE RTS-96 and a 2383 bus model of the Polish system) illustrates that the new approach is at least two orders of magnitude faster than Monte Carlo, without introducing measurable bias. Moreover, the approach enables one to compute the sensitivity of overall blackout risk to individual component-failure probabilities in the initiating contingency, allowing one to quickly identify low-cost strategies for reducing risk. By computing the sensitivity of

[1] [26] Pooya Rezaei, Paul D.H. Hines, Margaret J. Eppstein, "Estimating Cascading Failure Risk with Random Chemistry," *IEEE Transactions on Power Systems*, vol. 30, no. 5, pp. 2726–2735, September 2015.

risk to individual initial outage probabilities for the Polish system, we found that reducing three line-outage probabilities by 50% would reduce cascading failure risk by 33%. Finally, we used the method to estimate changes in risk as a function of load. Surprisingly, this calculation illustrates that risk can sometimes decrease as load increases.

2.1 Introduction

Large blackouts are low-probability, high-impact events; i.e., they happen infrequently, but when they do happen, they can lead to catastrophic social and economic effects, such as the North American blackouts of Aug. 2003 [1] and Sept. 2011 [3]. For this reason cascading failure risk assessment is increasingly required by reliability standards (e.g., [27]) and is a focus of IEEE Power and Energy Society activities [4].

A primary goal of reliability risk analysis methods is to produce statistical reliability measures, such as Expected Energy Not Supplied (EENS), that allow one to compare different versions of a particular system, or to evaluate changes in a system over time. The science and practice of Monte Carlo (MC) methods for power system reliability studies are well established [28], particularly for evaluating generation and transmission adequacy. However, for some types of problems, Monte Carlo methods can require many samples to produce high-confidence statistical results, causing the approach to be computationally prohibitive or even infeasible in some cases [29]. Some studies reduce the computational effort due to sampling by: 1) variance reduction techniques [30], 2) state-space pruning [31], 3) parallel and distributed computation [29], 4) pseudo-sequential simulation [32], or 5) Artificial Neural Networks [33]. Generally, the results provide small improvements (typically less than a factor of 10 speedup). To our knowledge, [33] describes an approach with the most substantial speedup: a factor of 45 over standard Monte Carlo.

Methods for applying sampling techniques to cascading failure risk estimation are less well established [4], for several reasons. First, the simulation of cascading failures remains

a difficult problem, making it difficult to estimate the eventual impact (typically measured in the amount of lost load) of a cascade-triggering disturbance. As a result, standard power system reliability models tend to capture only one or two outage generations, ignoring the impact of subsequent outages [21]. Second, even if cascading sizes can be accurately estimated, those sizes can be at any scale: from a few MW to tens of GW. The nature of cascading gives rise to the well-documented power-law in blackout sizes [13,34]. This implies that the occurrence probabilities of particular combinations of outages (and operator errors) that could trigger large cascading failures are very low, making it necessary to observe several representative events to obtain an accurate risk estimate [35]. Third, the size of the search space of all possible $n-k$ contingencies that might trigger a cascade, where n is the number of components that might fail and k is the number that did fail, is enormous and grows exponentially with n and k. This further increases the need for a large number of simulations.

Despite these challenges, there are a number of studies focused on the modeling of cascading failures (e.g., [15–17, 21]). A smaller number of papers have adapted sampling techniques to the problem of cascading failure risk estimation [21,36]. In doing so, some have used variance reduction techniques to reduce the computational effort [19,37–39], which led to a speedup factor of 5-10 in [37], and 2-4 in [19]. Non-sampling approaches, such as branching process models [40, 41], can provide efficient estimates of risk, but abstract away some details, such as the ability to compute the relative contributions of particular outages to overall risk.

A prior work in our group adapted a search algorithm, known as Random Chemistry (RC), to the problem of finding large collections of $n-k$ contingencies that lead to cascading failure [14]. However, this initial work did not explain how the approach could be used for risk estimation. In this chapter, we derive a method to use the Random Chemistry algorithm to estimate blackout risk due to cascading failure, given a few simplifying assumptions, and

compare the computational efficiency of our approach with that of Monte Carlo sampling. This chapter builds on preliminary results reported in [42] and [43], extending our method to compute the relative impacts of individual components on overall risk and showing how increasing load and generator dispatch method impact risk.

The remainder of the chapter is organized as follows. Section 2.2 defines cascading failure risk and introduces two general approaches to estimate risk. Section 2.3 describes our method for using Random Chemistry for cascading failure risk estimation, and section 2.4 presents simulation results. Finally, section 2.5 provides our conclusions.

2.2 Two approaches to risk estimation

A standard measure of risk due to a random disturbance is the product of event probability and its severity (or cost) [4]. If $S(\mathcal{C}, x)$ is a measure of the severity of the events proceeding from an arbitrary disturbance $\mathcal{C}$ to a system at a particular state x, then the risk due to $\mathcal{C}$ is:

$$R(\mathcal{C}, x) = \Pr(\mathcal{C})S(\mathcal{C}, x) \tag{2.1}$$

If we denote the set of all possible disturbances by Ω, then the system risk is:

$$R(x) = \sum_{\forall c \in \Omega} R(c, x) = \sum_{\forall c \in \Omega} \Pr(c)S(c, x) \tag{2.2}$$

In this chapter, $\mathcal{C}$ denotes a random disturbance, while c (the lower case) denotes an individual disturbance. Therefore, one can think of $S(\mathcal{C}, x)$ as a random variable that maps a random event $\mathcal{C}$ to its severity, and interpret $R(x)$ as $E[S(\mathcal{C}, x)]$, i.e., the expected value of $S(\mathcal{C}, x)$.

Since it may not be feasible to compute the severity of all disturbances for a system, one approach for estimating system risk is to estimate $R(x)$ from a smaller sample of all

possible disturbances. One option is Monte Carlo sampling, in which one draws randomly from Ω based on the probability function $\Pr(\mathcal{C})$. The average severity then converges to the true risk, given a sufficiently large set of samples:

$$\hat{R}_{MC}(x) = \frac{1}{|\Omega_a|} \sum_{c \in \Omega_a} S(c, x) \tag{2.3}$$

where $\hat{R}$ is an estimated value of R in this and subsequent notations, Ω_a is a set that results from sampling randomly from Ω, and $|\Omega_a|$ is the number of elements in Ω_a. Note that Ω_a may include duplicates and the empty set, depending on the sampling approach.

A key problem with this approach is that there are many events for which $S(c, x) = 0$, which means that Monte Carlo will spend a lot of time sampling from events that have no impact on $R(x)$. Alternatively, if one could sample exclusively from the subspace Ω_B such that $S(c, x) > 0, \forall c \in \Omega_B$, and we somehow knew the size of this subset, then risk could be more efficiently estimated by computing:

$$\hat{R}(x) = \frac{|\Omega_B|}{|\Omega_b|} \sum_{c \in \Omega_b} \Pr(c) S(c, x) \tag{2.4}$$

where Ω_b is a representative subset sampled from Ω_B , i.e., $\Omega_b \subseteq \Omega_B$. Clearly, (2.4) converges to (2.2) as $\Omega_b \to \Omega_B$. In order to avoid a biased outcome when $|\Omega_b| \ll |\Omega_B|$, Ω_b needs to be an unbiased sample, such that it provides a representative sample of Ω_B across a range of event sizes and probabilities. The idea in (2.4) is somewhat similar to importance sampling [44].

In this chapter, we develop a method for estimating cascading blackout risk in power systems based on (2.4), and compare the convergence speed with Monte Carlo sampling in (2.3).

2.3 Method

The specific focus of this chapter is estimating risk due to cascading failures triggered by exogenously-caused branch (transmission line or transformer) outage contingencies. In this case, each contingency $c \in \Omega$ is a subset of the branches in the grid ($c \subseteq \{1, ..., n\}$), and Ω is the set of all possible branch outage combinations. While there are other types of contingencies that might trigger cascades, branch outages provide a useful starting point. Adapting the method to incorporate other type of contingencies (e.g., generator outages) is trivial. In this chapter, we assume that the exogenously-caused branch outages are statistically independent, such that for two single contingencies c_i and c_j, $\Pr(c_i \cap c_j) = \Pr(c_i) \Pr(c_j)$. While there are methods in the literature for modeling common mode outages (e.g., [45]) and other types of correlations (e.g., [18]), the risk from these correlations is not captured in the results presented here. Verifying the efficiency of the Random Chemistry risk estimation method for the case of correlated outages and other types of contingencies remains for future work.

Let $S(c, x)$ represent the output of a simulator that gives blackout sizes in MW, resulting from any initiating contingency c applied to the system with state x such that $0 \leq S(c, x) \leq S_0$, where S_0 is the total load in the system. In general, Monte Carlo sampling can quickly estimate $R(x)$ for blackouts of small sizes. However, because of the heavy-tailed statistics of cascading failures, estimating the risk due to larger blackouts is more difficult. Here, we focus on computing the risk resulting from blackouts larger than some fraction $0 < \alpha < 1$ of S_0. Specifically, we study the risk of blackouts 5% and larger, i.e., for $S(\mathcal{C}, x) \geq 0.05 S_0$. In order to do so, we replace $S(\mathcal{C}, x)$ in (2.3) with $S_\alpha(\mathcal{C}, x)$, where:

$$S_\alpha(\mathcal{C}, x) = \begin{cases} S(\mathcal{C}, x) & S(\mathcal{C}, x) \geq \alpha S_0 \\ 0 & \text{otherwise} \end{cases} \tag{2.5}$$

2.3.1 Risk from minimal contingencies

A unique aspect of the Random Chemistry algorithm (see Appendix 2.A and [14]) is that it is designed to find "minimal" blackout-causing contingencies. A minimal blackout-causing contingency is a set of outages that result in a large blackout (in this chapter we define large as $\geq 5\%$), but would not result in a large blackout if any one of the outages in the multiple-contingency had not occurred. For brevity we refer to disturbances of this sort as malignancies. Formally, a set of outages d is a malignancy if $S(d,x) \geq 0.05S_0$ and $\nexists c' \in \Omega : c' \subset d \wedge S(c',x) \geq 0.05S_0$. In order to use the data from Random Chemistry, we need to be able to estimate the risk from all $n-k$ contingencies, including the non-minimal ones, from data about malignancies. To do so, we make the following assumption:

Assumption 1: *Given a malignancy d, which triggers a blackout of size $S(d,x)$, the blackout sizes triggered by all supersets of d can be estimated by the size of blackout triggered by d, i.e., $\forall c'' \supset d \rightarrow S(c'',x) = S(d,x)$.*

Clearly, Assumption 1 does not hold for every case. There are some superset contingencies that trigger smaller blackouts and some supersets that cause larger blackouts. In Appendix 2.B, we evaluate Assumption 1, comparing the actual blackout sizes of all $n-3$ supersets with the values that are estimated by minimal $n-2$ subsets for the Polish system (described in section 2.4). We find that Assumption 1 causes the $n-3$ risk estimate to be 2.5% higher than the actual value for $n-3$ risk. Given that the $n-3$ risk is 24.0% of the total risk, the total impact of Assumption 1 on the overall risk estimate is to increase it by only 0.6%.

As one adds more components to a minimal malignancy, making larger supersets, the blackout size difference between the two events becomes larger, but because the probability of high order events ($n-k$ for $k \geq 4$) is orders of magnitude lower than probability of its malignancy subset, the overall impact becomes much smaller, and at some point negligible for high order events.

This section shows, by a small example, how to use Assumption 1 to estimate risk efficiently using the minimal contingency data that Random Chemistry provides.

Let us assume that in a small system with 5 transmission lines, Random Chemistry has found an $n-3$ malignancy, $d_1 = \{1,2,3\}$. (By definition, this means that none of the $n-2$ subset contingencies, $c'_1 = \{1,2\}$, $c'_2 = \{1,3\}$ and $c'_3 = \{2,3\}$, cause a 5% or larger blackout.) Using our previous assumption that line failures are independent, the exact risk associated with d_1 and all its supersets is:

$$\begin{aligned} R(\hat{d_1}, x) =& S(d_1, x)p_1p_2p_3(1-p_4)(1-p_5)+ \\ & S(c''_1, x)p_1p_2p_3p_4(1-p_5)+ \\ & S(c''_2, x)p_1p_2p_3(1-p_4)p_5+ \\ & S(c''_3, x)p_1p_2p_3p_4p_5 \end{aligned} \tag{2.6}$$

where $\hat{d_1}$ denotes d_1 together with all its supersets: $c''_1 = \{1,2,3,4\}$, $c''_2 = \{1,2,3,5\}$, $c''_3 = \{1,2,3,4,5\}$, and p_i is the line-failure probability for line i. Given Assumption 1, $S(d_1, x) = S(c''_i, x), \forall i \in \{1,2,3\}$, which means that:

$$R(\hat{d_1}, x) = S(d_1, x)p_1p_2p_3[(1-p_4)(1-p_5) + p_4(1-p_5) + (1-p_4)p_5 + p_4p_5] \tag{2.7}$$

Expanding the term in the bracket shows that it equals 1, which means that:

$$R(\hat{d_1}, x) = S(d_1, x)p_1p_2p_3 = S(d_1, x)\Pr(\hat{d_1}) \tag{2.8}$$

where $\Pr(\hat{d_1})$ is the probability of the malignancy d_1 and all of its supersets, i.e., any event that includes at least the branches in d_1. A similar formulation holds for supersets of any malignancy. Therefore, Assumption 1 enables us to estimate risk of a malignancy and its supersets solely using the information provided by the malignancy itself. In general, for

each malignancy d, we have:

$$R(\hat{d}, x) = S(d, x) \Pr(\hat{d}) = S(d, x) \left(\prod_{i \in d} p_i \right) \tag{2.9}$$

2.3.2 General Random Chemistry risk estimation

Our method separately estimates the risk due to $n-2$ and $n-3$ malignancies. We use the symbol $\Omega_{m,k} \subset \Omega$ to be the set of all $n-k$ malignancies. After i runs, Random Chemistry will have found a certain number of events from each $\Omega_{m,k}$ set. Let i_k be the number of times that Random Chemistry has found a not-necessarily-unique member of $\Omega_{m,k}$ and $\Omega_{RC,k}$ be the set of unique members found. By tracking the rate at which unique members of $\Omega_{m,k}$ are found, if i_k is sufficiently large, we can estimate the size of $\Omega_{m,k}$ (see section 2.3.3). Let $\hat{m_k}$ be this estimate. Given this notation, and the derivation in (2.8), we can simultaneously capture the $n-k$ risk from a set of malignancies and all of their supersets based on (2.4) and (2.9), as follows:

$$\hat{R}_{RC,k}(x) = \frac{\hat{m_k}}{|\Omega_{RC,k}|} \sum_{d \in \Omega_{RC,k}} S(d, x) \left(\prod_{i \in d} p_i \right) \tag{2.10}$$

where $\hat{R}_{RC,k}(x)$ is the estimated $n-k$ blackout risk by Random Chemistry. The results in section 2.4 indicate that the sum of these values over k gives a reasonable estimate of total blackout risk:

$$\hat{R}_{RC}(x) = \sum_{k=2}^{k_{\max}} \hat{R}_{RC,k}(x) \tag{2.11}$$

We have set $k_{\max} = 5$ while running Random Chemistry previously in [14], since larger multiple contingencies are highly improbable, and (at least for the case of uncorrelated outages) have a minuscule contribution to the total risk. However, the size of the $n-5$ and $n-4$ sets are so large that for real-world systems, it is not computationally practical

to estimate $\hat{m}_5$ and $\hat{m}_4$. Thus we generally use $k_{\max} = 3$ for risk calculations. Since this captures the risk from an increasingly large collection of $n - \{2, 3\}$ malignancies and *all of their supersets*, the results appear to be highly representative of the true system risk (see section 2.4).

Note that there is a caveat in considering the malignancy supersets as in (2.10). Every contingency set causing a large blackout contains a malignancy, but this malignancy is not necessarily unique. The contingencies that contain more than one unique malignancy are considered more than once in (2.10). For example, if {1,2} and {1,3} were both malignancies in a system, the superset {1,2,3} would be taken into account two times in (2.10); once in $S(\{1, 2\}, x)p_1p_2$ and once in $S(\{1, 3\}, x)p_1p_3$. However, the number of these kinds of supersets is normally much lower than the total number of supersets of any order, so the overall error that they cause is negligible. In this chapter, we are mainly studying the $n-2$ and $n-3$ risk, so we counted the exact number of $n-3$ supersets that have been counted more than once in the Polish system. Our inspection indicated that out of the total of 1,562,760 $n-3$ supersets of $n-2$ malignancies, 21,771 supersets (1.4%) included more than one malignancy subset, and thus were counted more than once. Note that the exact number of malignancies that will be counted more than once depends on the particular system. It is also noteworthy that each of the higher order supersets may include more malignancies than each of the lower order ones, however, as mentioned before, the higher order contingencies have orders of magnitude lower probabilities and thus have an infinitesimal impact on the overall risk.

It is important to note that we find, in section 2.4, that Assumption 1 and the above caveat do not measurably change the risk estimation results relative to the Monte Carlo estimate, which computes risk based on the exact probability and blackout sizes of all contingencies.

2.3.3 Estimating the Size of Each $n-k$ Collection

Initially, Random Chemistry primarily finds malignancies that are unique (not found previously). However, as the number of identified malignancies increases, the algorithm finds duplicates more frequently. By measuring the rate at which the algorithm finds new unique contingencies of a given size k, one can estimate the total number of minimal dangerous $n-k$ contingencies that cause blackouts. There are a variety of ways to estimate the set-size $|\Omega_{m,k}|$ as Random Chemistry progresses, such that: $\lim_{i_k \to \infty} \hat{m}_k(i_k) = |\Omega_{m,k}|$. In [14], we suggested an approach based on measuring the rate at which the algorithm is finding new malignancies. In this chapter, we use another approach based on the number of unique malignancies found vs. the number of Random Chemistry runs. To illustrate, consider a jar of N balls numbered $1, ..., N$. If balls are removed from the jar one at a time with the same probability (and then replaced), one can mathematically show (see Appendix 2.C) that the expected number of unique balls drawn after i draws (N_i) follows:

$$N_i = N(1 - e^{ri}) \tag{2.12}$$

where $r = \ln\left(1 - \frac{1}{N}\right)$. Based on this idea, we suggest an alternative exponential model, which was empirically found to be more accurate for our application. We found that the number of unique malignancies found by Random Chemistry is best represented by the Cumulative Distribution Function (CDF) of the exponential Weibull distribution. Specifically, the number of unique $n-k$ malignancies in the set $\Omega_{RC,k}$ after i_k runs follows:

$$|\Omega_{RC,k}(i_k)| \sim \hat{m_k}\left(1 - e^{-(\frac{i_k}{\lambda})^{\mu}}\right)^{\nu} \tag{2.13}$$

The parameters λ, μ, ν and $\hat{m}_k$ (the estimate of interest) can be found by nonlinear least-squares fittings to a sequence of data for i_k and $|\Omega_{RC,k}(i_k)|$. Fig. 2.1 shows the results of this method, where the the sizes of $n-2$ and $n-3$ malignancy sets are estimated for the

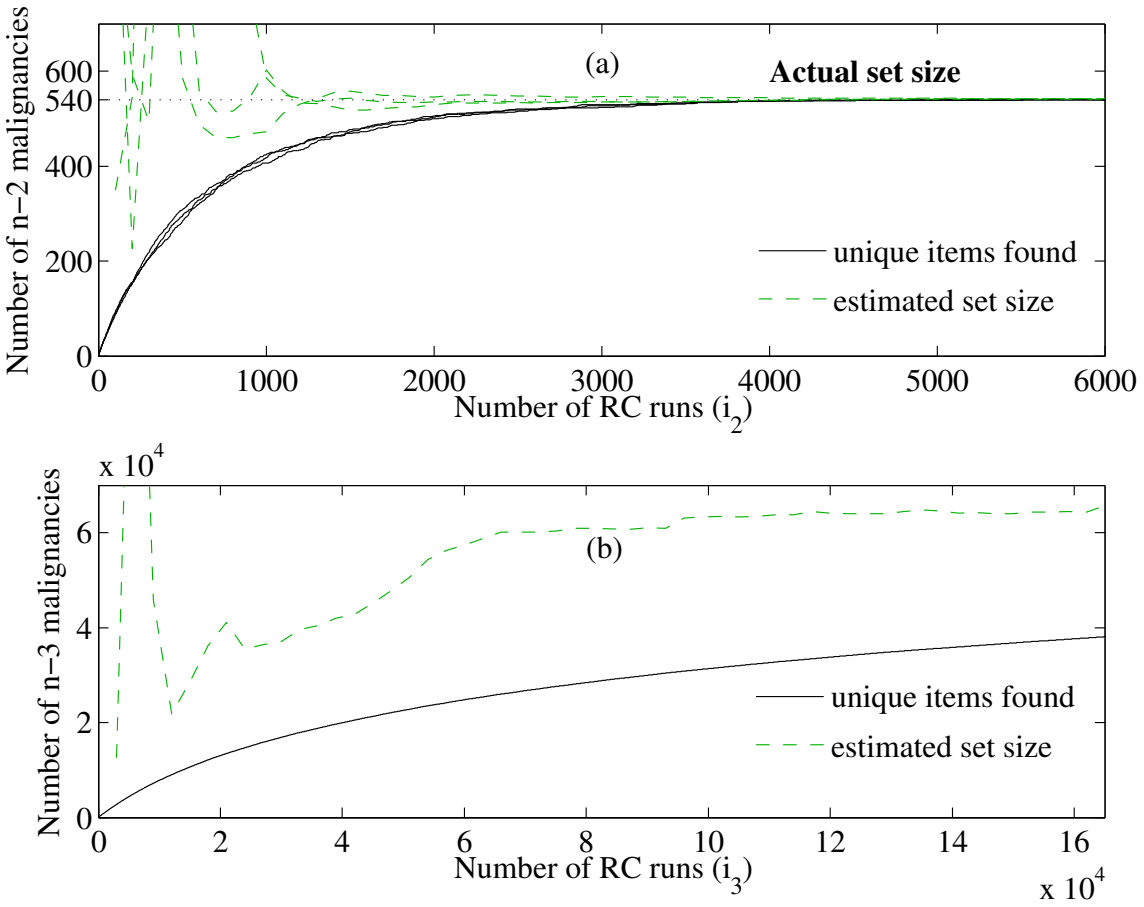

Figure 2.1: The number of unique (a) $n-2$, and (b) $n-3$ malignancies found ($\Omega_{RC,k}$,solid line) and the estimate of the set size ($\hat{m}_k$, dashed line) vs. the number of Random Chemistry runs that led to an $n-2$ (i_2) and $n-3$ (i_3) malignancy, respectively, in the Polish system.

Polish system. The results shown for $n-2$ are for three separate runs of Random Chemistry searching for malignancies in the Polish system (Fig. 2.1a). All three estimates converged to $\hat{m}_k = 540$, which is the true number of $n-2$ malignancies, as verified by exhaustive search. Fig. 2.1b shows that the estimate of $\hat{m}_3$ is converging to about 6.4×10^4.

2.3.4 Sensitivity of risk to component-failure probability

As previously suggested, it is possible to use the Random Chemistry risk estimation approach in (2.10) to find the sensitivity of the overall risk to individual component-failure

probability in the initiating contingency. To do so, we compute the partial derivative of $\hat{R}_{RC,k}(x)$ with respect to each branch failure probability p_i and sum the result over $k \in \{2, 3\}$ for all branches, as follows:

$$\frac{\partial \hat{R}_{RC,k}(x)}{\partial p_i} = \frac{\hat{m}_k}{|\Omega_{RC,k}|} \sum_{d \in \Omega_{RC,k}} S(d, x) \left(\prod_{\substack{j \in d \\ j \neq i}} p_j \right) \tag{2.14}$$

$$\frac{\partial \hat{R}_{RC}(x)}{\partial p_i} = \sum_{k=2}^{k_{\max}} \frac{\partial \hat{R}_{RC,k}(x)}{\partial p_i} \tag{2.15}$$

This type of sensitivity analysis is particularly useful in finding critical components in a transmission system (see section 2.4.3). Note that (2.15) provides the sensitivity of risk to individual outage probability in the initiating events, and to keep this chapter focused, we do not study the failure probabilities when a cascade propagates. In future work, we will identify the lines that fail frequently during the course of cascades, and study the impact on risk of upgrading these lines.

2.4 Results

We used two test systems to evaluate the proposed risk estimation method. The first is the 73-bus RTS-96, which has 120 branches and 8550 MW of total load [45]. The second test system is a model of the 2004 winter peak Polish power system, which is available with MATPOWER [46]. This test system has 2896 branches (transmission lines and transformers), 2383 buses, and 24.6 GW of total load. For the Polish case, some of the transmission lines were overloaded in the original system, so we increased line flow limits to be the larger of the existing limit and 1.05 times the pre-contingency line flows for each line, after increasing all loads by 10%. We prepared the pre-contingency test cases for both systems using a preventive security-constrained dc optimal power flow (SCDCOPF) to make both

cases $n-1$ secure with respect to branch outages (see Appendix 2.D). The $n-1$ security constraints in the SCDCOPF model ensure that all flows remain less than or equal to the long-term emergency (LTE) rating after a single branch outage. The LTE rating is assumed to be 110% of the normal flow limit for all lines. The generation cost data, which is needed for the OPF, is not readily available for RTS-96. In this chapter, we took the cost data from [47] based on the generation types in [45].

In both networks, we computed line failure probabilities from transmission line failure rates (λ, outages/year), and assumed that each failure lasts for 1 hour on average (that the mean time to repair is 1 hour). Thus, the probability of line i being in a non-working state during a particular sample is $p_i = \lambda_i/8760$, where 8760 is the number of hours in a year. Note that this approximation is valid only for the case where $\lambda_i/8760 \ll 1$, which is true, since all of the λ in the test systems are approximately 1. As the failure rate data were not available for the Polish system, we randomly assigned failure rates to transmission lines, such that the mean and variance of λ's were equal to those in the RTS-96. The data for both systems are available online [48, 49].

2.4.1 Simulator

To test our method, we used an updated version of the cascading failure simulator used in [14]. In this simulator (known as DCSIMSEP) line flows are computed using a dc power flow calculation. When outages result in long-term emergency (LTE) rating violations (assumed to be 110% of the normal line flow limit), transmission lines trip in an amount of time that is proportional to the magnitude of the overload, such that more extreme overloads result in faster outages. The time delay is set such that if the line flow is 50% above the normal limit (that is the long-term emergency rating, LTE), the line will trip in 15 seconds. When line outages result in the separation of a network into multiple connected components (islands), a combination of fast generator ramping, load shedding and generator

tripping are used to restore a balance between supply and demand in each island. After each simulation, DCSIMSEP reports the number of line outages and the amount of load shedding that occurred. Illustrative video and source code for the simulator are available at [50].

DCSIMSEP does not describe several known mechanisms of cascading failure, such as voltage collapse, dynamic instability or hidden failures in protection systems. However, the risk analysis process proposed here can be used in combination with any simulator that reports the blackout size, given an initiating contingency. Future work will test the impact of these additional mechanisms on the efficiency of the proposed approach.

2.4.2 Comparing Random Chemistry approach to Monte Carlo

We applied the proposed method to our two test cases, and estimated large blackout risk as a function of total computational effort. These results were compared to results from a standard Monte Carlo simulation. The number of calls to DCSIMSEP is used as our measure of computational effort, because cascading failure simulation takes up the vast majority of risk estimation run-time. Actual run-time is not used explicitly since it depends on many factors, including the extent to which code is optimized. Each cascading failure simulation (by a call to DCSIMSEP) in the risk estimation process takes 0.3 to 0.5 seconds on average for the Polish system[2], depending on the number of subsequent cascades. In our Monte Carlo implementation, a contingency is simulated only if the number of elements in the sampled contingency is 2 or larger, since the system was initially $n-1$ secure. While each Monte Carlo run needs either zero or one simulation, each successful Random Chemistry run requires approximately 47 simulations (when averaged over both successful and unsuccessful runs) on the Polish system.

Figs. 2.2a and 2.2b show the Monte Carlo and Random Chemistry risk convergence

[2]On a 2.66 GHz Intel Core i7 MacBook Pro with 8 GB of memory

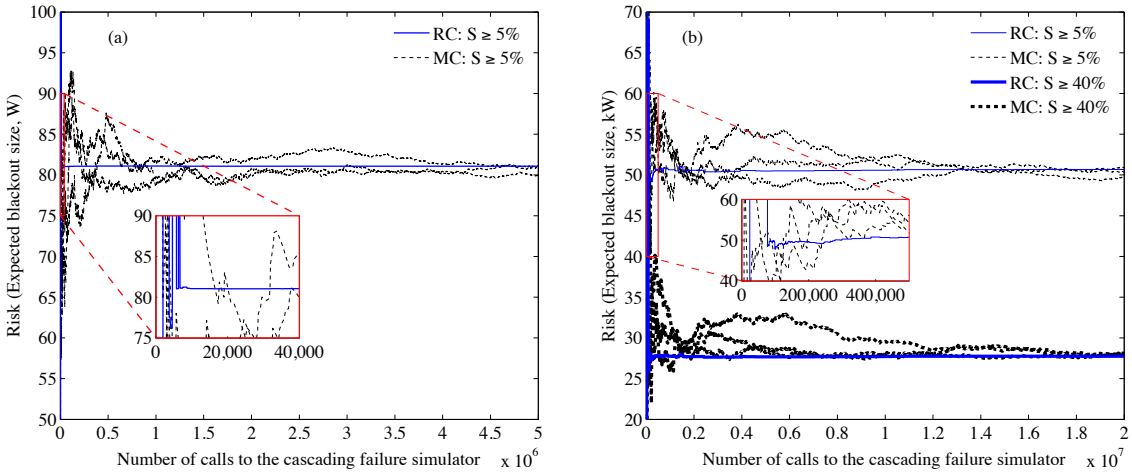

Figure 2.2: Cascading failure risk estimates using the Random Chemistry and Monte Carlo methods for the (a) RTS-96 and (b) Polish system, where S is the blackout size. For each test case, three representative Monte Carlo runs and one Random Chemistry run (since runs for the latter are very consistent) are shown.

for the RTS-96 and the Polish systems, respectively. More specifically, Fig. 2.2a shows the convergence of $E[S_{0.05}(\mathcal{C}, x)]$ for the RTS-96, while Fig. 2.2b shows the convergence of $E[S_{0.05}(\mathcal{C}, x)]$ and $E[S_{0.4}(\mathcal{C}, x)]$ for the Polish system. In the case of RTS-96, the largest blackout caused by $n-2$ and $n-3$ malignancies was less than 20% of total load, therefore we only explored $E[S_{0.05}(\mathcal{C}, x)]$.

Fig. 2.2 shows that the Random Chemistry approach is more than two orders of magnitude faster than Monte Carlo for both test systems. We also observe that Monte Carlo and Random Chemistry are converging to similar values, providing evidence that Assumption 1 does not measurably bias the results.

In addition, Table 2.1 compares the convergence numerically for $S \geq 5\%$ in the Polish system. We computed the mean, variance and 95% confidence intervals (the range between 2.5^{th} and 97.5^{th} percentiles) for both Random Chemistry and Monte Carlo by bootstrapping, where random samples were taken with replacement from the original data. Results are for 1000 resampling trials, where for each trial, the number of samples were chosen for both Random Chemistry and Monte Carlo such that they required the same number of calls to

the cascading failure simulator.

Table 2.1: Comparison of Monte Carlo (MC) and Random Chemistry (RC) risk (in kW) after 10^6 *and* 2×10^7 *calls to the simulator for 1000 bootstrapping trials*

	After 10^6 calls		After 2×10^7 calls	
	MC	RC	MC	RC
Mean	53.03	50.25	50.32	50.48
Variance	21.87	0.007	0.95	0.000045
95% Confidence Interval	44.54-62.84	50.07-50.36	48.34-52.29	50.46-50.49

Table 2.1 shows that after 10^6 calls to the simulator, the confidence interval for Monte Carlo is much wider than for Random Chemistry. Note that the very minor drift in the Random Chemistry confidence interval from 10^6 to 2×10^7 calls to the simulator is due to the improved estimate of $\hat{m_3}$ (Fig. 2.1b).

2.4.3 Investigating the components of large blackout risk

There are a number of advantages that arise from computing risk by sampling methods such as Random Chemistry or Monte Carlo. With both methods, one can disaggregate $\hat{R}(x)$ and compute the risk that comes from blackouts of different sizes, e.g., compute the risk due to small, medium, and large blackouts, or the risk from $n-2$ and $n-3$ contingencies, although it takes much longer for Monte Carlo to find a sufficient number of outages to do this type of disaggregation. Sections 2.4.3 and 2.4.3 illustrate this calculation, and section 2.4.4 shows the disaggregated (in blackout size) risk vs. load level.

A second advantage is the ability to find the sensitivity of $\hat{R}(x)$ to the failure-rates of particular transmission lines. Disaggregating $\hat{R}(x)$ and finding the most important components that impact $\hat{R}(x)$ could have tremendous value to system operators. For example, it may allow an operator to identify particular actions (such as hardening particularly vulnerable transmission lines, or reducing the load on some lines) that can substantially reduce large blackout risk.

Risk from blackouts of different sizes

To illustrate the separation of risk for different blackout sizes, Fig. 2.2b shows the risk for $E[S_{0.4}(\mathcal{C}, x)]$, i.e. for blackouts 40% or larger. Disaggregating risk by blackout size is particularly useful if one wants to know the impact of potential system changes, such as the addition of a new transmission line, or changes in load level. Understanding how these changes impact the risk of blackouts of different sizes should allow for more informed decision making. We study the problem of how risk changes with load in section 2.4.4.

Risk from $n-2$ and $n-3$ contingencies

It is noteworthy that the majority of the risk shown in Fig. 2.2 comes from $n-2$ malignancies. Because of the smaller number of $n-2$ malignancies relative to $n-3$ malignancies, the Random Chemistry $n-2$ risk estimate converges much faster than the $n-3$ risk estimate. However, well after the $n-2$ risk has converged, some small fluctuations in total risk remain, due to changes in the minimal $n-3$ set size estimation (see Fig. 2.1b).

In order to further understand the impact of $n-3$ contingencies on blackout risk, we further explored the details of contingency sets found for the Polish system. The $n-3$ risk is composed of two portions; a small part of the risk is due to $n-3$ malignancies (herein referred to as minimal $n-3$ risk) with the remainder coming from non-minimal $n-3$ contingencies that are supersets of $n-2$ malignancies. To find the latter portion, we post-processed the data to compute the probabilities of all $n-3$ supersets of $n-2$ malignancies, using the associated $n-2$ blackout size based on Assumption 1, to avoid simulating all the supersets. The results were similar (see Table 2.2) to what Monte Carlo finds when computing risk by sampling from both minimal and non-minimal contingencies.

Table 2.2 shows the $n-2$ and $n-3$ estimates of risk by both Monte Carlo and Random Chemistry methods for the Polish system. Although the Monte Carlo risk estimates are similar to those from Random Chemistry, Monte Carlo identifies far fewer minimal $n-3$ than

non-minimal $n-3$ contingencies, thus providing much less information about the minimal $n-3$ risk. Specifically, Random Chemistry found 540 $n-2$ and 38,212 $n-3$ malignancies, whereas Monte Carlo found only 440 $n-2$, 41 minimal $n-3$, and 830 non-minimal $n-3$ contingencies. Note that, as Table 2.2 shows, 96.7% of the Random Chemistry $n-3$ risk estimate (11.7 kW) was actually attributable to $n-2$ malignancies, with only 3.3% (0.4 kW) due to $n-3$ malignancies.

Risk Sensitivity

Fig. 2.3 shows the sensitivity of risk to individual branch outage probabilities (derived from their failure rates) in the Polish system, as computed from (2.15).

Clearly, the sensitivity data in Fig. 2.3 show a very heavy tail; a very small number of components affect risk disproportionately. This becomes particularly clear when we look at the impact of particular lines on total risk, by computing the risk sensitivity value times the outage probability. For example, given the risk sensitivity of 1.41×10^5 kW and the outage probability of 1.06×10^{-4} for branch 96 (which has the highest sensitivity value), and total risk of 50.5 kW in the Polish system (Fig. 2.2), we find that this branch can adjust 29% of overall cascading failure risk by modifying its failure probability.

These sensitivity values can be used to identify potential risk-mitigation strategies. For example, transmission lines that have a higher overall risk sensitivity factor might be targeted for increased vegetation management or improved fault detection relaying systems, which may reduce the associated line-outage probabilities. To illustrate this approach, we

Table 2.2: Estimated $n-2$ and $n-3$ risk in the Polish system.

	MC risk (kW)	RC risk (kW)	Percent of RC risk due to	
			$n-2$ minimal	$n-3$ minimal
$n-2$	37.1	36.4	100%	NA
$n-3$	11.5	12.1	96.7%	3.3%
Total*	50.3	50.5	99.2%	0.8%

*Note that Total includes risk from non-minimal $n-4$'s, $n-5$'s, etc.

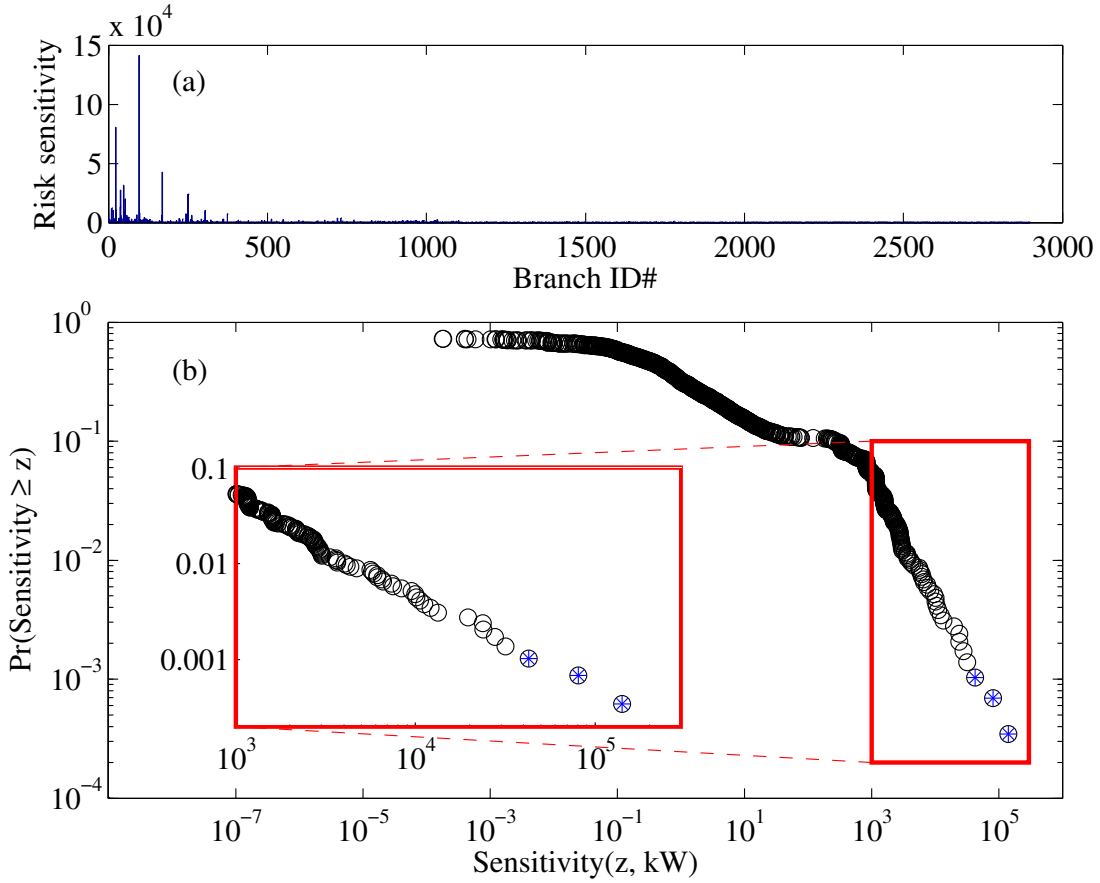

Figure 2.3: (a) Sensitivity of risk to branch failure probability for all 2896 branches in the Polish system, (b) Complementary Cumulative Distribution Function of sensitivities (one circle per branch); inset shows data for the 5% of branches with the largest sensitivities. The three lines with the highest sensitivities are marked with an asterisk.

identified the three branches with the highest sensitivity values, namely branches 96, 23 and 169. After identifying the branches, we reduced the three failure probabilities (p_{96}, p_{23} and p_{169}) by half, and re-computed risk. This resulted in a 33% reduction in total cascading failure risk. In another experiment [51], we reduced line rating for these three transmission lines by half in the initial dispatch of the system. This increased dispatch cost by a modest 1.6%, but decreased overall cascading failure risk by 61%. These two results suggest that new optimal power flow formulations could be designed to take into account the existing trade-off between blackout risk and normal operation costs.

2.4.4 Estimating risk as a function of load

Finally, in order to illustrate the potential of this approach to perform more in-depth studies of cascading failure risk, we used the Random Chemistry method to examine how cascading failure risk changes with different load levels and generator dispatch methods. To do so, we prepared $n-1$ secure versions of both systems for a range of load levels from 50% to 119% for RTS-96 and 50% to 115% for the Polish system. 119% was the highest load level at which SCDCOPF could find a solution without load shedding in the pre-contingency RTS-96 case. For the Polish system, load could increase up to 110% before a small amount of load shedding was needed to find a secure solution. For cases from 111% to 115% load, less than 1% load shedding was required to achieve $n-1$ security. For comparison purposes, we extended our study of the Polish system up to 115% load.

Fig. 2.4 shows risk in the RTS-96 system for all load levels for two different pre-contingency dispatch conditions. To make the analysis more useful, the risk associated with different blackout sizes are separately presented. Panel (a) shows the results produced from a SCDCOPF dispatch at each load level. In order to smooth out differences at adjacent points, each point on the graph shows the rolling average of risk across three consecutive integer percentage load levels (i.e., the datum at 90% load is the average for 89%, 90%, and

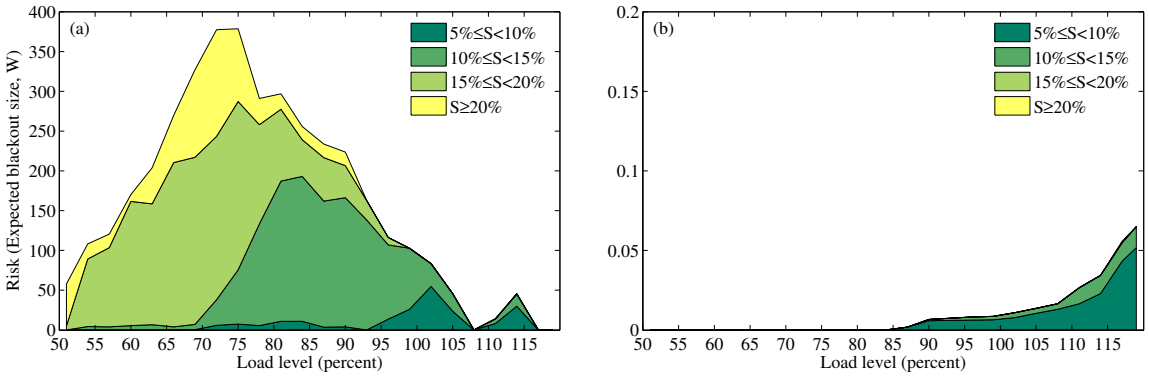

Figure 2.4: Cascading failure risk vs. load level for RTS-96: (a) SCDCOPF, and (b) Proportional dispatch.

91%).

It is interesting to note that very-large blackout risk is greatest at about 70% load level, and decreases significantly as the load increases beyond this level. The initial increase in risk is similar to the findings in [52], [13], [38] and [18], which report a phase transition in cascading failure risk as load increases. However, depending on the dispatch method for the pre-contingency system, the risk may decrease subsequently, as Fig. 2.4a shows for SCDCOPF dispatch. The later decrease in risk differs substantially from what is previously reported in the literature.

Fig. 2.4b shows risk for the same load levels but with a proportional dispatch method, in which we took the 119% load case from SCDCOPF, and uniformly decreased the loads and generators to each lower load level [53]. This dispatch method reduced risk substantially, and the relationship between load and risk now becomes monotonic. Large blackout risk is practically zero for the proportional dispatch cases. The pre-contingency dispatch in this case is obviously more expensive than that from the SCDCOPF, which indicates that there is an important tradeoff between generation dispatch costs and cascading failure risk.

Fig. 2.5 shows cascading failure risk vs. load level for the Polish system, using SCDCOPF for the pre-contingency dispatch. Again, the results suggest that that risk does not always increase with load level. In fact, risk decreases to some extent for load percentages between

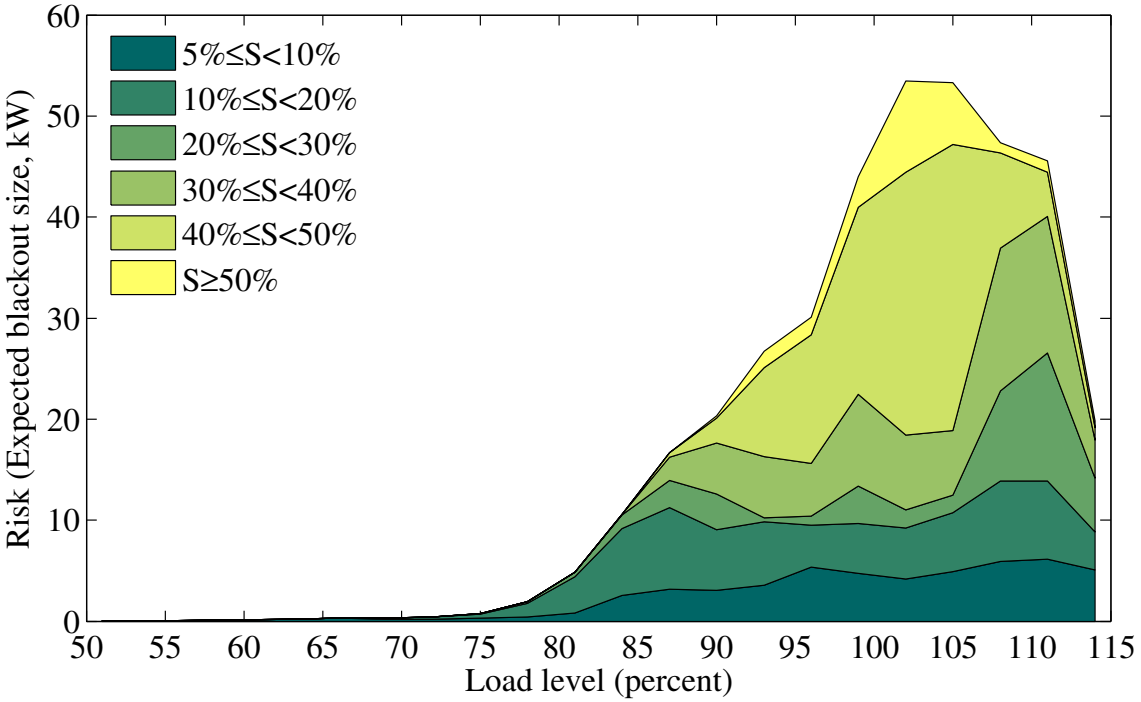

Figure 2.5: Cascading failure risk vs. load level for the Polish system, dispatched by SCDCOPF.

100% and 110%, and to a larger extent above 110% (the same cases for which some load shedding, less than 1%, occurs during the pre-contingency dispatch).

Inspection of the test systems indicates that the reduced risk at higher load levels results from the way that SCDCOPF uses more local generation with less long-distance transmission at higher load levels. In other words, at moderate load levels, the minimum cost generators are far from load centers, and important transmission corridors are loaded closer to their capacity. To illustrate this, Fig. 2.6 shows the total amount of power flow on the 5% most sensitive branches, found from (2.15), in RTS-96 and the Polish system. We observe in Fig. 2.6 that the total power flows on these critical lines follow the same general pattern as risk in Figs. 2.4 and 2.5 for both systems.

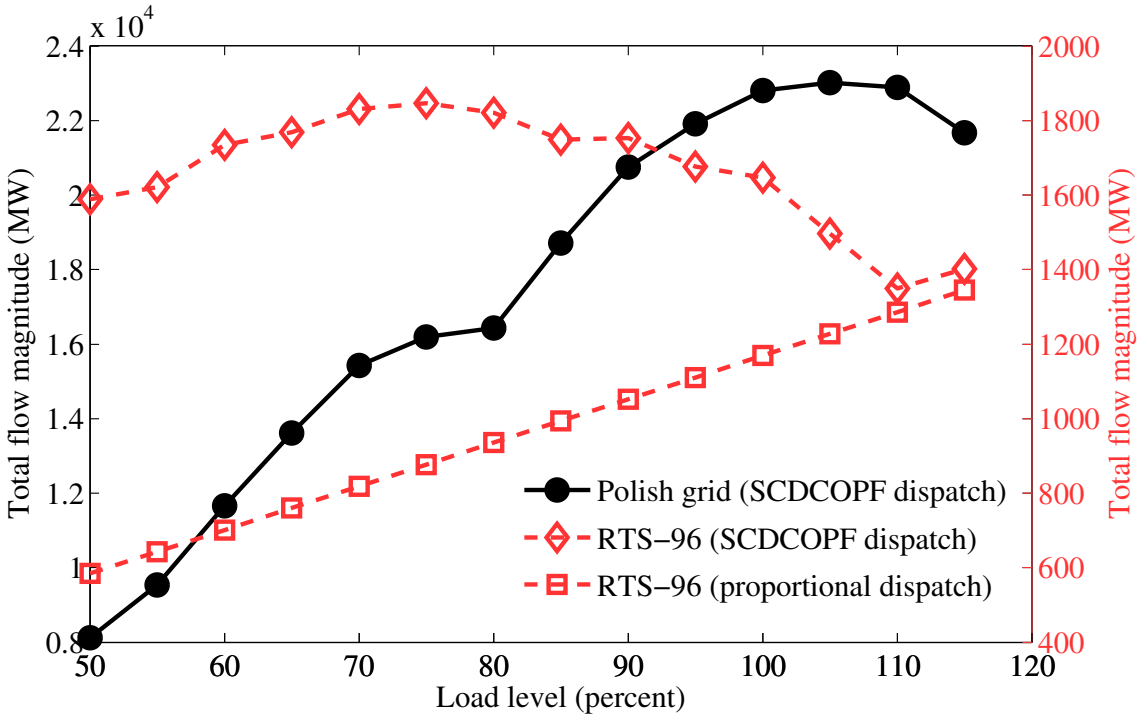

Figure 2.6: Total power flow magnitude on the 5% most sensitive branches in the Polish system (solid circles, left axis) and RTS-96 (open symbols, right axis).

2.5 Conclusion and Future Work

This chapter presents a new computationally efficient method, based on the Random Chemistry algorithm in [14], for estimating the risk of large (e.g., $\geq 5\%$ of system load) cascading blackouts. A comparison of this method to Monte Carlo simulation for two test cases (the IEEE RTS-96, and a model of the Polish transmission system) shows that the new approach is at least two orders of magnitude faster than Monte Carlo, and does not introduce measurable bias into the estimate. The computational efficiency of the Random Chemistry approach comes from the way that it directly searches for large blackout-causing contingencies, as opposed to Monte Carlo, which samples broadly from all possible contingencies.

We disaggregated risk with respect to the resulting blackout sizes and the sensitivity of risk to individual branch outage probabilities in the initiating events. For the latter case, we derived a method to use the data generated by the Random Chemistry approach to quickly estimate the impact of component outage probabilities on the overall risk. For the Polish system, the results indicate that reducing the unplanned outage probabilities on three transmission lines (e.g., by more aggressive vegetation management) would produce a 33% reduction in overall cascading failure risk.

In order to illustrate the utility of the proposed approach, we computed how the risk of blackouts of various sizes changes with load level. Surprisingly, the results indicate that risk can sometimes decrease with increasing load, e.g., if generators are dispatched according to a preventative security constrained optimal power flow. However, if generators are dispatched proportionally (all generations and loads change in equal ratios with respect to a load level with low risk), blackout risk is much smaller and risk increases monotonically with load. This illustrates an important tradeoff between economic efficiency and blackout risk.

These results suggest a number of important topics for future research. First, the results presented here rely on the assumption that branch outages are uncorrelated and come from

a relatively simple cascading failure simulator. Future work will seek to confirm that the efficiency gains associated with the Random Chemistry approach persist after modeling correlated outages and additional mechanisms of cascading. In addition, we studied only the sensitivity of risk to initiating events; studying the sensitivity of risk to events during a cascade remains for future work. Finally, future research is needed to transform the data that result from Random Chemistry into effective strategies for reducing blackout risk.

Appendices

2.A Summary of the Random Chemistry Algorithm

The Random Chemistry algorithm is a stochastic set-size reduction search strategy that can be used to efficiently (in logarithmic time) find minimal subsets that are associated with a certain outcome of interest. The algorithm was applied to genomic data mining in [54], and was adapted to the problem of finding $n-k$ blackout-initiating contingencies in power grids [14]. In summary, the Random Chemistry algorithm operates as follows. Initially, we use the cascading failure simulator from [14] (DCSIMSEP [50]) to find a large multiple contingency c (an $n-k_{\text{init}}$ contingency, where $k_{\text{init}} \geq 40$) that results in a large blackout. Because k_{init} is so large, this step typically requires very few tries. Then, the algorithm stochastically reduces c according to a logarithmically decreasing set size reduction schedule (in this work we used $\{k_{\text{init}} = 80, k_2 = 40, k_3 = 20, k_4 = 14, k_5 = 10, k_6 = 7, k_{\text{final}} = 5\}$) by testing random subsets of the desired size until one is found that causes a large blackout. If no such subset is found within a pre-specified maximum number of tries T (we used $T = 20$), the run is restarted from a new random $n-k_{\text{init}}$ contingency. The remaining set of size $k_{\text{final}} = 5$ is exhaustively searched (starting from $k = 2$) until a minimal $n-k$ blackout-causing contingency ($2 \leq k \leq k_{\text{final}}$) is identified. This cycle can then be repeated to obtain large collections of $n-k$ minimal hazardous contingencies.

2.B Exploring Assumption 1

In this section, we test Assumption 1 for the Polish system by comparing the actual blackout sizes of all $n-3$ supersets of all $n-2$ malignancies with the estimated values, i.e., the blackout size of each $n-2$ subset. For each $n-2$ malignancy, there are $n-2 = 2894$ supersets that were simulated with DCSIMSEP for this comparison. We then computed the percent deviation of each $n-3$ blackout size from its malignancy subset:

$$\epsilon = \frac{S_{act} - S_{est}}{S_{est}} \times 100$$

where S_{act} is the actual blackout size of an $n-3$ superset, and S_{est} is the blackout size of its $n-2$ subset. Fig. 2.7 shows the proportional frequency of these deviations. We found that these deviations are generally in the range of -1.9% (10^{th} percentile) to 0.9% (90^{th} percentile). Ultimately, Assumption 1 resulted in the estimated $n-3$ blackout risk to be 2.5% higher than the exact value obtained by using the actual $n-3$ blackout sizes.

Note that Assumption 1 provides a weaker estimation when larger than one-extra-element supersets of malignancies are considered. However, with larger supersets, the contingencies become highly improbable, and make a negligible contribution to the total risk. Thus, we only need Assumption 1 to work for supersets with few additional elements added to a malignancy. This partially explains why the above assumption does not measurably change the Random Chemistry risk estimation results in section 2.4, relative to what is computed by Monte Carlo.

2.C Derivation of Equation (2.12)

This appendix presents the derivation of (2.12), the expected number of uniquely numbered objects found (N_i) after i draws from a jar of N objects numbered 1...N.

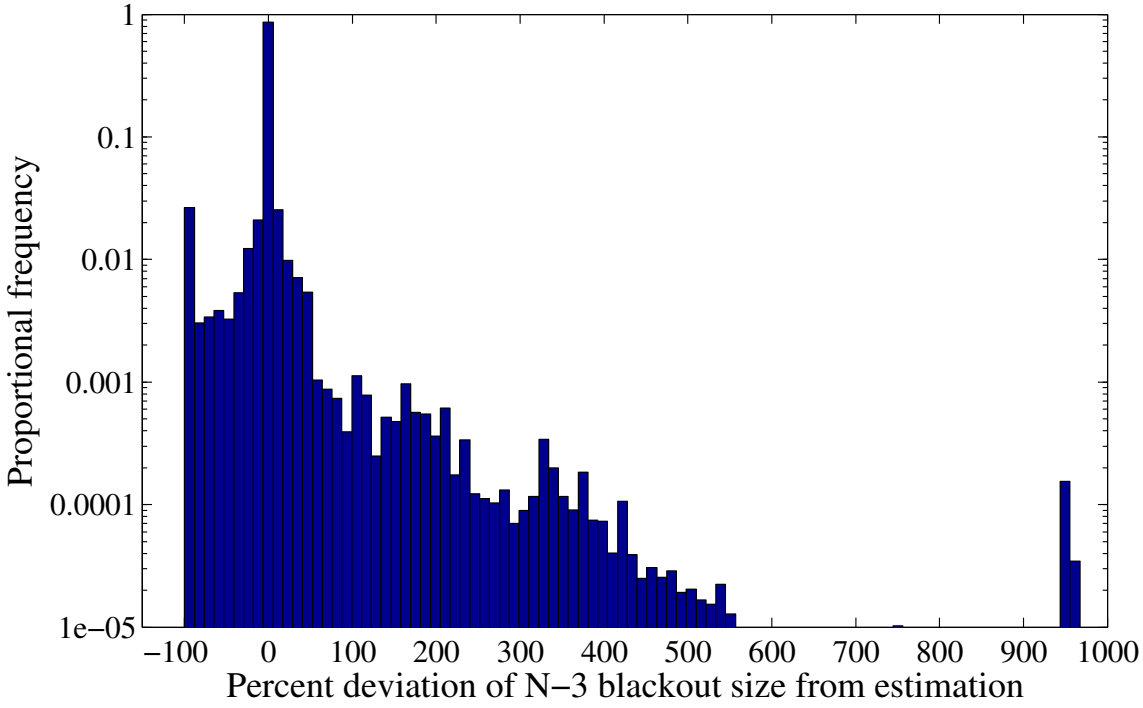

Figure 2.7: Proportional frequency of percent difference in actual minus estimated blackout sizes caused by non-minimal $n-3$ contingencies.

After the first draw, one will have found precisely 1 unique object. In subsequent draws, the expected number of unique items found is:

$$N_i = N_{i-1} + \frac{N - N_{i-1}}{N} = rN_{i-1} + 1 \tag{2.16}$$

where $r = 1 - \frac{1}{N}$. Equation (2.16) is a recursive function, for which we would like to find a closed-form expression. To do so, one can divide both sides by r^i, which gives:

$$\frac{N_i}{r^i} = \frac{N_{i-1}}{r^{i-1}} + \frac{1}{r^i} \tag{2.17}$$

Let

$$\mathcal{N}_i = \frac{N_i}{r^i} \tag{2.18}$$

Then:

$$\mathcal{N}_i = \mathcal{N}_{i-1} + \frac{1}{r^i} \tag{2.19}$$

$\mathcal{N}_0 = 0$, so:

$$\mathcal{N}_i = \sum_{j=1}^{i} \frac{1}{r^j} = \frac{N\left(1 - r^i\right)}{r^i}$$

Based on (2.18): $N_i = N\left(1 - r^i\right) = N(1 - e^{i\ln(r)})$, as presented in (2.12).

2.D Security-constrained optimal power flow for pre-contingency dispatch

For the initial results in this chapter, we computed the pre-contingency power flow state for each load level using a Security-Constrained DC Optimal Power Flow (SCDCOPF). As a result, each pre-contingency network is $n - 1$ secure for any single line outage. Although the DC Optimal Power Flow (DCOPF) is a relatively simple linear programming problem, a full SCDCOPF including all line outages as contingencies can become computationally expensive, especially for larger systems, because of extensive number of contingencies. To

reduce the computational effort, we solve a decomposed SCDCOPF based on the method proposed in [55]. The decomposed SCDCOPF is described as follows.

Initially, DCOPF is solved to find minimal generation cost dispatch constrained by power flow equations and line flow limits, with the following formulation:

$$\min_{\mathbf{P}_g, \mathbf{P}_d} \quad \mathbf{c}_g^T \mathbf{P}_g - \mathbf{c}_d^T \mathbf{P}_d \tag{2.20}$$

$$\text{s.t.} \quad \mathbf{P}_{\bar{\mathbf{r}}} = \mathbf{B}_{\overline{\mathbf{rr}}} \boldsymbol{\theta}_{\bar{r}} \tag{2.21}$$

$$\sum_{i=1}^{|G|} P_{g,i} = \sum_{j=1}^{|D|} P_{d,j} \tag{2.22}$$

$$\mathbf{F} = \mathbf{X}_b^{-1} \mathbf{A} \boldsymbol{\theta}_{\bar{r}} \tag{2.23}$$

$$-\mathbf{F}_{\max} \leq \mathbf{F} \leq \mathbf{F}_{\max} \tag{2.24}$$

$$0 \leq \mathbf{P}_g \leq \mathbf{P}_{g,\max} \tag{2.25}$$

$$0 \leq \mathbf{P}_d \leq \mathbf{P}_{d0} \tag{2.26}$$

where $\mathbf{P}_g$ and $\mathbf{P}_d$ denote vectors of real power generation and load in the network, and G and D are sets of buses with generators and loads respectively. $\mathbf{c}_g$ and $\mathbf{c}_d$ are vectors of generator marginal costs and the cost of load shedding at each bus, respectively (both in $\$/MWh$). $\mathbf{P}_{\bar{\mathbf{r}}}$, $\mathbf{B}_{\overline{\mathbf{rr}}}$ and $\boldsymbol{\theta}_{\bar{r}}$ are respectively the vector of real power injections, bus susceptance matrix, and the vector of bus voltage angles for all buses except the reference bus. $\mathbf{F}$ denotes the line power flow vector. $\mathbf{X}_b$ is a matrix with each diagonal entry representing the reactance of each line, and zero non-diagonal entries. $\mathbf{A}$ is the node-branch incidence matrix, where the number of rows and columns are equal to the number of branches and buses respectively.

Constraints (2.21) and (2.22) enforce the DC power flow constraints, and constraint (2.23) calculates flows from bus voltage angles. Constraints (2.24), (4.5g) and (2.26) restrict line flows, real power generation and load to be between their upper and lower bounds. Constraint (2.26), together with the second term in (2.20), enables the possibility of load shedding, which ensures that the problem is always feasible. In order to ensure that load

shedding does not occur unless absolutely necessary, we set the entries of $\mathbf{c}_d$ to have large positive values, which are all greater than $\mathbf{c}_g$. In this chapter, we assume equal values of c_d for all loads.

In order to make each case $n-1$ secure, we add contingency constraints. Here, we use the Line Outage Distribution Factors (LODF) matrix to find post-contingency line flows after each line outage [56], which is an $m \times m$ matrix, where m represents the number of branches. Assuming line j is tripped in the network, each entry h_{ij} of the LODF matrix gives the relative change in flow on line i due to the outage of line j. Therefore, each post-contingency flow constraint has the following form:

$$-F'_{i,\max} \leq f_i + h_{ij} f_j \leq F'_{i,\min} \tag{2.27}$$

where $F'_{i,\max}$ denotes the short term rating of line i. f_i and f_j denote the pre-contingency power flows on lines i and j respectively. In order to solve a full SCDCOPF, one can add as many as $m(m-1)$ contingency constraints to the problem. However, explicitly adding these constraints makes problem prohibitively computational expensive, especially for large m. To reduce the computational cost, we implement a decomposed SCOPF, based on [55], in which contingency constraints are incrementally added to the problem until the solution is $n-1$ secure. The flowchart of one cycle of this algorithm is shown in Fig. 2.8. Typically, only 2 or 3 repetitions are needed to find an $n-1$ secure solution.

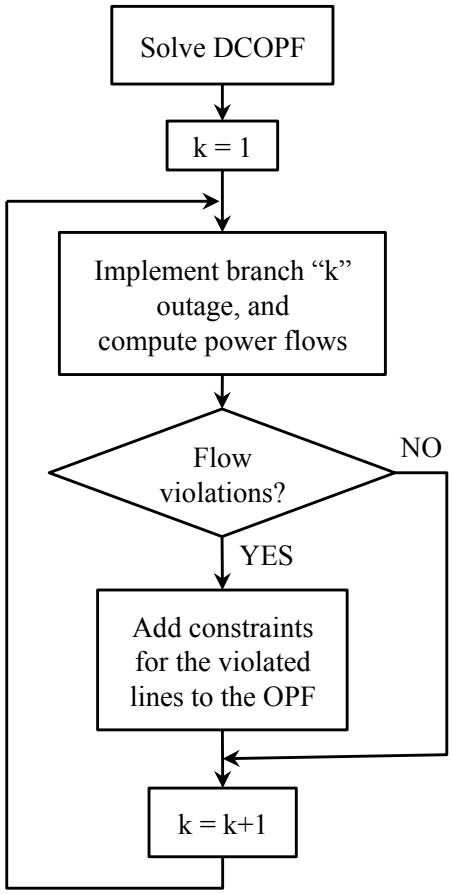

Figure 2.8: One cycle of the decomposed SCDCOPF (based on [55])

Chapter 3

Simulating Cascading Failures in Power Systems Using AC Power Flow

Abstract

Understanding and mitigating cascading failures is essential to the safe operation of power grids. Because of this importance, transmission utilities are required to analyze large sets of multiple contingencies and the possibility of cascading failure as a part of their planning studies [27]. In spite of this requirement, commercially available tools for cascading failure analysis are very limited, and improved simulation tools are currently of great interest to the industry. This chapter describes a cascading failure simulator that uses the ac power flow model. Using ac power flow in simulating cascading failures involves a critical challenge: the power flow equations frequently become unsolvable when the system is under stress after sequential outages. The real world equivalent of this loss of solution to the system of equations is a phenomenon called voltage collapse, which is an unstable state of the system that typically leads to a blackout of some size. This chapter presents an effective method in overcoming this challenge by finding a practical load shedding that would make the equations solvable again.

3.1 Introduction

The dc power flow model is a useful starting point for cascading research, because the model is numerically stable and fast. However, it cannot describe voltage deviations or reactive power flows, which are known to be particularly important contributors to many historical cascades. The nonlinear ac equations are a more accurate and accepted model of power flows, which are usually solved numerically using the Newton-Raphson method. However, the ac equations do not have a unique solution, and have a fractal region of convergence based on the starting point. In addition, a poorly chosen starting point or step size in Newton-Raphson may cause divergence.

Another reason why power flow might not converge is when no solution exists for the system of equations leading to voltage collapse. This case is the focus of this chapter, because it arises very often in simulating cascading failures with a quai-steady-state model. Voltage collapse typically leads to load shedding (blackout) after a dramatic reduction in voltage of some buses and perhaps operation of under-voltage relays. There are typically three ways that simulators deal with this situation in the literature. Firstly, the simulation stops because of lack of a power flow solution, and that case is considered a blackout of the entire system [57, 58]. However, during voltage collapse in real world cascading failures, e.g. 2003 northeast blackout, some of the loads black out until the remainder of the system re-stabilizes. Another way to overcome voltage collapse in a simulation is to reduce all loads by a fraction in blocks in the entire system [20] or in the region with the highest mismatch [18], and try solving power flow repeatedly until a solution is found. In reality, large cascades that involve voltage collapse do not affect the whole system. For example, in the case of 2003 northeast blackout, loads were not disconnected in the entire country. This is because voltage collapse is typically a relatively local problem, and is more likely to cause load shedding within a region near the source of the voltage collapse. Reducing loads in

multiple steps has another drawback that is the need to repeat many trials and errors before a solution is found. Finally, a dc optimal power flow is solved in [19] to shed some loads, but there is no guarantee that the system becomes solvable, so some scenarios are considered a blackout of the whole system. This chapter describes a method to estimate the required load shedding to make an unsolvable power flow case solvable again. The approach used here roughly represents a combination of phenomena that lead to load shedding when a power system approaches voltage collapse. When ACSimSep finds an unsolvable power flow case it chooses load shedding that will move the system towards the region of solvability. In our experience, the method needs two iterations at most to make a case solvable in large-scale power systems under highly stressed conditions.

The remainder of this chapter is organized as follows. Section 3.2 describes the distributed slack bus power flow algorithm with optimal multiplier that is used in ACSimSep. Section 3.3 explains a method that finds a solution to deal with unsolvable power flow cases. This method is incorporated in ACSimSep algorithm, which is covered in Section 3.4. Section 3.5 compares ac and dc cascading failure simulation results both in individual cases and in estimating risk with the Random Chemistry method (Chapter 2). Finally, Section 3.6 discusses conclusions of the chapter.

3.2 Power flow with distributed slack bus and optimal multiplier

There are two common formulations for ac power flow equations: rectangular and polar coordinates for voltage phasors. In the polar formulation, the voltage at each bus i is represented as:

$$V_i = |V_i| e^{j\theta_i} \tag{3.1}$$

whereas in rectangular formulation:

$$V_i = a_i + jb_i \tag{3.2}$$

Power flow equations can then be represented as:

$$\mathbf{S} = \mathbf{f}(\mathbf{x}) \tag{3.3}$$

where $\mathbf{S}$ is a vector of constant real and reactive power injections at each bus where they are specified, $\mathbf{x}$ is a vector of bus voltage magnitude and angles (in the polar formulation) or bus voltage real and imaginary parts (in the rectangular formulation). In power flow analysis, all system buses are one of the following types: PQ, PV and slack. In a PQ bus, which is used to model load buses, active power P and reactive power Q are specified. In a PV bus, which is used to model generation buses, active power P and voltage magnitude V are specified. Because we cannot predict the losses, at least one bus needs to be considered as slack, in which voltage magnitude and angle are specified. Choosing one bus as slack is necessary to have a reference angle and be able to solve the equations numerically.

The performance of power flow convergence varies based on the formulation type and the extent to which the case is stressed. The polar formulation typically provides a better first order approximation of power flow equations, which improves convergence [59]. The polar format also results in fewer equations and variables than rectangular. The difference is equal to the number of PV buses in the system. This is because the voltage magnitudes, which are specified for PV buses, are directly used as variables in polar formulation, and so will be dropped for PV buses. Therefore, our simulator uses a polar formulation of the ac

power flow, which gives us:

$$\mathbf{S} = [P_1, P_2, \ldots, P_{n-1}, Q_1, Q_2, \ldots, Q_m]^T \tag{3.4}$$

$$\mathbf{x} = [\theta_1, \theta_2, \ldots, \theta_{n-1}, |V_1|, |V_2|, \ldots, |V_m|]^T \tag{3.5}$$

where P_i and Q_i are, respectively, the real and reactive power injections, and m is the number of PQ buses in the system. Real power is specified at all buses except the slack, where voltage is $1\angle 0$. Also:

$$\mathbf{f} = \left[f_{P_1}(\mathbf{x}), f_{P_2}(\mathbf{x}), \ldots, f_{P_{n-1}}(\mathbf{x}), f_{Q_1}(\mathbf{x}), f_{Q_2}(\mathbf{x}), \ldots, f_{Q_m}(\mathbf{x})\right]^T \tag{3.6}$$

After some algebra we have [60]:

$$f_{P_i}(\mathbf{x}) = |V_i| \sum_{j=1}^{n} \{|V_j|(G_{ij}\cos(\theta_i - \theta_j) + B_{ij}\sin(\theta_i - \theta_j))\} \tag{3.7}$$

$$f_{Q_i}(\mathbf{x}) = |V_i| \sum_{j=1}^{n} \{|V_j|(G_{ij}\sin(\theta_i - \theta_j) - B_{ij}\cos(\theta_i - \theta_j))\} \tag{3.8}$$

where $Y_{ij} = G_{ij} + jB_{ij}$ are elements of the bus admittance matrix $\mathbf{Y}$.

The most common approach is to solve (3.3) using a standard Newton-Raphson method:

$$\mathbf{x}_{k+1} = \mathbf{x}_k + \Delta\mathbf{x}_k \tag{3.9}$$

$$\Delta\mathbf{x}_k = -\mathbf{J}(\mathbf{x}_k)^{-1}\left[\mathbf{f}(\mathbf{x}_k) - \mathbf{S}\right] \tag{3.10}$$

where $\mathbf{J}(\mathbf{x}^k)$ is the jacobian matrix at iteration k. Under normal power system conditions, the standard Newton-Raphson with a flat starting point (voltage angles equal to 0 and voltage magnitudes equal to 1) typically works well. However, when a system is under stress, it sometimes diverges. A solution that helps convergence in this situation is to use a variable step size after the direction has been found in (3.10) [59, 61, 62]. This step size is

chosen to minimize the squared norm of the power flow mismatch function $\mathbf{g}(\mathbf{x}) = \mathbf{f}(\mathbf{x}) - \mathbf{S}$, and so is called the optimal multiplier method:

$$\begin{aligned}\mu_k &= \arg\min_{\mu} \frac{1}{2} \left(\|\mathbf{f}(\mathbf{x}_k + \mu\Delta\mathbf{x}_k) - \mathbf{S}\|_2\right)^2 \\ &= \arg\min_{\mu} \frac{1}{2} \left(\|\mathbf{g}(\mathbf{x}_k + \mu\Delta\mathbf{x}_k)\|_2\right)^2 \end{aligned} \tag{3.11}$$

which will change (3.9) to:

$$\mathbf{x}_{k+1} = \mathbf{x}_k + \mu_k \Delta\mathbf{x}_k \tag{3.12}$$

Equation (3.11) is a function in terms of μ and can be solved using the golden section search or parabolic interpolation algorithms [63]. Using the optimal multiplier from (3.11) causes the squared norm to get smaller (or remain constant) in each iteration, and so avoids divergence. Numerical experience shows that in the optimal multiplier method, convergence is quite good, even for very ill-conditioned or heavily-loaded systems [62].

In simulating cascades, where in many cases, a huge disturbance causes a large imbalance between generation and load, it is no longer appropriate to have a single slack bus. The ac power flow in our studies uses a distributed slack bus model in which many generators participate in ramping [64]. Only a small modification is required in equations to implement participating factors for generators. Now, (3.3) changes to:

$$\mathbf{S} + \rho\mathbf{h} = \mathbf{f}(\mathbf{x}) \tag{3.13}$$

with:

$$\mathbf{S} = [P_1, P_2, \ldots, P_n, Q_1, Q_2, \ldots, Q_m]^T \tag{3.14}$$

$$\mathbf{x} = [\theta_1, \theta_2, \ldots, \theta_{n-1}, |V_1|, |V_2|, \ldots, |V_m|, \rho]^T \tag{3.15}$$

where $\mathbf{h}$ is the column vector of participating factors for generators on the elements that are

added to a generator power in $\mathbf{S}$ and is zero otherwise. ρ is a new variable in power flow that, after being multiplied by $\mathbf{h}$, determines how much power is added to or subtracted from each participating generator. Distributed slack bus roughly simulates generator responses to frequency changes (e.g., droop control), where generators share varying loads among themselves. In our simulations, participating factors ($\mathbf{h}$) are set proportional to maximum generation limit for each generator.

3.3 Resolving unsolvable power flow

When load level increases in a power network, the system gets closer to its stability limit, beyond which it cannot operate. Using the power flow equations, one can determine the solvable and unsolvable region in terms of system parameters [62]. Fig. 3.1 depicts three different regions in a multi-dimensional parameter space. The parameters include active and reactive loads on all buses, active power injection and voltage set-points for generators. The normal operating region is where power flow solves and all state variables are within their limits. The undesirable region includes the parameter values where power flow solves (thus the system can also operate), but some of the limits are violated, e.g. some lines are overloaded. If the system is operating in that region, an optimal power flow strategy can find the best controls to move the system to return to the desirable region. One example of this type of restorative optimal control is developed in Chapter 4. The third operating region is where power flow is unsolvable. If the system moves to that region because of some disturbance, a blackout of some size would happen due to voltage collapse. In simulating cascading failures, this occurs relatively frequently. In this section, a method is developed to find a practical direction to move in the multi-dimensional parameter space back to the solvable region.

To illustrate, consider a simple two bus test system with a transmission line connecting the two buses (Fig. 3.2). Bus 1 is the slack bus, and bus 2 has a load on it connected with

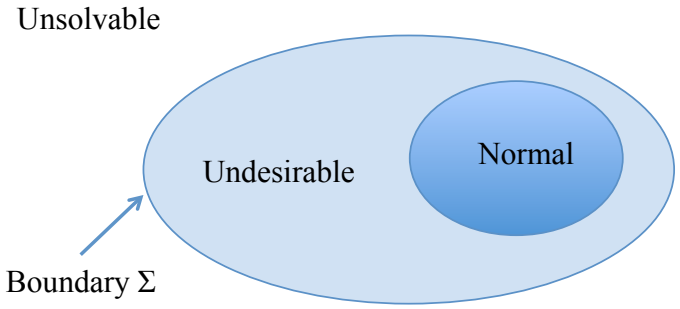

Figure 3.1: Operating regions in terms of system parameter space

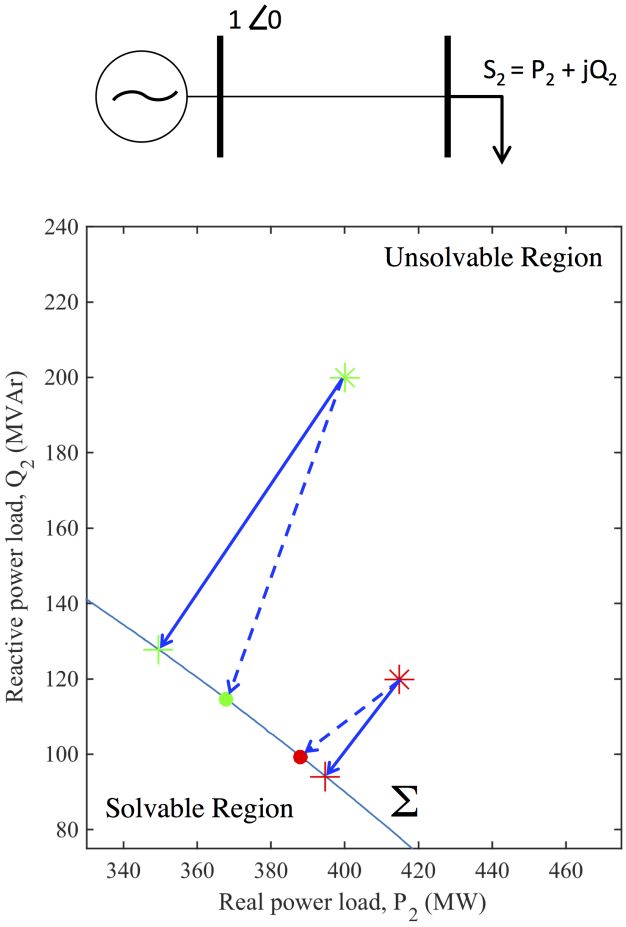

Figure 3.2: Parameter space of the two bus system. In each set of three markers connected with arrows, asterisks show the starting load point in power flow; circles show $\mathbf{f}(\mathbf{x}^*)$ where $\mathbf{x}^*$ is the value of $\mathbf{x}$ at the end of solving power flow; pluses show the minimum distance point from load points in the solvable region. Arrows show plausible directions to move in the parameter space back to solvable region.

a lossless transmission line with reactance of 0.1 per unit. Fig. 3.2 shows the solvable and unsolvable power flow regions in terms of active and reactive power of the load. The two regions are separated by the boundary Σ. If one starts solving power flow for any of the load points in the unsolvable region (e.g., the asterisks in Fig. 3.2), the optimal multiplier power flow ends up on a point x^* where $\mathbf{f}(\mathbf{x}^*)$ is on the boundary Σ (circles in Fig. 3.2). The jacobian of power flow equations is singular on this boundary, which means that it has a zero eigenvalue there. Furthermore, the left eigenvector associated with the zero eigenvalue of the jacobian $\mathbf{J}(\mathbf{x}^*)$ is perpendicular to Σ at $\mathbf{f}(\mathbf{x}^*)$ [65–67]. The dashed arrows in Fig. 3.2 connect $\mathbf{S}$ to $\mathbf{f}(\mathbf{x}^*)$ and show a plausible direction to move in the parameter space to return to the solvable region. In cases with many buses and transmission lines, the boundary is no longer as flat as in Fig. 3.2 (see [68]), so solving power flow does not necessarily give the best direction for load shedding. To ensure that a load shedding direction would move back to the solvable region, a more effective approach is to move in the minimum distance direction from the load point ($\mathbf{S}$) to the boundary Σ (solid arrows in Fig. 3.2). In general, $\mathbf{f}(\mathbf{x}^*)$ is not at the minimum distance from $\mathbf{S}$. Finding the minimum distance vector has another benefit and that is enabling one to estimate the amount of load shedding that is required to move back to the solvable region while holding the power factor constant. This is explained later in this section and also in [67].

To find the minimum distance from solvable region, the power flow problem is formulated as an unconstrained optimization problem [62]:

$$\min_{\mathbf{x}} \quad F(\mathbf{x}) = \frac{1}{2}[\mathbf{f}(\mathbf{x}) - \mathbf{S}]^T[\mathbf{f}(\mathbf{x}) - \mathbf{S}] \tag{3.16}$$

If the power flow is solvable, minimizing $F(\mathbf{x})$ gives a power flow solution with a zero objective function at the solution. If the ac equations are not solvable, (3.16) provides the point with a minimum distance from the unsolvable point to the boundary Σ in the parameter space. An iterative method is proposed in [62] to find this minimum distance

by solving the power flow and updating $\mathbf{S}$ in each iteration. This approach works well for cases when the unsolvable point is not far from the boundary. In highly stressed cases, where the initial point $\mathbf{S}$ is very far from the boundary, the method frequently diverges. This is due to the underlying assumption that Σ is nearly flat. This is not necessarily the case; if the boundary is curvy, the method fails. To avoid this problem, ACSimSep uses a nonlinear least squares optimization method, namely the Levenberg-Marquardt algorithm in MATLAB, to optimize (3.16) directly. By exploiting sparsity this algorithm can typically find an optimal solution in a few seconds on a personal computer for a large system.

If there are many loads in a system, the parameter space becomes of higher dimensions, and the vector that connects the load point to a boundary point (either with a minimum distance or not) will have non-zero values on many of its coordinates, which translates into load shedding at a large percentage of system buses. A more practical approach when power flow is unsolvable is to shed loads that are the most sensitive in reducing the distance to solvable region, i.e., the most effective loads. In addition, it is a better representation of actual utility practice to shed loads with a constant power factor (constant ratio of active and reactive power). Let β be the Euclidean distance of the initial load point $\mathbf{S}$ from the solvable region. Fig. 3.3 illustrates this distance for the two bus test system with a load of 400 MW and 200 MVAr. As mentioned earlier, the true minimum distance load shedding is not practical since it involves changes in a large number of buses. Instead, the sensitivity of the change in β to change in loads is more useful. In general, the sensitivity of β to different controls could be found, e.g., active/reactive power injection of loads and capacitor bank switching, depending on their availability. A method is proposed in [67] from the results in [66] to find these sensitivities. However, the sensitivity to real and reactive power of loads (elements of $\mathbf{S}$) could be found directly in the vector of minimum distance. And that is what we need to estimate load shedding to get back to the solvable region. To illustrate, let $\mathbf{u}$ be a vector of available controls (real and reactive power of all loads in $\mathbf{S}$ for now),

and $\beta_{\mathbf{u}}$ be the vector of sensitivities, i.e., $\beta_{u_i} = \frac{\Delta\beta}{\Delta u_i}$. Then β_{u_i} is essentially equal to the ith element in the vector of minimum distance ($\mathbf{S}_m - \mathbf{S}$ in Fig. 3.3), and an estimate of required change in ith control to get back to the solvable region is given by $\frac{\beta}{\beta_{u_i}}$. This can be illustrated for the two bus case in Fig. 3.3, where power flow is solved for an initial load of $400 + 200j$. Let w_m be the normalized vector of minimum distance. We have:

$$w_m = \frac{\mathbf{S}_m - \mathbf{S}}{|\mathbf{S}_m - \mathbf{S}|} = [\beta_{P_2}, \beta_{Q_2}]^T \tag{3.17}$$

Then ΔP_2, which is the required change in P_2 to get back to the solvable region can be estimated by $\frac{\beta}{\beta_{P_2}}$. The estimation error is the difference between the boundary (Σ) and the tangent plane on the minimum distance point (circle in Fig. 3.3). Similarly, ΔQ_2 can be estimated by $\frac{\beta}{\beta_{Q_2}}$. However, we are interested in change in a direction where power factor is constant, so we need to find β_{S_2}. Sensitivity of β to change in apparent power for load i, β_{S_i}, can be computed in terms of β_{P_i} and β_{Q_i} as follows:

$$\begin{aligned}
\Delta\beta &= \beta_{P_i}\Delta P_i + \beta_{Q_i}\Delta Q_i \\
&= \beta_{P_i}\Delta S_i \cos\phi + \beta_{Q_i}\Delta S_i \sin\phi \\
&= \left[\beta_{P_i}\cos\phi + \beta_{Q_i}\sin\phi\right]\Delta S_i
\end{aligned} \tag{3.18}$$

Thus β_{S_i} is given by:

$$\beta_{S_i} = \beta_{P_i}\cos\phi + \beta_{Q_i}\sin\phi \tag{3.19}$$

where $\cos\phi$ is the load power factor. After computing β_{S_i} for all buses, we choose the buses with the largest sensitivities to shed until $\beta = \sum \beta_{S_i}\Delta S_i$ depending on available apparent power on the buses.

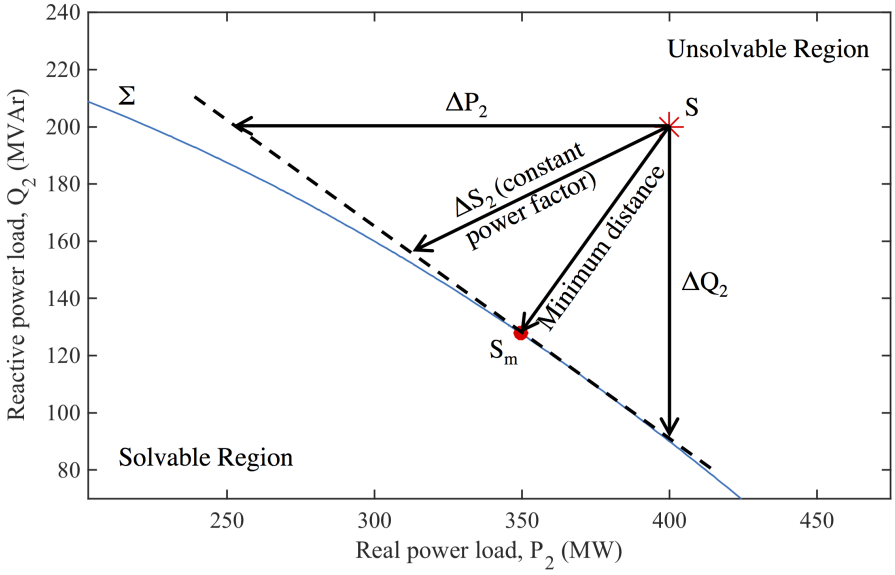

Figure 3.3: Illustration of constant power factor direction in the parameter space of the two bus system. $\mathbf{S}$ *shows the initial load to solve power flow.* $\mathbf{S_m} - \mathbf{S}$ *shows the minimum distance vector.* ΔP_2*,* ΔQ_2*, and* ΔS_2 *show the estimated shedding from active, reactive and apparent power respectively.*

3.4 ACSimSep algorithm

Figure 3.4 shows an algorithm flowchart for ACSimSep. All of the steps are the same as in DCSimSep (section 1.2), except Step 5 and a minor modification in how rebalance is done. Rebalance in Step 4 is done such that the total generation is equal to the total load plus 5%. This is to take power losses into account. The final rebalancing is completed by the participation factors of all generators in the island. In Step 5, ACSimSep computes the power flow, and if the power flow does not converge, the method from section 3.3 is used to find sensitivity factors at each bus in Step 5a. Then, it sheds 50% more load than what is estimated to be necessary to return the solution to within the solvable region, to ensure that the resulting operating point is well inside the solvable region. Because some load is shed in that island, ACSimSep then rebalances the island again by ramping down generators for one minute and then tripping them starting from the smallest generators until generation

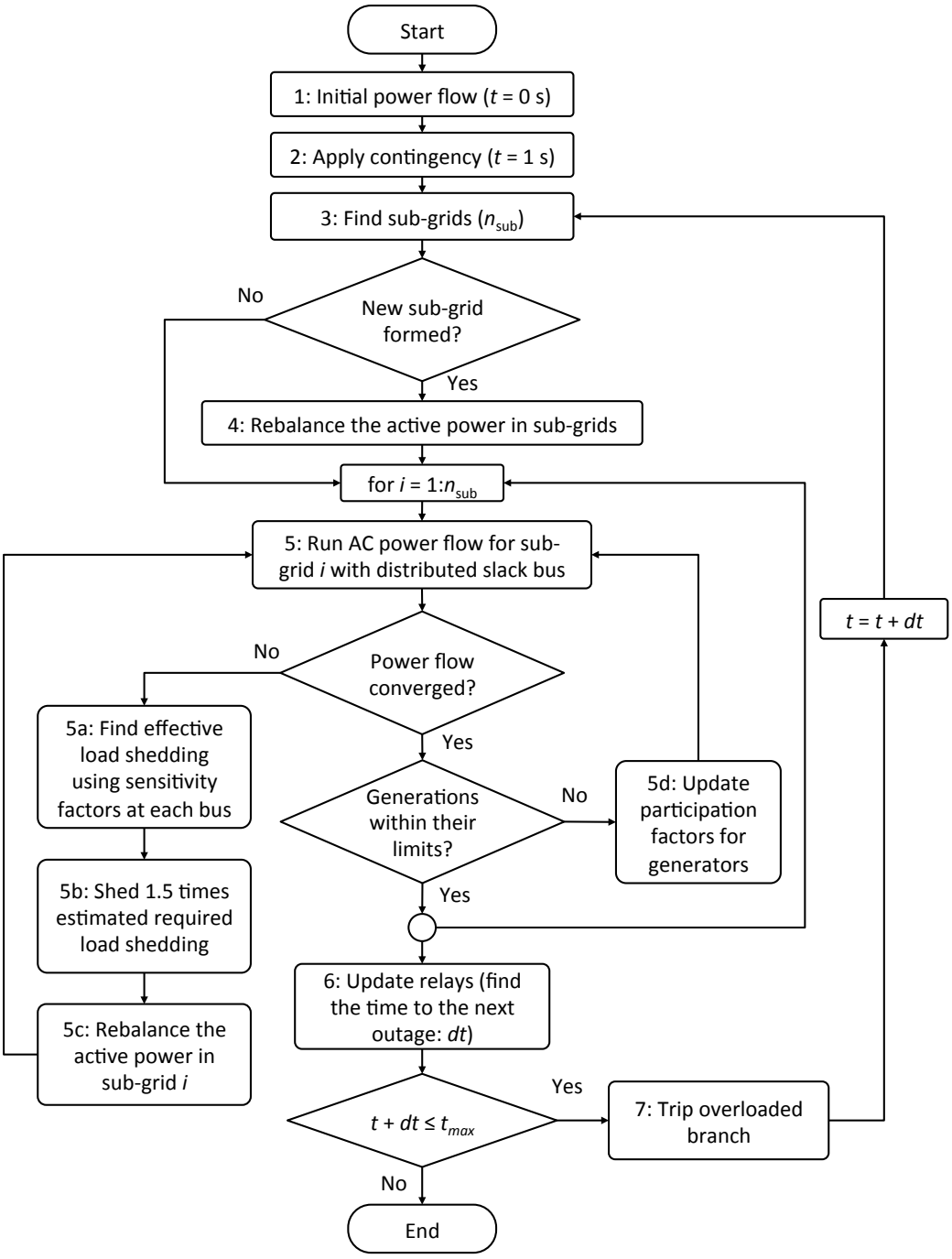

*Figure 3.4: The diagram of ACSimSep: An **AC** power flow **Sim**ulator of power system **Sep**aration*

is equal to load plus 10%. Again, the rest of the adjustment is done by participation factors of all generators in the island. After the power flow converges, generators are checked to make sure they observe maximum generation limit (minimum is set to zero at this time). If some generators are producing at above their maximum allowed capacity, their participation factor is set to zero and power flow is solved again. This is done until all generators are within their limits. Furthermore, if total maximum generation is not enough to supply all loads in the island (participation factors are all zero), 5% of (initial) loads are shed in that island and power flow is solved again.

Note that occasionally the specific form of the solvable and unsolvable regions and the boundary Σ may cause the estimated load shedding to not be sufficient to move the operating point to within the solvable region. Therefore, Steps 5, 5a, 5b and 5c are repeated until the power flow converges. Simulation results show that one additional iteration can usually find a convergent power flow, even in extremely stressed cases.

3.5 Comparing ac and dc simulation

In this section, the goal is to examine similarities and differences between the dc and the ac simulators. To do so, we use the IEEE RTS-96 test case [45]. The data for this system are available online [49]. The initial load level of the system is set to 79%, i.e., all loads in the system are multiplied by a factor of 0.79. This load level was previously shown to have a particularly high blackout risk (see section 2.4.4). The pre-contingency system was initially set to be $n-1$ secure using a dc security-constrained optimal power (SCOPF). Note that because the SCOPF uses the dc power flow, the ac case is not perfectly $n-1$ secure. This section describes the cascading events predicted from the two models, using two different $n-2$ contingencies as an example: one for which the two simulators predict a similar set of outages and blackout sizes, and a second for which the two simulators produce very different results.

Fig. 3.5(a) shows the progress of first simulation, where lines 312-323 and 315-324 are tripped initially. These outages cause an overload on line 314-316, which subsequently outages, after which the power flow does not converge. The ac model then sheds loads on buses 303, 308, and 307 and 302 to find a power flow solution, after which line 313-323 is overloaded and eventually outages. At this point the system divides into two sub-grids, and a large mismatch between generation and load causes generator tripping in the larger island and load shedding in the smaller island. A similar sequence of events occurs in the case of dc simulation, aside from the fact that we do not have a non-convergent power flow, and all load shedding is due to the rebalancing process. Interestingly, both simulations end with 18.9% of lost load.

Fig. 3.5(b) illustrates the second simulation with ACSimSep, in which lines 203-224 and 214-216 are tripped initially. In the ac simulation, a small amount of load shedding occurs on one bus (107) to avoid voltage collapse, but the majority of the load shedding occurs after the system is divided into two islands, after three endogenous outages. This simulation ends in a 6.2% blackout in the ac simulation. In the dc simulation the initiating contingency does not cause any overloads in the system, as line flows are computed to be below limits after the initial outages. Therefore, the dc simulation does not report any load shedding.

In addition, we computed the risk sensitivity from Section 2.3.4 with both dc and ac simulators to find how sensitivity of overall risk to individual component-failure probability changes for all branches. We used the IEEE RTS-96 with a load level of 100%. Interestingly, the three most critical branches remain the same in both dc and ac simulations. Table 3.1 shows the ten most risk-sensitive branches in the IEEE RTS-96, ordered by their sensitivity values.

In another test, we checked the number of $n-2$'s found by the dc simulator that remain a malignancy with the ac simulator, i.e., cause a $\geq$ 5% blackout. From the 540 $n-2$

Table 3.1: Ten most risk-sensitive branches in the IEEE RTS-96

order	1	2	3	4	5	6	7	8	9	10
Branch number (w/ DCSimSep)	104	103	102	30	109	28	27	107	106	18
Branch number (w/ ACSimSep)	104	103	102	109	107	106	11	6	86	7

malignancies in the Polish system, found in Chapter 2, only nine of them did not cause a large ($\geq 5\%$) blackout.

The above results indicate that although the dc simulator uses a simplified model of the power grid, it can still provide some useful information on how cascades propagate in a given system. The dc simulator becomes particularly beneficial if simulation time is a priority. The difference is very noticeable in any realistically sized power system. For example, every run of the ac simulator on the Polish system takes 4.2 seconds (on average) when using Random Chemistry (the simulation stops as soon as $S >= 5\%$), and 34.7 seconds (on average) for simulation of each malignant $n-2$. These times reduce to 0.57 and 3.7 seconds, respectively, with the dc simulator [1]. Finding the extent to which the dc simulator could provide useful information without a huge bias in results compared to the more acceptable ac simulator, remains for the future work.

3.5.1 Estimating risk as a function of load

Chapter 2 proposed a method to estimate risk using Random Chemistry. One of the merits of the method is that it is not dependent on a particular simulator, and so could be used by the operator's simulator of choice. Fig. 3.6 compares the ac and dc simulators in estimating blackout risk as a function of load for the IEEE RTS-96 test system.

While the ac and dc models show different absolute levels of risk, the overall pattern is quite similar. Because the ac simulator captures load shedding due to voltage collapse

[1] On a MacBook Pro with a 2.66 GHz processor and 8 GB of RAM

in addition to imbalanced situations, it is able to find the higher risk of larger blackouts ($\geq 20\%$) after the system is highly stressed.

3.6 Conclusions

Power flow equations can become unsolvable under heavily loaded conditions in a power system. In cascading failure simulation, branches are disconnected in a network when they remain overloaded for a sufficient time, which very often leads to an unsolvable case. This phenomenon is known as voltage collapse. This chapter described an effective method to estimate a practical load shedding that is required to make unsolvable cases solvable again. The proposed load shedding is then followed up by reducing generations based on ramping capabilities and then tripping generators if ramping is not enough. The load shedding can represent a combination of control and protection system responses, such as under voltage load shedding and operator interventions that altogether move the state of the system back to normal operating region. The proposed method is used in an ac simulator that has some similarities with the previous dc simulator, but also some important differences in that it can benefit from simulating blackouts due to voltage collapse. Simulations show that although the dc and ac simulations are sometimes similar, but generally, the dc simulator underestimates the size of a blackout especially in heavily loaded cases.

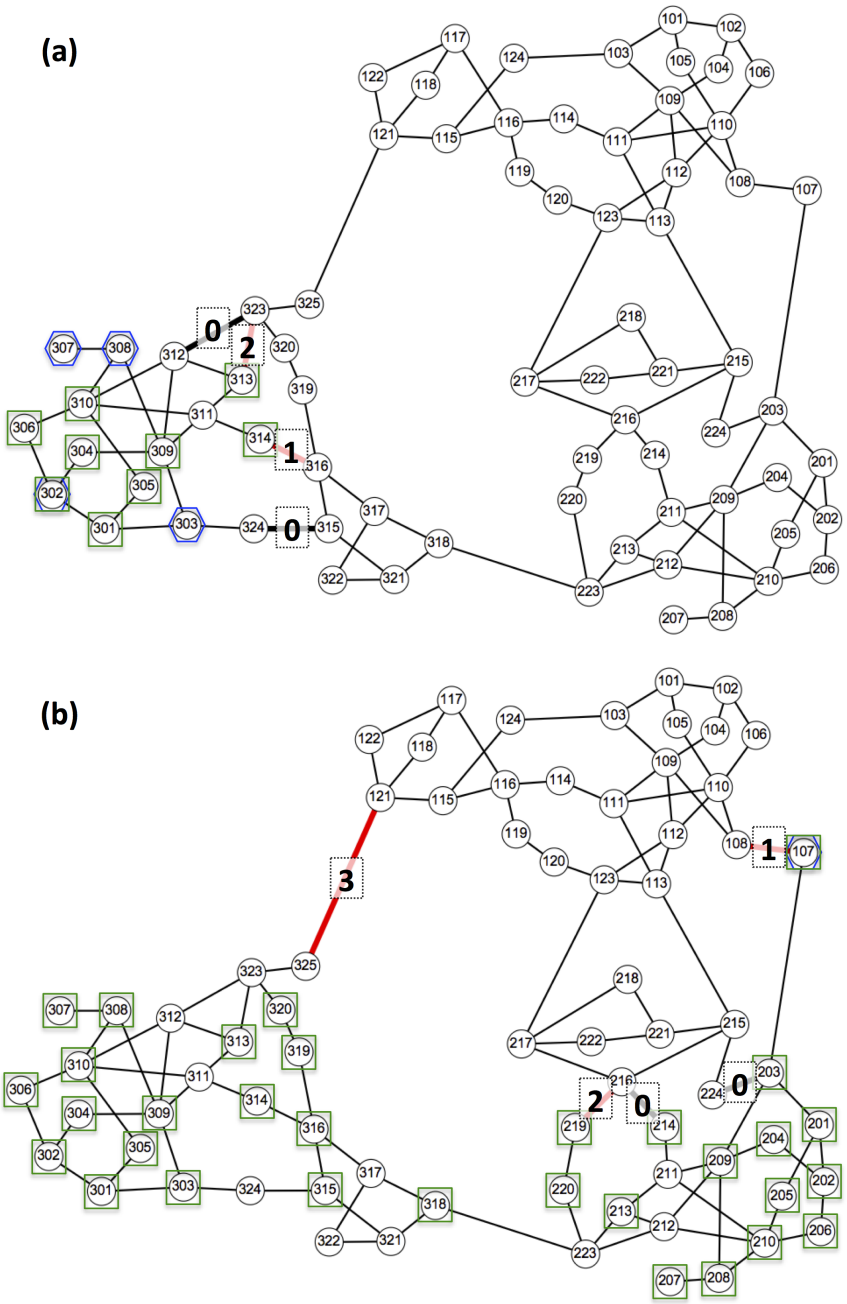

Figure 3.5: Illustration of the simulation of two $n-2$ contingencies on the IEEE RTS-96 case with ACSimSep: (a) 312-323 and 315-324, and (b) 203-224 and 214-216. Initial line outages are shown in black and subsequent dependent outages are shown in red. The numbers show the order in which the lines trip, with zeros indicating the two initiating branch outages. The buses where load shedding occurs to avoid voltage collapse are surrounded by a hexagon, and the buses where load shedding results from the rebalancing process are surrounded by a square.

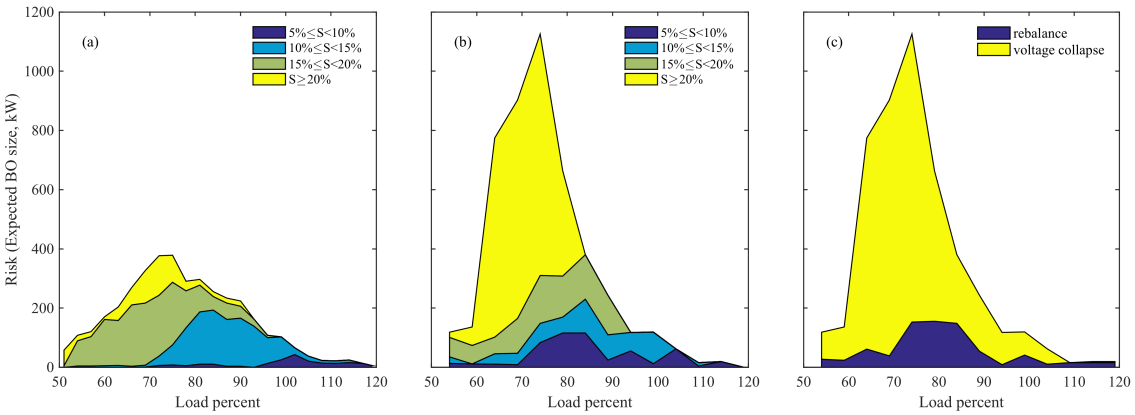

Figure 3.6: Cascading failure risk versus load level in the IEEE RTS-96 case: (a) DCSimSep results, (b,c) ACSimSep results. Risk is shown for different blackout size ranges in (a,b). Panel (c) separates the risk due to the two different load shedding mechanisms: re-balancing and voltage collapse.

Chapter 4

Distributed Predictive Emergency Control to Mitigate Cascading Failures

Abstract

One of the most effective ways to mitigate blackout sizes is to use emergency control strategies once stress is detected in a power system. Centralized methods normally provide the optimal solution in these situations. However, they suffer from high communication and computation burdens. Distributed methods fit well with current power system control practices, in which many control centers manage disjoint regional networks. In addition, they are more robust to attacks or failures in the control system. This chapter proposes a distributed receding horizon emergency control method, in which agents have a limited information and control area. The decision variables are load shedding and generator reduction in a local neighborhood of agents. Simulation results for a large-scale real power grid model show that compared with a central controller, the agents can find high quality solutions to reduce blackout sizes so long as the neighborhoods are large enough.

4.1 Introduction

The ultimate goal in understanding cascading failures is to develop methods to mitigate cascading blackouts. This chapter focuses on potential distributed approaches to reduce the size of a blackout after some overloads are detected. These methods fall into post-contingency mitigation methods, such as special protection or remedial action schemes (SPS/RAS) [69]. Typically, a SPS seeks to rapidly implement stress-reducing control actions, such as shedding load or reducing power generation, to control overloads or dynamic instabilities that might trigger a cascading event, after a contingency occurs. Later analysis of many real-world cascading events has shown that some careful control strategies could drastically reduce the size of the blackout. One common strategy is load shedding, which could have been effective in numerous previous blackouts—the 2003 northeast blackout [1], 2003 Italy blackout [70] and 2011 blackout in the US Southwest [3] to name a few. The core objective for emergency control schemes of this sort is to avoid a large amount of load shedding in a cascading blackout by performing smaller-sized targeted load sheddings and generation control.

A first step toward solving this problem is to design a central emergency control scheme to be used after detecting an overload in the system. The control variables could involve generation control, load shedding, and other controls, e.g., capacitor switching, tap-changer operation, and FACTS devices, depending on their availability in the system. Traditionally, load shedding has been studied for under-frequency protection. Under-frequency load shedding (UFLS) schemes become useful when large disturbances lead to generation deficit in a power system, e.g., after separation of the power grid or generator outages. Adaptive strategies have been proposed to avoid frequency instability [71–75]. An optimal load shedding algorithm is proposed in [76] to stop cascades. Building up on this work, a robust control method of cascading failures in power grids is later proposed in [77] that incorporates noise

and model errors.

Because cascades typically progress gradually (over minutes), at least in the initial stages, Model Predictive Control (MPC) has been shown to be particularly effective in arresting the spread of cascades before they propagate to large blackouts [57, 58, 78]. Model predictive control is particularly useful for controlling systems with hard constraints on their input and state variables. Classical control methods like PID control cannot naturally incorporate constraints and thus need to address constraints *a posteriori* [79]. MPC benefits from having an estimated model of the system, and so it can predict the system state based on the current state and input variables, by solving an optimization problem with constraints over a time horizon. It then implements the next immediate control variables and repeats the process. The reader can refer to [79–81] for an overview of MPC methods. MPC is widely used in both academia and industry, especially in the chemical process industry [82]. It has a range of applications from controlling robot manipulators to clinical anesthesia [83]. In power and energy systems, many papers have studied centralized MPC schemes. For example, MPC has been studied for voltage control in a number of applications: in transmission systems under normal and emergency conditions [84]; in distribution systems with distributed generation [85]; and in isolated hybrid wind-diesel generation systems [86]. Wind generation systems have also been controlled by MPC schemes [87–89]. The predictive optimization of MPC becomes particularly beneficial when using the wind forecast data.

Another useful application of MPC is centralized emergency control of power systems after contingencies. One of the early adoptions in this regard was in [90], which used load shedding, capacitor switching and tap changer operation to preserve voltage stability. One of the authors of the same work later proposed a predictive under-frequency load shedding scheme for frequency stability [91]. To prevent voltage instability in a power system, [92, 93] used MPC without considering thermal overloads and the possibility of cascading. Most recently, Almassalkhi and Hiskens [57, 58] proposed an overload mitigation

scheme by shedding load and changing generations with a focus on mitigating cascading blackouts. They considered energy storage and wind power curtailment in their scheme.

Centralized control schemes benefit from information from the entire system, and thus can provide finite horizon optimal control. However, they may be impractical to implement due to the substantial computational requirements, and the excessive amount of information that needs to be communicated across the system. Because of these shortcomings, multi-agent control has attracted a lot of attention. The literature on multi-agent systems is quite vast. The reader can refer to [94] for a general review of the topic. The challenge is often to get close-to-optimal performance without a substantial time delay. Generally, multi-agent methods need to make a trade-off between solution quality and the computation time. Talukdar et al. [95] show how autonomous agents, without strategic planning or centralized coordination, can converge to solutions of arbitrarily high quality, but there is no guarantee in reaching the optimal solutions. Modi et al. [96] proposed an algorithm to solve the Distributed Constraint Optimization Problem, which is a modeling that arises in multi-agent systems. The algorithm guarantees to find the optimal solution if time allows, and provides solutions with less quality given a limited time.

Cooperation among agents is one way to achieve better quality solutions. Cooperative algorithms can allow effective task performance in networked dynamic systems, where a group of agents reach an agreement–usually called a consensus–by negotiating with their neighbors [97]. Consensus problems form the foundation of the field of distributed computing in computer science, where a computational problem is divided into many tasks solved by one or more computers that could exchange messages [98]. In the past decade, there has been a lot of interest in multi-agent consensus problems in networked systems from different disciplines of engineering and science. Some of the applications arise in collective behavior of swarms [99], synchronization of coupled oscillators [100], formation control for multi-robot systems [101], and optimization-based cooperative control [102]. In power and energy

systems, multi-agent schemes have been used for a small number of applications including condition monitoring of equipments, distributed control of microgrids and power system restoration. An overview of previous applications of multi-agent approaches to power engineering is given in [103, 104]. More recently, [105] compares several decentralized predictive control schemes for power network applications.

In emergency control of power systems, multi-agent schemes have been used in [106] to prevent voltage collapse, but they do not consider thermal overloads in the transmission system. A multi-agent method (with some variations) is proposed in [78, 107, 108] to reduce overloads in power networks and thus mitigate cascading blackouts. When it comes to emergency control in power systems, there are no reasons why the solution to the emergency control problem needs to be decentralized [78]. First, a cascading failure could propagate in a system such that it affects components that are not necessarily in close proximity. Unless those elements were controlled by one entity, a centralized method might not be useful in practice, because there is no single entity to implement that method, and the associated entities might not be interested in relinquishing control of their infrastructure to maintain their privacy. The second reason to advocate a decentralized strategy is robustness. A centralized decision process can be more prone to failure as a result of any of its components failing. Finally, the reaction time is potentially shorter in a decentralized rather than a centralized approach, because of the ability to solve many smaller problems in parallel, using data that can be gathered with smaller communication delays.

This chapter proposes a multi-agent emergency control strategy to reduce overloads, building up on the ideas in [78]. The method could use either dc or ac power flow equations to model a power system, and estimates variations in line flows using dc power flow equations based on the initial state of the system. The dc power flow equations in the controller are an approximate linearization of ac power flow. To overcome the inaccuracies of dc power flow, the controller uses an MPC-based scheme, and solves the problem in multiple steps

considering the effects in a time window in the future instead of a one-step optimization. After implementing only one step, the controller receives new measurements, updates its model, and solves the problem again. The closed-loop nature of MPC can also account for delays of the control actions that is missing in one-step controllers.

In the design presented here, all of the distributed agents on each bus have such a controller that finds the optimal load shedding and generator reduction in their neighborhood to alleviate overloads using only information available locally. One of the shortcomings of the methods in [78] was that the agents' solutions frequently resulted in an imbalanced system (more generation than load, or vice-versa), thus requiring a re-balance between consecutive iterations of the algorithm. Primary and secondary frequency control are normally in charge of re-balancing generation and load in a power system, so the methods in [78] could work well but would impose a high burden on the frequency control systems between consecutive iterations of the cascade mitigation algorithm. The agents' negotiation algorithm here guarantees that the total generation reduction is equal to the total load shedding so as to maintain the balance of the system. The results show that given a sufficiently large local neighborhood, agents can find arbitrarily high quality solutions that are similar to a centralized scheme.

4.2 Centralized iterative emergency control

This section describes the formulation of a central emergency controller, which is then used to develop a distributed predictive multi-agent scheme in Section 4.4. The goal is to mitigate overloads by shedding the minimum amount of load. The controller estimates variations of loads and generations with dc power flow equations. The formulation is as follows:

$$\underset{\Delta\mathbf{P}_G, \Delta\mathbf{P}_D}{\text{Minimize}} \quad -\mathbf{1}^{\mathbf{T}}\,\Delta\mathbf{P}_D + \mathbf{c}^{\mathbf{T}}\,\mathbf{s} \tag{4.1a}$$

$$\text{subject to:} \quad \Delta\mathbf{f} = \mathbf{X}_b^{-1}\mathbf{A}^{\mathbf{T}}\,\Delta\boldsymbol{\theta} \tag{4.1b}$$

$$-\mathbf{f}_{\max} - \mathbf{s} \leq \mathbf{f}_0 + \Delta\mathbf{f} \leq \mathbf{f}_{\max} + \mathbf{s} \tag{4.1c}$$

$$\mathbf{B}\,\Delta\boldsymbol{\theta} = \Delta\mathbf{P}_G - \Delta\mathbf{P}_D \tag{4.1d}$$

$$-\min(\mathbf{P}_{G0}, \mathbf{R}) \leq \Delta\mathbf{P}_G \leq 0 \tag{4.1e}$$

$$-\mathbf{P}_{D0} \leq \Delta\mathbf{P}_D \leq 0 \tag{4.1f}$$

$$\mathbf{s} \geq 0 \tag{4.1g}$$

$$\Delta\theta_i = 0,\ \forall i \in \Omega_{\text{ref}} \tag{4.1h}$$

where $\Delta\mathbf{P}_D$ and $\Delta\mathbf{P}_G$ are vectors of changes in load and generation, respectively. $\mathbf{1}$ is a vector with all of its elements equal to one, and $\mathbf{1}^{\mathbf{T}}$ is its transpose. $\mathbf{s}$ denotes a vector with elements equal to the amount of overload on each line, and $\mathbf{c}$ is a vector of penalty factors for overloads. Constraint (4.1b) computes the changes in flows of all lines $\Delta\mathbf{f}$ from: changes in bus voltage angles $\Delta\boldsymbol{\theta}$; the matrix $\mathbf{X}_b$ with diagonal entries representing the reactance of each line and zero non-diagonal entries; and the node-branch incidence matrix $\mathbf{A}$. Each element $A_{ij} = 1$ if the flow on line j leaves node i, -1 if it enters node i, and 0 otherwise. Constraint (4.1c) ensures that the line flows remain between their specified limits. Here, (4.1c) is defined as a soft constraint to ensure that there always exist a solution to (4.1). The null solution ($\Delta\mathbf{P}_G = \Delta\mathbf{P}_D = 0$) is always a feasible (but frequently not optimal) solution to (4.1). Constraint (4.1d) enforces the dc power flow equations for the changes in variables, where $\mathbf{B}$ is the bus susceptance matrix. Constraint (4.1f) restricts all loads to remain between 0 and their initial value, and constraint (4.1e) limits generation changes by vector of ramping rates $\mathbf{R}$ so long as the ramping is not larger than the initial generation. Note that generators cannot increase their production in this formulation to

avoid undesirable rampings in sequential application of emergency control given there is no cost function for generators. Adding such cost functions remains for future work. Finally, constraint (4.1h) sets $\Delta\theta$ of reference buses to zero, where Ω_{ref} is the set of reference buses containing one bus from each island.

One desirable feature of the proposed controller is that it estimates the variation in generation and load instead of using their values directly in the equations. The controller takes the measurements as initial values for its model and then estimates how a minimum load shedding and generator reduction can reduce flows. Therefore, the system could work with ac power flow model, while still using a dc controller. The idea is that the controller could efficiently estimate flow changes around an operating point due to small changes in generation and load. Simulation results indicate that using such a controller can effectively reduce blackout sizes after a set of contingencies causes overloads in a system.

If line flows are limited with a hard constraint (without slack variables $\mathbf{s}$), there would be cases where the correction of flows is very expensive (or infeasible) in one step. In those cases, it might be more beneficial if the controller reduces the overload gradually to move the system toward a less stressed operating point. Another benefit of the proposed controller is that the soft constraint in (4.1c) avoids infeasibility, and also enables one to use the controller in multiple steps sequentially in order to gradually mitigate overloads. This makes the controller well suited for a model predictive control (MPC) strategy. Section 4.3 briefly introduces MPC, and then describes the controller formulation in an MPC framework.

4.3 Receding Horizon Model-Predictive Control

The core idea of MPC is to optimize future system response given the current state of the system and control inputs. MPC is useful in that it can incorporate constraints for all variables unlike traditional control methods. Using MPC, one could optimize the control objective and include constraints in a finite time horizon. Let $\mathbf{u}$, $\mathbf{x}$ and $\mathbf{y}$ represent system

inputs, states and outputs, respectively. A typical control objective is to drive outputs to their reference values (denoted by $\mathbf{y}_{\text{ref}}$). At each time step MPC optimizes an objective function, such as minimizing $\|\mathbf{y} - \mathbf{y}_{\text{ref}}\|_2^2$ over a time horizon starting from the current time. Then the control inputs for the first immediate time step are implemented; the state of the system is measured again and the optimization is repeated over a new time horizon, which has moved one time step forward. The process usually continues until the control objective is satisfied. Because of this behavior this approach is sometimes called *receding horizon* control. Since the predictions and measurements are repeated at each time step, MPC shows closed-loop behavior.

MPC calculations are typically based on a discrete time representation of the system under study. The state space model is:

$$\mathbf{x}[k+1] = \mathbf{A}\,\mathbf{x}[k] + \mathbf{B}\,\mathbf{u}[k] \tag{4.2a}$$

$$\mathbf{y}[k] = \mathbf{C}\,\mathbf{x}[k] \tag{4.2b}$$

where k denotes the sample time for the variables, and state space matrices are represented by $\mathbf{A}$, $\mathbf{B}$ and $\mathbf{C}$. Normally, there is not a direct term $\mathbf{D}$ from input to output in MPC models [79,109]. This is because the outputs (and state variables) are already given at time k, and cannot be affected by present time $\mathbf{u}[k]$, which the optimizer will compute. A general MPC formulation is:

$$\underset{\mathbf{u}}{\text{Minimize}} \qquad \sum_{k=1}^{N_p} \|\mathbf{y}[k] - \mathbf{y}_{\text{ref}}\|_{\mathbf{Q}}^2 \tag{4.3a}$$

$$\mathbf{x}[0] = \mathbf{x}_0 \tag{4.3b}$$

$$\mathbf{y}_{\min} \le \mathbf{y}[k] \le \mathbf{y}_{\max} \quad k = 1, 2, \ldots, N_p \tag{4.3c}$$

$$\mathbf{u}_{\min} \le \mathbf{u}[k] \le \mathbf{u}_{\max} \quad k = 0, 1, \ldots, N_p - 1 \tag{4.3d}$$

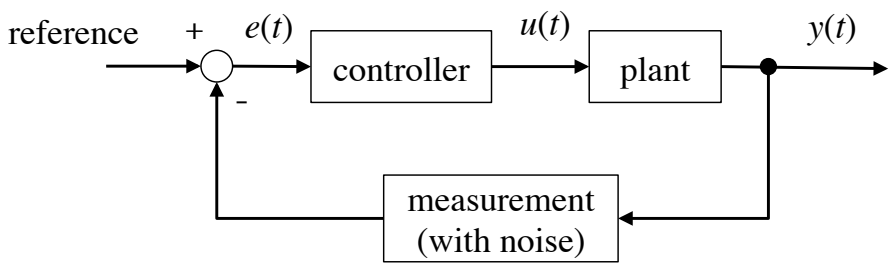

Figure 4.1: Block diagram of a plant with controller.

where $\mathbf{Q}$ is a diagonal matrix of weights, and $\mathbf{x}_0$ is the given state of the system at the present time ($k = 0$). The number of samples in the optimization time horizon is N_P. Note that for a vector $\mathbf{p}$ we have: $\|\mathbf{p}\|^2_{\mathbf{Q}} = \mathbf{p}^T\mathbf{Q}\mathbf{p}$. Also, the relationship between input, output and state variables is given by (4.2a) and (4.2b). As long as $\mathbf{Q}$ is diagonal with positive values, $\mathbf{Q}$ would be positive semi-definite and the problem becomes convex. Efficient solvers exist to solve a convex Quadratic Program (QP). Fig. 4.1 shows the block diagram of a typical controller computing inputs for a plant to set its outputs to a reference value.

The goal in some problems—including the emergency control problem in this chapter—is to minimize the variations of inputs $\Delta\mathbf{u}$ instead of having some reference values $\mathbf{u}_{\text{ref}}$. One way to include input variations in the equations is to re-write them as follows [109]:

$$\begin{pmatrix} \mathbf{x}[k+1] \\ \mathbf{u}[k] \end{pmatrix} = \underbrace{\begin{pmatrix} \mathbf{A} & \mathbf{B} \\ 0 & \mathbf{I} \end{pmatrix}}_{\hat{\mathbf{A}}} \begin{pmatrix} \mathbf{x}[k] \\ \mathbf{u}[k-1] \end{pmatrix} + \underbrace{\begin{pmatrix} \mathbf{B} \\ \mathbf{I} \end{pmatrix}}_{\hat{\mathbf{B}}} \Delta\mathbf{u}[k] \tag{4.4a}$$

$$\mathbf{y}[k] = \underbrace{\begin{pmatrix} \mathbf{C} & 0 \end{pmatrix}}_{\hat{\mathbf{C}}} \begin{pmatrix} \mathbf{x}[k] \\ \mathbf{u}[k-1] \end{pmatrix} \tag{4.4b}$$

where $\Delta\mathbf{u}[k] = \mathbf{u}[k] - \mathbf{u}[k-1]$. Note that in this formulation the input variables are replaced with their variations while the inputs themselves are added to the state variables. The new state space matrices are $\hat{\mathbf{A}}$, $\hat{\mathbf{B}}$ and $\hat{\mathbf{C}}$. Similarly, the emergency control problem incorporates

variations of load and generation while minimizing the variations. Section 4.4 describes how to formulate the emergency control problem in an MPC framework that could be solved by both a central controller and also distributed agents in a network.

4.4 Distributed model-based predictive emergency control

As mentioned earlier, a distributed emergency control scheme is more practical than a centralized controller because it is more robust to failures, and it will need less computations and communication. In addition, a distributed scheme is more natural because power system control centers have limited control areas. However, there is always a challenge in decomposing a centralized optimization problem without deteriorating solution quality. This section describes a distributed predictive emergency control strategy based on the central controller in Section 4.2. Simulation results on a model of the Polish power grid show that the approach can give comparable solutions to the central controller so long as the local neighborhood is sufficiently large enough.

Similar to (4.1) changes of loads and generators are the decision variables with the difference that the problem is solved over a time horizon inspired by MPC, and that the controllers are now independent agents located on all buses in a power system. The agents receive information from a local neighborhood and only have authority to issue control signals to other agents within that neighborhood. Fig. 4.2 shows the diagram of the distributed controller on each agent. The following paragraphs explain each step of the method:

Step 1: Agent i (on bus i) collects measurement data including generation $\mathbf{P}_{G,i}$ and load $\mathbf{P}_{D,i}$ on bus i and flows $\mathbf{f}_i$ of all lines that are connected to it.

Step 2: The agent checks if there is any overload on the lines connected to it. If there

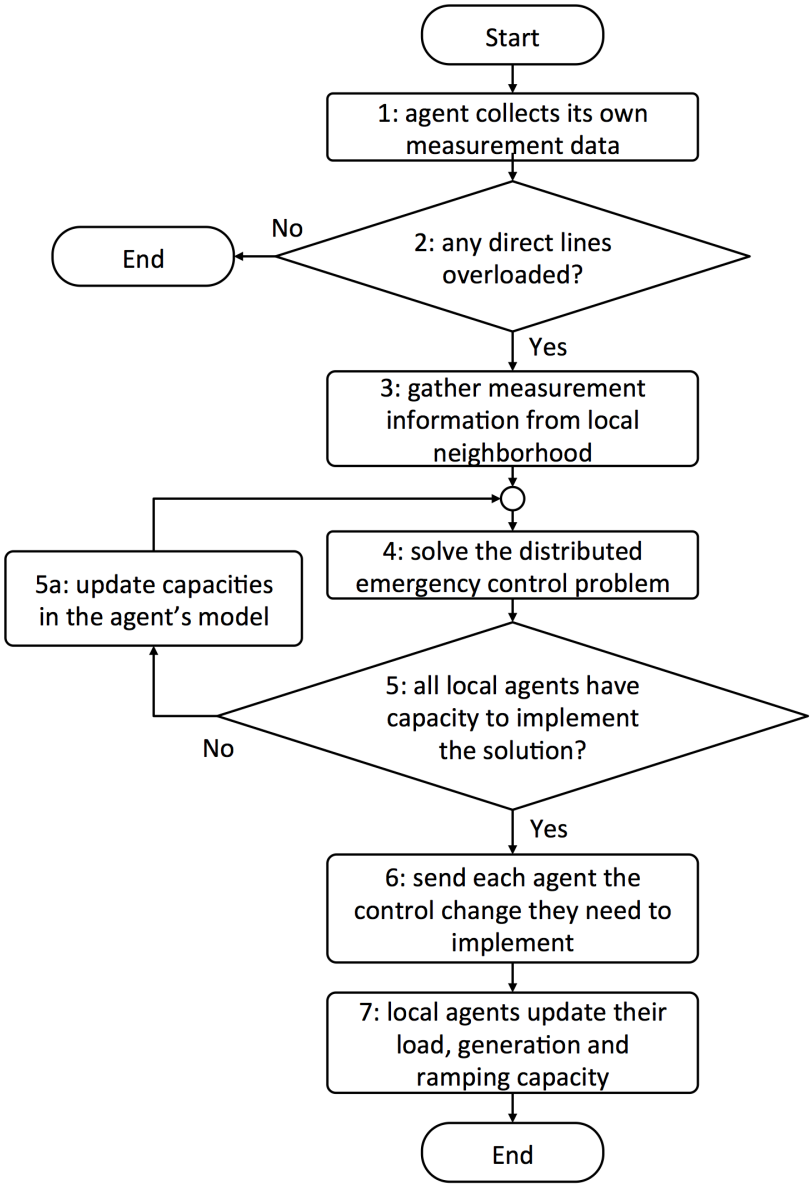

Figure 4.2: Diagram of the distributed controller of agents on all system buses.

are no overloads, it does not need to do anything.

Step 3: If there are one or more overloads on the line in $\mathbf{f}_i$, each agent j in a local neighborhood $\mathcal{V}$ sends their measurement data $[\mathbf{P}_{G,j}^T, \mathbf{P}_{D,j}^T, \mathbf{f}_j^T]^T$ and the tripped lines (if any) to agent i. In our simulations, a local neighborhood of a bus includes all buses that are N_{hop} away from it counting the (minimum) number of branches between them. For example, if $N_{\text{hop}} = 1$ the neighborhood of a bus includes all the buses that are directly connected to it, and so on for higher N_{hop}. Furthermore, a local neighborhood of a line is the union of local neighborhoods of the two buses on each end of the line. Note that the local neighborhood of a bus does not change during an event if some of the lines in this neighborhood are outaged. The communication system is assumed to be independent of the power system. Here $\mathcal{V}$ is set to be the local neighborhood of overloaded lines connected to agent i.

Step 4: Agent i solves the distributed emergency control problem (4.5) with decision variables including the change in load and generation for all buses $j \in \mathcal{V}$.

Step 5: Load shedding and generation reduction in the solution of distributed control problem (4.5) are always equal. But since agent i is not aware of any load shedding requested by other agents that are potentially solving another overload in the same neighborhood simultaneously, the capacity for load shedding and generator ramping may have changed in the neighborhood since agent i received the measurement data. To ensure that the solution can be completely implemented without violating the generation/load balance, agent i checks if there is enough capacity in the local neighborhood. If there is not enough capacity, agent i updates its information and solves (4.5) again until there is enough capacity to implement its solution in the local neighborhood $j \in \mathcal{V}$. In this step, agent i also receives information from its local neighborhood about the load sheddings or generator reductions that any of the agents $j \in \mathcal{V}$ will implement in the same iteration. Agent i will then incorporate those variable changes in its formulation. This is done to avoid extra load

shedding in case some of the local agents have already received a command from other solving agents to reduce their load/generation.

Step 6: If the solution is approved by all local agents, each of them receives a confirmation message to implement the solution at the end of the iteration.

Step 7: Local agents update their remaining load shedding and generation ramping capacity based on the change that agent i has requested, and then confirmed in Step 6.

After all agents go through the process in Fig. 4.2 all agents implement the changes that have been requested from them in that iteration. Note that for each line only one bus (at either end) needs to implement the algorithm in Fig. 4.2.

The following paragraphs explain the distributed emergency control problem (step 4) that each agent i solves in more details. Let k denote the sample time. The change of variables for a single time step is represented by $\delta x[k] = x[k] - x[k-1]$ and a change relative to the current time ($k = 0$) is represented by $\Delta x[k] = x[k] - x[0]$. The control inputs at time k are changes of generation $\delta \mathbf{P}_{G,\mathcal{V}}[k]$ and load $\delta \mathbf{P}_{D,\mathcal{V}}[k]$ in a subset $\mathcal{V}$ of all buses in the system, where $\mathcal{V}$ includes all buses in a local neighborhood of overloaded lines conneced to i. The formulation of the distributed predictive emergency controller is

as follows:

$$\underset{\delta\mathbf{P}_{G,\mathcal{V}},\delta\mathbf{P}_{D,\mathcal{V}}}{\text{Minimize}} \quad \sum_{k=0}^{N_P-1} \mathbf{c}_1^T\, \delta\mathbf{P}_{D,\mathcal{V}}[k] + \sum_{k=1}^{N_P} \mathbf{c}_2^T\, \mathbf{s}[k] \tag{4.5a}$$

$$\text{subject to:} \quad \mathbf{B}\Delta\boldsymbol{\theta}[k+1] = \mathbf{B}\Delta\boldsymbol{\theta}[k] + \delta\mathbf{P}_{G,\mathcal{V}}[k] + \delta\mathbf{P}_{D,\mathcal{V}}[k] \quad k = 0,\dots,N_p-1 \tag{4.5b}$$

$$\Delta\mathbf{f}[k] = \mathbf{X}_b^{-1}\mathbf{A}^{\mathbf{T}}\,\Delta\boldsymbol{\theta}[k] \quad k = 0,\dots,N_p-1 \tag{4.5c}$$

$$-\mathbf{f}_{\max,\mathcal{E}} - \mathbf{s}[k] \le \mathbf{f}_{\mathcal{E}}[k] \le \mathbf{f}_{\max,\mathcal{E}} + \mathbf{s}[k] \quad k = 1,\dots,N_p \tag{4.5d}$$

$$-\mathbf{R}_{\mathcal{V}} \le \delta\mathbf{P}_{G,\mathcal{V}}[k] \le 0 \quad k = 0,\dots,N_p-1 \tag{4.5e}$$

$$\delta\mathbf{P}_{D,\mathcal{V}}[k] \le 0 \quad k = 0,\dots,N_p-1 \tag{4.5f}$$

$$\Delta\mathbf{P}_{G,\mathcal{V}}[k] \ge -\mathbf{P}_{G,\mathcal{V}}[0^-] \quad k = N_p-1 \tag{4.5g}$$

$$\Delta\mathbf{P}_{D,\mathcal{V}}[k] \ge -\mathbf{P}_{D,\mathcal{V}}[0^-] \quad k = N_p-1 \tag{4.5h}$$

$$\mathbf{s}[k] \ge 0 \quad k = 1,\dots,N_p \tag{4.5i}$$

$$\delta\theta_i[k] = 0 \quad k = 1,\dots,N_p, i \in \Omega_{\text{ref}} \tag{4.5j}$$

where $\mathbf{c}_1$ and $\mathbf{c}_2$ denote the cost of load shedding and overload, respectively. The set of all lines connected to all buses in $\mathcal{V}$, for which agent i has received flow information, are denoted by $\mathbf{f}_{\mathcal{E}}$. The vector of initial load and generation is represented by $\mathbf{P}_{D,\mathcal{V}}[0^-]$ and $\mathbf{P}_{G,\mathcal{V}}[0^-]$, respectively, which are equal to the value of load/generation measured one step before the current time $k = 0$. Other variables are the same as the central emergency problem (4.1) with the difference that a subscript $\mathcal{V}$ includes only the variables for the local buses in $\mathcal{V}$ or the lines $\mathcal{E}$ connected to them. For example, $\mathbf{R}_{\mathcal{V}}$ denotes ramping rates for all buses in $\mathcal{V}$. In the objective function, the idea is to penalize overloads more severe than load shedding to implement soft constraints for overloads. Loads could have different shedding costs based on their importance. In our simulations, we typically set $c_{1,i} = 1$ and $c_{2,j} = 1000$.

Note that size of the distributed problem is much smaller than the central problem in both the number of variables and constraints, and the difference in the time it takes to solve

the problem over multiple time steps in a time horizon is noticeable for a realistically sized network. The variables are defined only on a local neighborhood, which also reduces the number of constraints in (4.5e–4.5h). In addition, the overload constraints in (4.5d,4.5i) are defined in a smaller neighborhood $\mathcal{E}$. Section 4.5 explains the simulation results for the distributed approach and compares the results with the centralized controller in terms of solution quality.

4.5 Results

The emergency control algorithm from Fig. 4.2 is incorporated in both dc and ac cascading failure simulators after Step 5, where power flow is solved (see Fig. 1.2 for dc and Fig. 3.4 for ac simulator). This section illustrates the results of simulation on a model of the 2004 winter peak Polish power system, which is available with MATPOWER [46]. This test system has 2896 branches (transmission lines and transformers) and 2383 buses. The reader can refer to Chapter 2 for details regarding how this system was initially dispatched and how failure probabilities were computed to estimate blackout risk. The data for this system is available online [48].

As described earlier, the agents in the distributed controller communicate with the nodes in their local neighborhood that are N_{hop} away from them counting the number of branches as hops. They also include them in their optimization problem and might request them to change their control variables if their solution to the control problem requires that. Fig. 4.3 shows the distribution of the number neighbors for all nodes in the Polish power network. It is interesting to note that the maximum number of neighbors grows rapidly for as N_{hop} gets larger, which causes the variance to be much higher for larger N_{hop}.

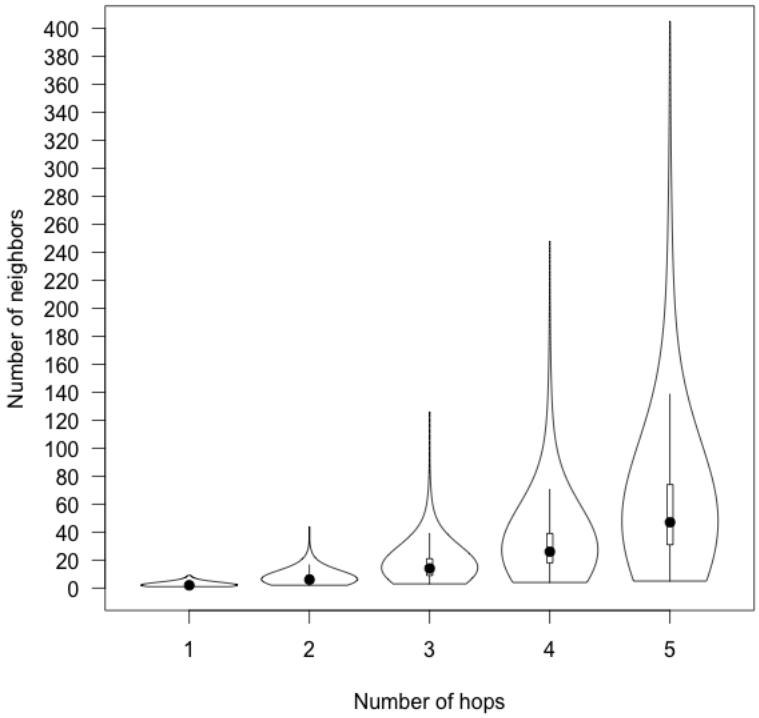

Figure 4.3: Violin plot of the number of neighbors for all nodes in the Polish network. Black dots show the median, while the boxes show 25^{th} to 75^{th} percentiles, and the black lines show the range of data without outliers. The density of data is also shown vertically for each case.

4.5.1 Illustration of the distributed controller

To illustrate how the distributed control operates, we look at one simulation example here before looking at how the method works overall for a larger set of initiating outages. Fig. 4.4 shows how blackout size changes in time for an initiating $N-2$ contingency, namely, outage of branches 23 and 855 in the system using ACSimSep. Panel (a) of Fig. 4.4 demonstrates how the current magnitude of a subset of highly loaded branches decreases gradually over time, while panels (b) and (c) show blackout size in terms of demand loss and number of branch outages, respectively. For comparison, outage of the same contingency is implemented without having any corrective control in the system. Fig. 4.5 shows the results with no control. The system is clearly more stressed without the controller, which ultimately results in a much larger blackout in terms of both the Megawatts of demand loss and the number of tripped branches.

4.5.2 Overall performance of distributed emergency controller

To determines if the distributed controller is advantageous, we need to look at its performance for a number of cascading failure cases, and compare results with cases that have a centralized controller or no controller at all. To do so, we found 7784 $n-2$ contingencies that caused some overload in the Polish system, and randomly selected 1000 of these to build our reference set of contingencies. Figs. 4.6 and 4.7 show results of simulating the multi-agent system with the dc and ac simulators, respectively. Different cases include no control, distributed controller with $N_{\text{hop}} = 1, \ldots, 4$ $(D_1, \ldots, D_4)$ and the centralized controller.

As the size of neighborhood in the multi-agent controller grows, blackout sizes reduce in both the dc and ac simulators. For both simulators a neighborhood of $N_{\text{hop}} = 4$ gives similar results to a central controller that needs substantially more communication and computation. The difference in size of computations becomes highly noticeable when solving

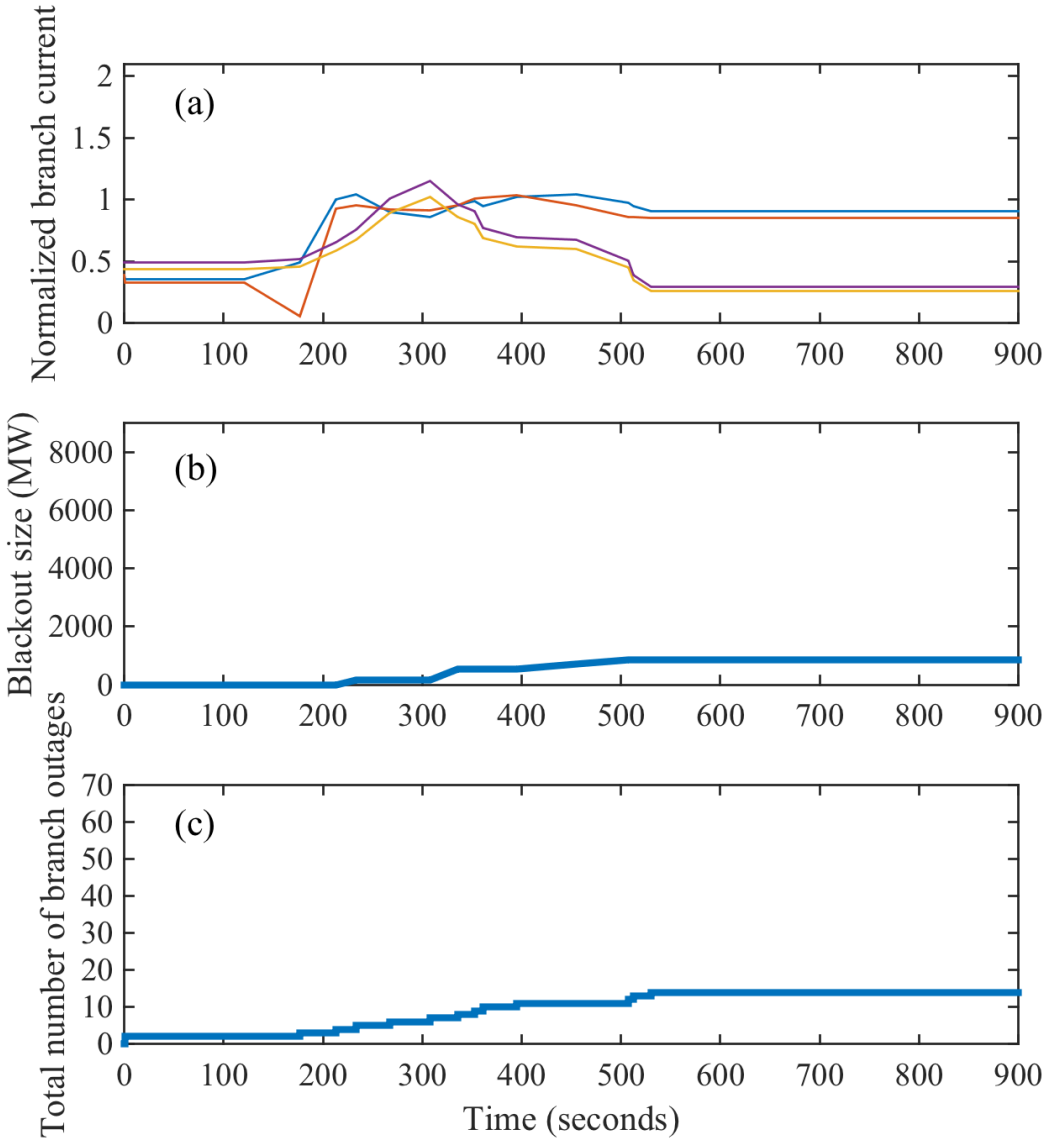

Figure 4.4: Simulation of a cascading failure initiated by an $n-2$ contingency (outage of branches 23 and 855) in the Polish grid when the distributed emergency controller with $N_{hop} = 4$ and time horizon of $N_p = 3$ is active. (a) Current magnitude of a subset of branches normalized over long-term emergency line rating. The subset is the lines that violate their rating during simulation and have average current magnitude higher than 80% of their flow limit. (b) Total demand that cannot be supplied in the process of the cascade. (c) Number of branch outages in the cascade.

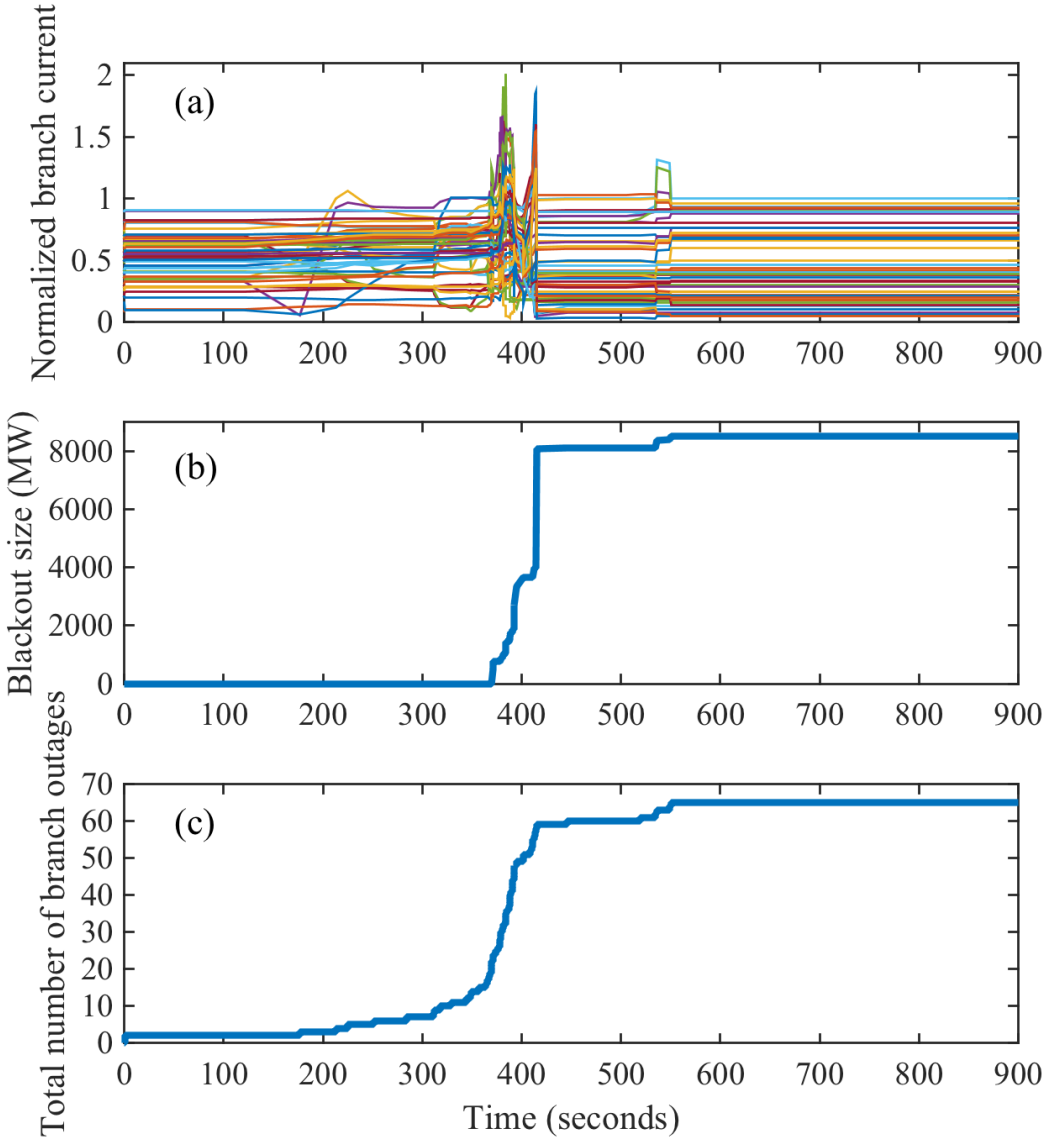

Figure 4.5: Simulation of a cascading failure initiated by an $n-2$ contingency (outage of branches 23 and 855) in the Polish grid with no control. (a) Current magnitude of a subset of branches normalized over long-term emergency line rating. The criteria to choose the subset is the same as Fig. 4.4. (b) Total demand that cannot be supplied in the process of the cascade. (c) Number of branch outages in the cascade.

the optimization over a time horizon in an MPC framework.

A trade-off exists in the distributed controller between the solution quality and the communication burden. To compare the communication burden between different multi-agent cases, we counted the number of messages that need to be sent or received among agents during the simulations. For each agent, the maximum number of messages sent/received (per iteration) were recorded during each cascade simulation. Fig. 4.8 shows the distribution of maximum number of messages for all agents. Note that two iterations of the cascade simulation are a maximum 60 seconds apart. If an outage is going to occur earlier than 60 seconds, the simulator reduces the amount of time until the next iteration. However, control actions are not implemented unless at least 60 seconds has passed from the previous control actions. Therefore, these number of messages are all that needs to be communicated in a time not less than one minute. If an agent is solving an emergency control problem, it gathers information from all its local agents; this gathering requires two messages. Furthermore, the agent needs to check available capacities after it solves its local problem and make sure that it knows the control actions that are requested in that same iteration by other agents from the local agent. So, this involves another two messages for both the sender and responder. In the end, the solving agent will send the required control change to its local agents, which counts as one message for both sender and receiver. Fig. 4.8 demonstrates that there are a few cases where one agent sends/receives many more messages compared with most of the cases where many fewer messages are required for the scheme to work effectively.

4.6 Conclusions

This chapter proposed a distributed predictive emergency control method, in which agents find load shedding and generator reduction to reduce overloads. The agents solve their problem over a time horizon—inspired by Model Predictive Control—and have limited

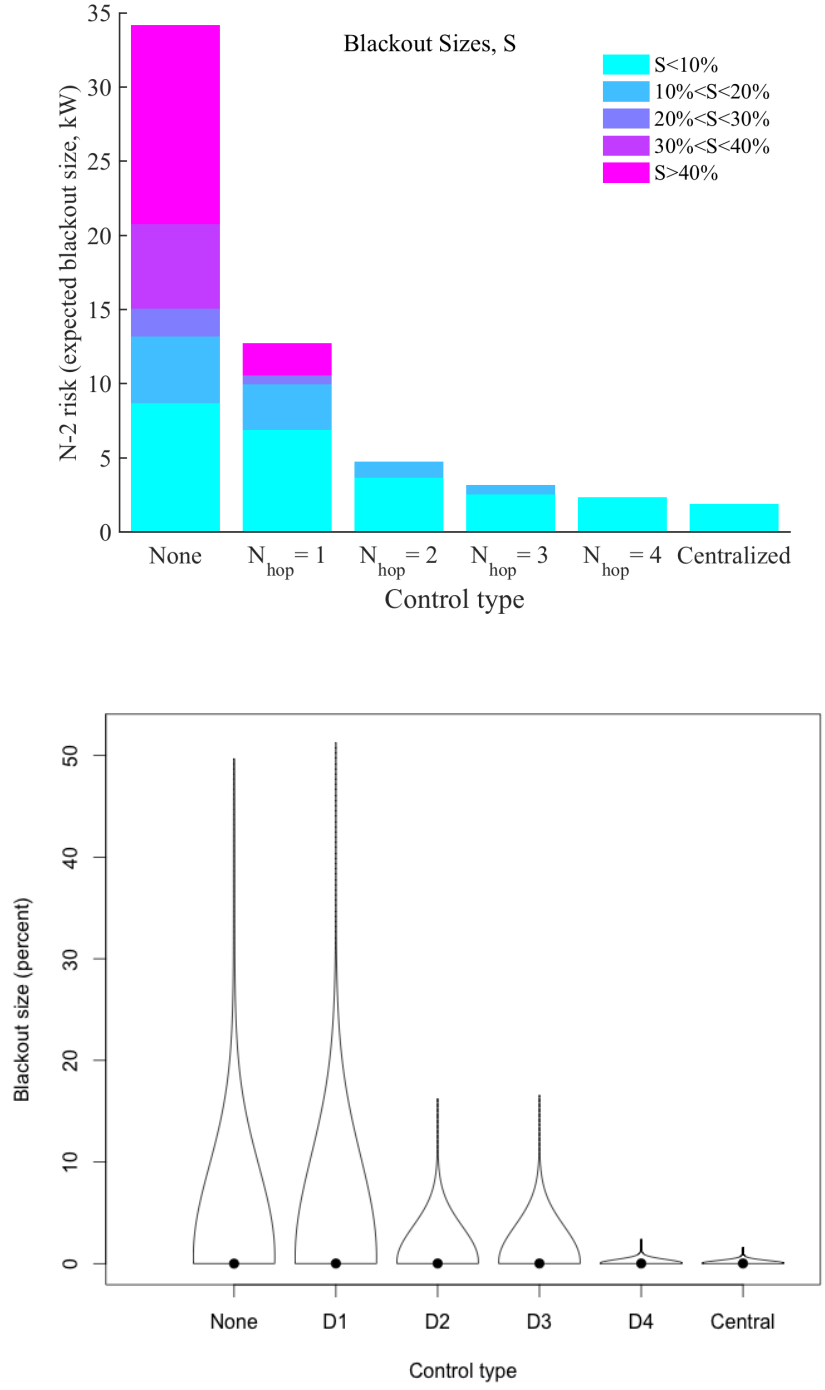

Figure 4.6: Simulation of a subset of $n-2$ contingencies in the Polish system with no control, distributed control and central control using DCSimSep. Distributed control cases are labeled D_1 to D_4, where the subscript shows the number of hops N_{hop} in the local neighborhood of agents. (a) Blackout risk for different blackout size ranges. (b) Violin plot of blackout sizes.

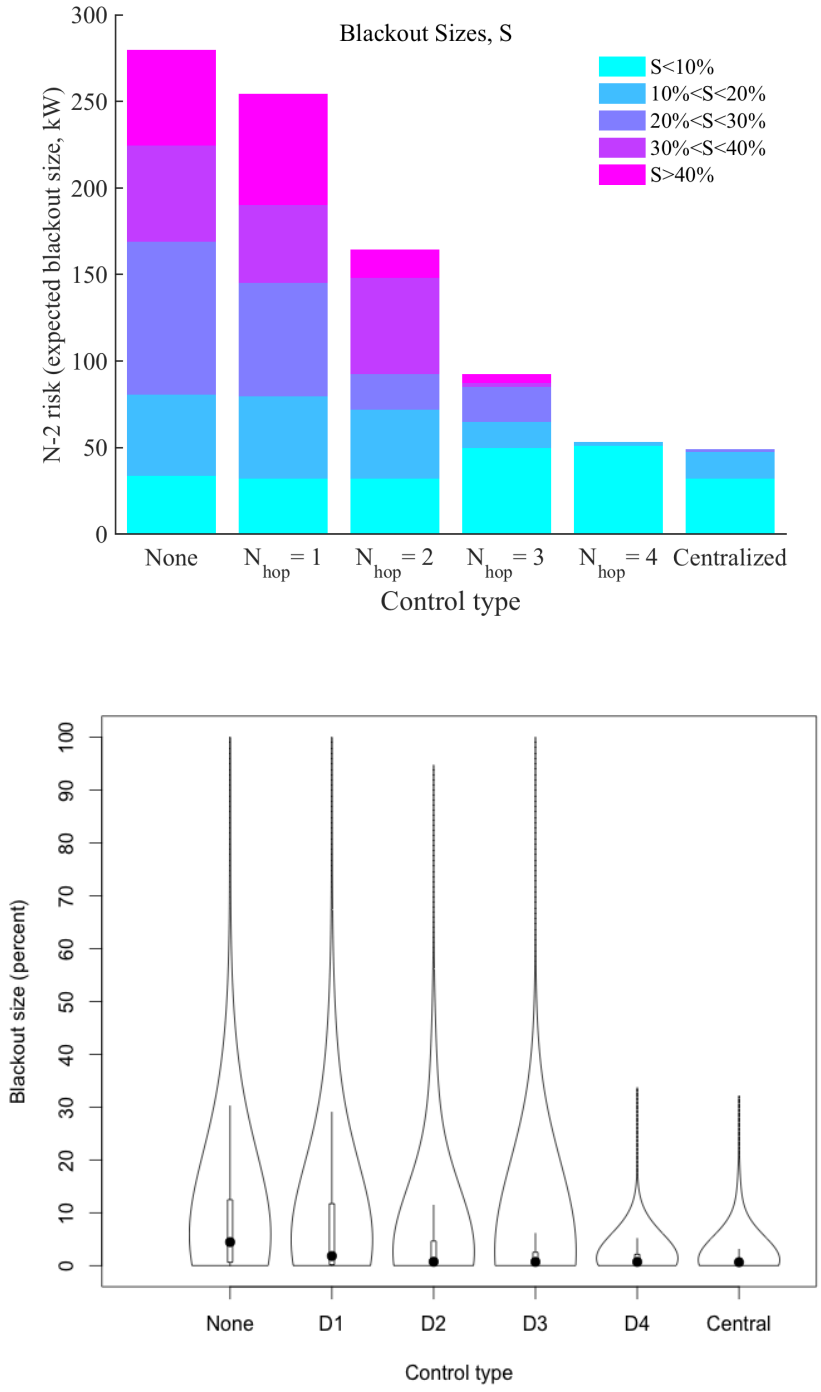

Figure 4.7: Simulation of a subset of $n-2$ contingencies in the Polish system with no control, distributed control and central control using ACSimSep. Distributed control cases are labeled D_1 to D_4, where the subscript shows the number of hops N_{hop} in the local neighborhood of agents. (a) Blackout risk for different blackout size ranges. (b) Violin plot of blackout sizes.

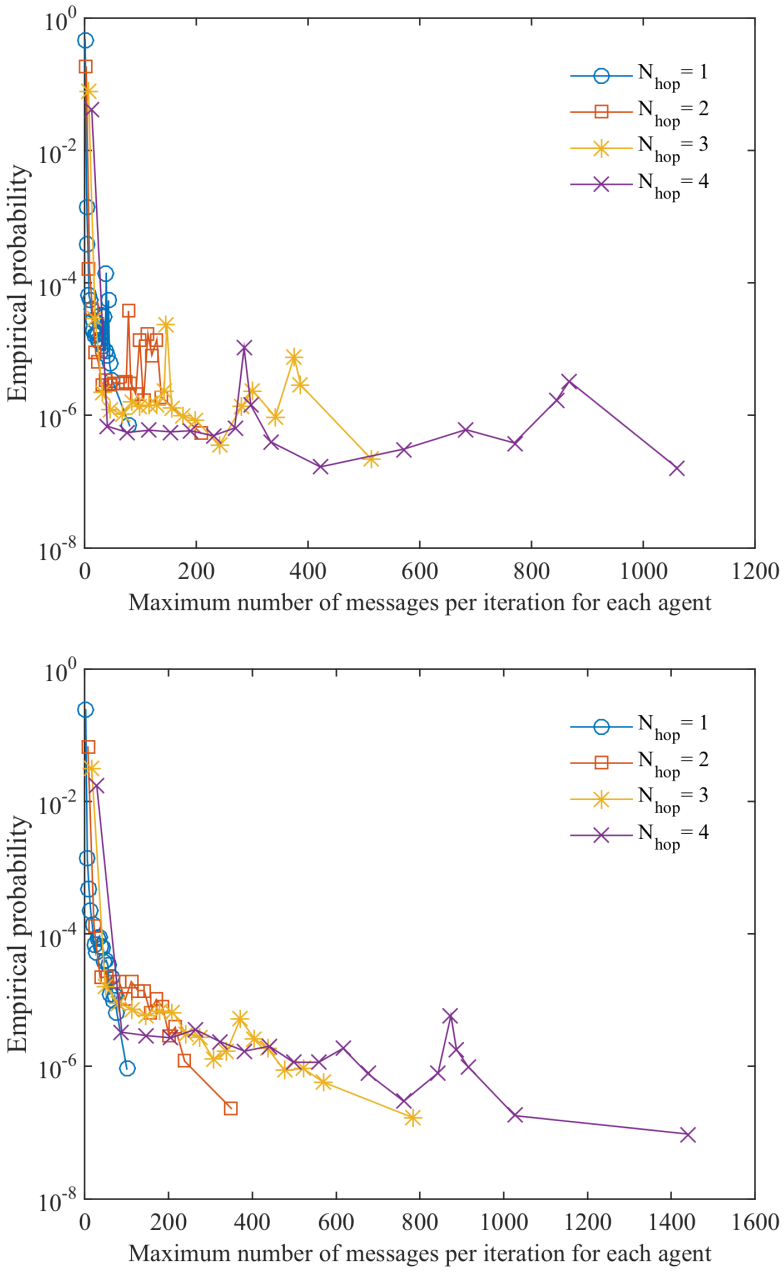

Figure 4.8: Distribution of maximum (over iterations of a simulation) number of messages sent/received by each agent per iteration in all simulations

information and authority, compared with a centralized method. Simulation results for a model of a large-scale power grid model show that the distributed method can provide high quality solutions as long as their control neighborhood is large enough. In the Polish system, a control/information neighborhood of buses that are maximum four branches away from a solving agent (bus) is enough to yield similar results to a centralized controller. Future work will study the impacts of selecting neighborhoods based on electrical properties rather than topological distances.

Chapter 5

Conclusions and Future Work

Despite substantial advances in communication, information and control technology, large blackouts still occur relatively frequently. This is because power systems are complex dynamical systems with many components that are interacting and sometimes working very close to their limits. Advanced information technology tools, which are important components of smart grid, facilitate new ways to operate a power system more efficiently and reliably. However, they may also contribute to new ways that the system could fail. Thus we need to understand and mitigate failures in power grids. Most of the time, power system outages are limited to one, or at most a few neighborhoods. However, failures occasionally cascade to become large blackouts. This dissertation focuses on cascading failures in a power network.

To understand how a cascade may propagate, we need accurate simulation tools, as we cannot experiment with a real power system for obvious reasons. Chapter 1 of the dissertation reviews current simulators in the literature, and explains in more detail, DCSimSep, a simulator based on dc power flow model. This simulator is then used in Chapter 2, in which a novel and efficient method is proposed to estimate cascading failure risk based on a search algorithm called Random Chemistry. The method was shown to be at least two orders of magnitude faster than a conventional Monte-Carlo simulation in estimating risk

for two test systems including a real large-scale power grid. Using this method one could efficiently estimate how risk changes by load level in a power system. Interestingly, risk does not grow monotonically as load increases when the initial system is dispatched using an $n-1$ security constrained optimal power flow. In addition, the method can identify critical components in the system and then suggest preventive measures for reducing risk. For example, more aggressive maintenance strategies that could reduce failure probabilities by half for the three most critical transmission lines in a model of the Polish grid could reduce risk by 33%. Another way to reduce risk is to reduce flows on critical transmission lines. For instance, reducing ratings by half for the three critical lines in the same system could reduce risk by 61%.

Using the dc power flow equations to simulate cascading failures is useful to quickly estimate risk, since dc power flow always provides a solution to the system of equations. However, the ac power flow equations are a more accurate and widely accepted model of power system operation. The challenge in using an ac simulator is that under stressed conditions no solution exists to the ac power flow equations. This lack of solution translates into a phenomenon known as voltage collapse in a power system. To overcome these cases, Chapter 3 of this dissertation proposes an effective method to shed load and reduce system stress so that the equations have a solution again. This solution is taken as the next operating point of the system to continue the simulation. Chapter 3 also shows the impact of using an ac simulator on cascading failure risk. The risk now includes blackouts due to voltage collapse in addition to previous risk, which was only due to imbalanced generation and load.

Other than preventive measures for reducing risk, it is also possible to design corrective control methods to reduce blackout size after some overloads in the system. This dissertation focuses on optimal load shedding and generator reduction before a cascade propagates. After-the-fact analysis of many historical cascading failures, such as the 2003 Northeast

blackout, suggested that a smaller targeted load shedding could mitigate a large blackout. Accordingly, Chapter 4 proposes a distributed receding horizon emergency control strategy that can give high quality solutions without a need to large amount of communication and computation required by a central controller. The controller is based on the dc optimal power flow method, but it could work on an ac system as well, because it incorporates change of power system variables. This chapter shows how the method can reduce the overall size of blackouts using both the dc and ac simulators. Depending on the size of control neighborhoods in the distributed controller, the amount of communications required for the method can vary, but they are all well within the capabilities of modern communication networks.

There are a number of different ways that the work in this dissertation could be extended. The current ac simulator provides one way to simulate blackouts due to imbalanced generation and load situation in addition to voltage collapse conditions. As discussed earlier, cascades involve many mechanisms. Some, but not all of these can be modeled using steady state power flow equations. For example, some methods are proposed in the literature to estimate system frequency based on steady state equations. And so the simulator could potentially be extended to model frequency instability cases.

The Random Chemistry risk estimation method has primarily been tested with the dc simulator presented in this dissertation. The same power grid model appears to have higher cascading failure risk (more ways to produce large blackouts) when measured with the ac simulator, because of the capability to model voltage collapse. Whether or not the Random Chemistry method is still efficient with an ac simulator when a larger number of contingencies exist is an open question. Some additional strategies may be required to maintain the efficiency of the risk estimation approach given the larger number of potential failure modes.

Additionally, the proposed risk estimation method works well if we assume that initiating

outages are independent. However, in many cases, triggering events may be correlated. For example storms may cause failures in a number of elements that are geographically close. Correlated outages typically increase the probability of simultaneous events relative to the computations in this dissertation. Thus the estimated risk in our works is close to a lower bound for the actual risk in a system. Incorporating correlated outages in estimating risk remains for future work.

This dissertation suggests some ideas for mitigating risk, given the risk estimate provided by Random Chemistry. Other approaches that translate the information from the risk estimate to identify direct actionable strategies that reduce risk is another topic for future study.

The proposed distributed controller is based on dc optimal power flow. A more accurate linearization of ac power flow equations, such as using the first order terms in power flow jacobian, could provide better solutions in mitigating cascades.

The proposed controller models makes use of only one negotiation scheme. Many other negotiation strategies exist that could potentially improve solution quality, but identifying the most effective method requires further tests and comparisons in both the resulting blackout sizes and communication burden.

Finally, the current controller uses topological distance between nodes in the power system to form local control and communication neighborhoods. The control can potentially be more effective if the neighborhoods are determined based on electrical properties of the network. For example, the Power Transfer Distribution Factor (PTDF) matrix, which gives an estimate of change of flows with injection on nodes, might be useful in setting the local neighborhoods.

Bibliography

[1] , "Final Report on the August 14, 2003 Blackout in the United States and Canada," tech. rep., US-Canada Power System Outage Task Force, April 2004.

[2] D. J. Prezant, J. Clair, S. Belyaev, D. Alleyne, G. I. Banauch, M. Davitt, K. Vandervoorts, K. J. Kelly, B. Currie, and G. Kalkut, "Effects of the august 2003 blackout on the New York City healthcare delivery system: a lesson for disaster preparedness," *Critical Care Medicine*, vol. 33, no. 1, pp. S96–S101, 2005.

[3] "Arizona-Southern California outages on September 8, 2011," tech. rep., FERC and NERC, 2012.

[4] M. Vaiman, K. Bell, Y. Chen, B. Chowdhury, I. Dobson, P. Hines, M. Papic, S. Miller, and P. Zhang, "Risk assessment of cascading outages: Methodologies and challenges," *IEEE Transactions on Power Systems*, vol. 27, no. 2, pp. 631– 641, 2012.

[5] P. Hines, J. Apt, and S. Talukdar, "Large blackouts in North America: Historical trends and policy implications," *Energy Policy*, vol. 37, pp. 5249–5259, 2009.

[6] A. Clauset, C. Shalizi, and M. Newman, "Power-law distributions in empirical data," *SIAM Review*, vol. 51, no. 4, pp. 661–703, 2009.

[7] D. Newman, B. Carreras, V. Lynch, and I. Dobson, "Exploring complex systems aspects of blackout risk and mitigation," *IEEE Transactions on Reliability*, vol. 60, no. 1, pp. 134 –143, 2011.

[8] D. Kosterev, C. Taylor, and W. Mittelstadt, "Model validation for the August 10, 1996 WSCC system outage," *IEEE Transactions on Power Systems*, vol. 14, pp. 967 – 979, 1999.

[9] J. Song, E. Cotilla-Sanchez, P. D. H. Hines, and G. Ghanavati, "Dynamic modeling of cascading failure in power systems," *IEEE Transactions on Power Systems*, vol. (in review, preprint: arXiv:1411.3990), 2015.

[10] M. Panteli and D. S. Kirschen, "Situation awareness in power systems: Theory, challenges and applications," *Electric Power Systems Research*, vol. 122, pp. 140–151, 2015.

[11] P. Hines, E. Cotilla-Sanchez, and S. Blumsack, "Do topological models provide good information about vulnerability in electric power networks?," *Chaos: An interdisciplinary journal of non-linear science*, vol. 20, no. 3, 2010.

[12] WSCC Operations Committee, "Western Systems Coordinating Council Disturbance Report For the Power System Outages that Occurred on the Western Interconnection on July 2, 1996 and July 3, 1996," tech. rep., Western Systems Coordinating Council, 1996.

[13] B. A. Carreras *et al.*, "Critical points and transitions in an electric power transmission model for cascading failure blackouts," *Chaos: An interdisciplinary journal of nonlinear science*, vol. 12, no. 4, pp. 985–994, 2002.

[14] M. Eppstein and P. Hines, "A "Random Chemistry" algorithm for identifying collections of multiple contingencies that initiate cascading failure," *IEEE Transactions on Power Systems*, vol. 27, no. 3, pp. 1698–1705, 2012.

[15] J. Qi, S. Mei, and F. Liu, "Blackout model considering slow process," *IEEE Transactions on Power Systems*, vol. 28, pp. 3274–3282, Aug 2013.

[16] R. Pfitzner, K. Turitsyn, and M. Chertkov, "Statistical classification of cascading

failures in power grids," in *IEEE Power and Energy Society General Meeting*, pp. 1–8, July 2011.

[17] M. Rahnamay-Naeini, Z. Wang, N. Ghani, A. Mammoli, and M. Hayat, "Stochastic analysis of cascading-failure dynamics in power grids," *IEEE Transactions on Power Systems*, vol. 29, pp. 1767–1779, July 2014.

[18] D. P. Nedic, I. Dobson, D. S. Kirschen, B. A. Carreras, and V. E. Lynch, "Criticality in a cascading failure blackout model," *International Journal of Electrical Power and Energy Systems*, vol. 28, no. 9, pp. 627–633, 2006.

[19] Q. Chen and L. Mili, "Composite power system vulnerability evaluation to cascading failures using importance sampling and antithetic variates," *IEEE Transactions on Power Systems*, vol. 28, no. 3, pp. 2321–2330, 2013.

[20] S. Mei, Y. Ni, G. Wang, and S. Wu, "A study of self-organized criticality of power system under cascading failures based on ac-opf with voltage stability margin," *IEEE Transactions on Power Systems*, vol. 23, pp. 1719 – 1726, Nov. 2008.

[21] P. Henneaux, P.-E. Labeau, and J.-C. Maun, "Blackout probabilistic risk assessment and thermal effects: Impacts of changes in generation," *IEEE Transactions on Power Systems*, vol. 28, pp. 4722–4731, Nov 2013.

[22] D. Mazauric, S. Soltan, and G. Zussman, "Computational analysis of cascading failures in power networks," in *Proceedings of the ACM SIGMETRICS/International Conference on Measurement and Modeling of Computer Systems*, SIGMETRICS '13, (New York, NY, USA), pp. 337–338, ACM, 2013.

[23] E. G. Cate, K. Hemmaplardh, J. W. Manke, and D. Gelopulos, "Time frame notion and time response of the models in transient, mid-term and long-term stability programs," *IEEE Transactions on Power Apparatus and Systems*, vol. PAS-103, pp. 143–151, Jan 1984.

[24] I. Roytelman and S. Shahidehpour, "A comprehensive long term dynamic simulation for power system recovery," *IEEE Transactions on Power Systems*, vol. 9, pp. 1427–1433, Aug 1994.

[25] B. Stott, J. Jardim, and O. Alsac, "Dc power flow revisited," *IEEE Transactions on Power Systems*, vol. 24, no. 3, pp. 1290 – 1300, 2009.

[26] P. Rezaei, P. Hines, and M. Eppstein, "Estimating cascading failure risk with random chemistry," *IEEE Transactions on Power Systems*, vol. 30, pp. 2726–2735, Sept 2015.

[27] NERC Standard TOP-004-2, *Transmission Operations*, 2007.

[28] R. N. Allan and R. Billinton, *Reliability Evaluation of Power Systems*. Plenum Press, 1996.

[29] C. Borges, D. Falcao, J. Mello, and A. Melo, "Composite reliability evaluation by sequential Monte Carlo simulation on parallel and distributed processing environments," *IEEE Transactions on Power Systems*, vol. 16, no. 2, pp. 203–209, 2001.

[30] R. Billinton and A. Jonnavithula, "Composite system adequacy assessment using sequential Monte Carlo simulation with variance reduction techniques," *IEE Proceedings-Generation, Transmission and Distribution*, vol. 144, no. 1, pp. 1–6, 1997.

[31] C. Singh and J. Mitra, "Composite system reliability evaluation using state space pruning," *IEEE Transactions on Power Systems*, vol. 12, no. 1, pp. 471–479, 1997.

[32] A. Leite da Silva, L. da Fonseca Manso, J. De Oliveira Mello, and R. Billinton, "Pseudo-chronological simulation for composite reliability analysis with time varying loads," *IEEE Transactions on Power Systems*, vol. 15, no. 1, pp. 73–80, 2000.

[33] A. Leite da Silva, L. de Resende, L. da Fonseca Manso, and V. Miranda, "Composite reliability assessment based on Monte Carlo simulation and Artificial Neural

Networks," *IEEE Transactions on Power Systems*, vol. 22, no. 3, pp. 1202–1209, 2007.

[34] B. Carreras, D. Newman, I. Dobson, and A. Poole, "Initial evidence for self-organized criticality in electric power system blackouts," in *Proceedings of the 33rd Annual Hawaii International Conference on System Sciences*, Jan 2000.

[35] I. Dobson, B. Carreras, and D. Newman, "How many occurrences of rare blackout events are needed to estimate event probability?," *IEEE Transactions on Power Systems*, vol. 28, pp. 3509–3510, Aug 2013.

[36] O. A. Mousavi, R. Cherkaoui, and M. Bozorg, "Blackouts risk evaluation by Monte Carlo simulation regarding cascading outages and system frequency deviation," *Electric Power Systems Research*, vol. 89, no. 0, pp. 157 – 164, 2012.

[37] D. Kirschen, D. Jayaweera, D. Nedic, and R. Allan, "A probabilistic indicator of system stress," *IEEE Transactions on Power Systems*, vol. 19, pp. 1650–1657, Aug 2004.

[38] J. Chen, J. S. Thorp, and I. Dobson, "Cascading dynamics and mitigation assessment in power system disturbances via a hidden failure model," *International Journal of Electrical Power & Energy Systems*, vol. 27, no. 4, pp. 318–326, 2005.

[39] J. Kim, J. Bucklew, and I. Dobson, "Splitting method for speedy simulation of cascading blackouts," *IEEE Transactions on Power Systems*, vol. 28, no. 3, pp. 3010–3017, 2013.

[40] H. Ren and I. Dobson, "Using transmission line outage data to estimate cascading failure propagation in an electric power system," *IEEE Transactions on Circuits and Systems–II: Express Briefs*, vol. 55, no. 9, pp. 927–931, 2008.

[41] I. Dobson, "Estimating the propagation and extent of cascading line outages from utility data with a branching process," *IEEE Transactions on Power Systems*,

vol. 27, no. 4, pp. 2146–2155, 2012.

[42] P. Rezaei, P. Hines, and M. Eppstein, "Estimating cascading failure risk: Comparing Monte Carlo sampling and random chemistry," in *IEEE Power and Energy Society General Meeting*, pp. 1–5, July 2014.

[43] P. Rezaei and P. Hines, "Changes in cascading failure risk with generator dispatch method and system load level," in *IEEE PES Transmission and Distribution Conference and Exposition*, pp. 1–5, 2014.

[44] W. G. Cochran, *Sampling Techniques*. Wiley, 2nd ed., 1963.

[45] C. Grigg, P. Wong, P. Albrecht, R. Allan, M. Bhavaraju, R. Billinton, Q. Chen, C. Fong, S. Haddad, S. Kuruganty, W. Li, R. Mukerji, D. Patton, N. Rau, D. Reppen, A. Schneider, M. Shahidehpour, and C. Singh, "The ieee reliability test system-1996. a report prepared by the reliability test system task force of the application of probability methods subcommittee," *IEEE Transactions on Power Systems*, vol. 14, no. 3, pp. 1010–1020, 1999.

[46] R. Zimmerman, C. Murillo-Sánchez, and R. Thomas, "MATPOWER: Steady-state operations, planning, and analysis tools for power systems research and education," *IEEE Transactions on Power Systems*, vol. 26, pp. 12 –19, feb. 2011.

[47] "http://www.eia.gov/."

[48] "https://github.com/phines/dcsimsep/blob/master/data/ps_polish_all.mat."

[49] "https://github.com/phines/dcsimsep/blob/master/data/ps_RTS_all_modified_gencost.mat."

[50] P. Hines, "DCSimSep: A simulator of cascading separation in power grids. https://github.com/phines/dcsimsep."

[51] P. Rezaei, M. J. Eppstein, and P. D. H. Hines, "Rapid assessment, visualization and

mitigation of cascading failure risk in power systems," in *Proc. of the 48th Annual Hawaii International Conference on System Sciences*, Jan 2015.

[52] H. Liao, J. Apt, and S. Talukdar, "Phase transitions in the probability of cascading failures," in *Electricity Transmission in Deregulated Markets: Conference at Carnegie Mellon University*, (Pittsburgh, PA), 2004.

[53] "https://github.com/phines/dcsimsep/blob/master/data/ps_RTS_all_proportional_dispatch.mat."

[54] M. J. Eppstein, J. L. Payne, B. C. White, and J. H. Moore, "Genomic mining for complex disease traits with "Random Chemistry"," *Genetic Programming and Evolvable Machines*, vol. 8, no. 4, pp. 395–411, 2007.

[55] Y. Li and J. McCalley, "Decomposed scopf for improving efficiency," *IEEE Transactions on Power Systems*, vol. 24, no. 1, pp. 494–495, 2009.

[56] A. J. Wood and B. F. Wollenberg, *Power Generation, Operation and Control*. Wiley, 1996.

[57] M. Almassalkhi and I. Hiskens, "Model-predictive cascade mitigation in electric power systems with storage and renewables–part i: Theory and implementation," *IEEE Transactions on Power Systems*, vol. 30, pp. 67–77, Jan 2015.

[58] M. Almassalkhi and I. Hiskens, "Model-predictive cascade mitigation in electric power systems with storage and renewables–part ii: Case-study," *IEEE Transactions on Power Systems*, vol. 30, pp. 78–87, Jan 2015.

[59] J. E. Tate and T. J. Overbye, "A comparison of the optimal multiplier in polar and rectangular coordinates," *IEEE Transactions on Power Systems*, vol. 20, no. 4, pp. 1667–1674, 2005.

[60] A. Bergen and V. Vittal, *Power Systems Analysis*. Pearson/Prentice Hall, 2000.

[61] S. Iwamoto and Y. Tamura, "A load flow calculation method for ill-conditioned power

systems," *IEEE Transactions on Power Apparatus and Systems*, no. 4, pp. 1736–1743, 1981.

[62] T. J. Overbye, "A power flow measure for unsolvable cases," *IEEE Transactions on Power Systems*, vol. 9, no. 3, pp. 1359–1365, 1994.

[63] W. H. Press, S. A. Teukolsky, W. T. Vetterling, and B. P. Flannery, *Numerical recipes in C*, vol. 2. Cambridge university press Cambridge, 1996.

[64] M. Ćalović and V. Strezoski, "Calculation of steady-state load flows incorporating system control effects and consumer self-regulation characteristics," *International Journal of Electrical Power and Energy Systems*, vol. 3, no. 2, pp. 65 – 74, 1981.

[65] I. Dobson, "Observations on the geometry of saddle node bifurcation and voltage collapse in electrical power systems," *IEEE Transactions on Circuits and Systems I: Fundamental Theory and Applications*, vol. 39, pp. 240 –243, mar 1992.

[66] I. Dobson and L. LIMING, "Computing an optimum direction in control space to avoid saddle node bifurcation and voltage collapse in electric power systems," *IEEE Transactions on Automatic Control*, vol. 37, no. 10, pp. 1616–1620, 1992.

[67] T. J. Overbye, "Computation of a practical method to restore power flow solvability," *IEEE Transactions on Power Systems*, vol. 10, no. 1, pp. 280–287, 1995.

[68] I. Hiskens and R. J. Davy, "Exploring the power flow solution space boundary," *IEEE Transactions on Power Systems*, vol. 16, no. 3, pp. 389–395, 2001.

[69] M. Begovic, D. Novosel, D. Karlsson, C. Henville, and G. Michel, "Wide-area protection and emergency control," *Proceedings of the IEEE*, vol. 93, no. 5, pp. 876–891, 2005.

[70] "Final report of the investigation committee on the 28 september 2003 blackout in italy," tech. rep., Union for the Co-ordination of Transmission of Electricity, 2004.

[71] P. Anderson and M. Mirheydar, "An adaptive method for setting underfrequency load

shedding relays," *IEEE Transactions on Power Systems*, vol. 7, pp. 647–655, May 1992.

[72] V. Chuvychin, N. Gurov, S. Venkata, and R. Brown, "An adaptive approach to load shedding and spinning reserve control during underfrequency conditions," *IEEE Transactions on Power Systems*, vol. 11, pp. 1805–1810, Nov 1996.

[73] H. You, V. Vittal, and Z. Yang, "Self-healing in power systems: an approach using islanding and rate of frequency decline-based load shedding," *IEEE Transactions on Power Systems*, vol. 18, pp. 174–181, Feb 2003.

[74] V. Terzija, "Adaptive underfrequency load shedding based on the magnitude of the disturbance estimation," *IEEE Transactions on Power Systems*, vol. 21, pp. 1260–1266, Aug 2006.

[75] H. Seyedi and M. Sanaye-Pasand, "New centralised adaptive load-shedding algorithms to mitigate power system blackouts," *Generation, Transmission Distribution, IET*, vol. 3, pp. 99–114, January 2009.

[76] D. Bienstock, "Optimal control of cascading power grid failures," in *50th IEEE conference on Decision and control and European control conference (CDC-ECC)*, pp. 2166–2173, IEEE, 2011.

[77] D. Bienstock and G. Grebla, "Robust control of cascading power grid failures using stochastic approximation," 04 2015.

[78] P. Hines, *A Decentralized Approach to Reducing the Social Costs of Cascading Failures*. PhD thesis, Carnegie Mellon University, 2007.

[79] J. M. Maciejowski, *Predictive control: with constraints*. Pearson education, 2002.

[80] F. Borrelli, A. Bemporad, and M. Morari, *Predictive control for linear and hybrid systems*. Cambridge University Press, 2011, In press (version updated: April 22, 2014).

[81] E. F. Camacho and C. B. Alba, *Model predictive control*. Springer Science & Business Media, 2013.

[82] J. Richalet, A. Rault, J. Testud, and J. Papon, "Model predictive heuristic control: Applications to industrial processes," *Automatica*, vol. 14, no. 5, pp. 413–428, 1978.

[83] E. F. Camacho and C. Bordons, *Model predictive control in the process industry*. Springer Science & Business Media, 2012.

[84] M. Zima and G. Andersson, "Model predictive control employing trajectory sensitivities for power systems applications," in *Decision and Control, 2005 and 2005 European Control Conference. CDC-ECC'05. 44th IEEE Conference on*, pp. 4452–4456, IEEE, 2005.

[85] G. Valverde and T. Van Cutsem, "Model predictive control of voltages in active distribution networks," *IEEE Transactions on Smart Grid*, vol. 4, no. 4, pp. 2152–2161, 2013.

[86] A. Kassem and A. Abdelaziz, "Reactive power control for voltage stability of standalone hybrid wind-diesel power system based on functional model predictive control," *Renewable Power Generation, IET*, vol. 8, no. 8, pp. 887–899, 2014.

[87] M. Soliman, O. Malik, and D. T. Westwick, "Multiple model predictive control for wind turbines with doubly fed induction generators," *IEEE Transactions on Sustainable Energy*, vol. 2, no. 3, pp. 215–225, 2011.

[88] M. Mirzaei, N. K. Poulsen, and H. H. Niemann, "Robust model predictive control of a wind turbine," in *American Control Conference (ACC), 2012*, pp. 4393–4398, IEEE, 2012.

[89] A. Khatamianfar, M. Khalid, A. V. Savkin, and V. G. Agelidis, "Improving wind farm dispatch in the australian electricity market with battery energy storage

using model predictive control," *IEEE Transactions on Sustainable Energy*, vol. 4, no. 3, pp. 745–755, 2013.

[90] M. Larsson, D. J. Hill, and G. Olsson, "Emergency voltage control using search and predictive control," *International journal of electrical power and energy systems*, vol. 24, no. 2, pp. 121–130, 2002.

[91] M. Larsson, "An adaptive predictive approach to emergency frequency control in electric power systems," in *Decision and Control, 2005 and 2005 European Control Conference. CDC-ECC'05. 44th IEEE Conference on*, pp. 4434–4439, IEEE, 2005.

[92] R. R. Negenborn, A. G. Beccuti, T. Demiray, S. Leirens, G. Damm, B. De Schutter, and M. Morari, "Supervisory hybrid model predictive control for voltage stability of power networks," in *American Control Conference, 2007. ACC'07*, pp. 5444–5449, IEEE, 2007.

[93] B. Gong and I. Hiskens, "Two-stage model predictive control for voltage collapse prevention," in *Power Symposium, 2008. NAPS'08. 40th North American*, pp. 1–7, IEEE, 2008.

[94] M. Wooldridge, *An introduction to multiagent systems*. John Wiley and Sons, 2009.

[95] S. Talukdar, L. Baerentzen, A. Gove, and P. De Souza, "Asynchronous teams: Co-operation schemes for autonomous agents," *Journal of Heuristics*, vol. 4, no. 4, pp. 295–321, 1998.

[96] P. J. Modi, W.-M. Shen, M. Tambe, and M. Yokoo, "Adopt: Asynchronous distributed constraint optimization with quality guarantees," *Artificial Intelligence*, vol. 161, no. 1, pp. 149–180, 2005.

[97] R. Olfati-Saber, A. Fax, and R. M. Murray, "Consensus and cooperation in networked multi-agent systems," *Proceedings of the IEEE*, vol. 95, no. 1, pp. 215–233, 2007.

[98] N. A. Lynch, *Distributed algorithms*. Morgan Kaufmann, 1996.

[99] N. Moshtagh and A. Jadbabaie, "Distributed geodesic control laws for flocking of nonholonomic agents," *IEEE Transactions on Automatic Control*, vol. 52, no. 4, pp. 681–686, 2007.

[100] R. Sepulchre, D. Paley, and N. Leonard, "Collective motion and oscillator synchronization," in *Cooperative control*, pp. 189–205, Springer, 2005.

[101] R. Olfati-Saber and R. M. Murray, "Distributed cooperative control of multiple vehicle formations using structural potential functions," in *IFAC World Congress*, pp. 346–352, Citeseer, 2002.

[102] T. Keviczky, F. Borrelli, and G. J. Balas, "A study on decentralized receding horizon control for decoupled systems," in *American Control Conference (ACC), 2004*, vol. 6, pp. 4921–4926, IEEE, 2004.

[103] S. D. McArthur, E. M. Davidson, V. M. Catterson, A. L. Dimeas, N. D. Hatziargyriou, F. Ponci, and T. Funabashi, "Multi-agent systems for power engineering applications—part i: Concepts, approaches, and technical challenges," *IEEE Transactions on Power Systems*, vol. 22, no. 4, pp. 1743–1752, 2007.

[104] S. D. McArthur, E. M. Davidson, V. M. Catterson, A. L. Dimeas, N. D. Hatziargyriou, F. Ponci, and T. Funabashi, "Multi-agent systems for power engineering applications—part ii: Technologies, standards, and tools for building multi-agent systems," *IEEE Transactions on Power Systems*, vol. 22, no. 4, pp. 1753–1759, 2007.

[105] R. M. Hermans, A. Jokić, M. Lazar, A. Alessio, P. P. van den Bosch, I. A. Hiskens, and A. Bemporad, "Assessment of non-centralised model predictive control techniques for electrical power networks," *International Journal of Control*, vol. 85, no. 8, pp. 1162–1177, 2012.

[106] D. Panasetsky, P. Etingov, and N. Voropai, "Multi-agent approach to emergency

control of power system," in *Electric Utility Deregulation and Restructuring and Power Technologies, 2008. DRPT 2008. Third International Conference on*, pp. 2157–2161, IEEE, 2008.

[107] P. Hines and S. Talukdar, "Controlling cascading failures with cooperative autonomous agents," *International Journal of Critical Infrastructures*, vol. 3, pp. 192 – 220, 2007.

[108] P. Hines and S. Talukdar, "Reciprocally altruistic agents for the mitigation of cascading failures in electrical power networks," in *Proceedings of the International Conference on Infrastructure Systems*, (Rotterdam), 2008.

[109] E. W. Jacobsen, "Lecture 13: Model predictive control." Unpublished lecture notes from 2E1252 Control Theory and Practice, KTH Royal Institute of Technology, 2005.